



This work is protected by copyright and other intellectual property rights and duplication or sale of all or part is not permitted, except that material may be duplicated by you for research, private study, criticism/review or educational purposes. Electronic or print copies are for your own personal, non-commercial use and shall not be passed to any other individual. No quotation may be published without proper acknowledgement. For any other use, or to quote extensively from the work, permission must be obtained from the copyright holder/s.

# Development of mathematical models for freight cars subject to dynamic loading



Anzhela Shestakova

School of Computing and Mathematics

Keele University

This dissertation is submitted for the degree of

*Doctor of Philosophy*

Keele December 2015

# Acknowledgement

First and foremost, I express sincere thanks to my supervisor Prof Julius Kaplunov for the continuous support, encouragement, motivation, advice and immense knowledge. His guidance helped me during the whole time of the research project and the writing of this thesis. It has been an honour to be his student in my PhD project. Additionally, I am very grateful to all the members of staff at Keele and Brunel Universities.

I gratefully acknowledge support and funding from the industrial project with AMSTED Rail, USA, especially from Prof Igor Aleynikov, Dr Brent Wilson and Dr Brad Hopkins.

Last but not the least, I would like to thank my friend Andriy Shestakov and my family: my parents Zinaida and Vladimir Kravchuk, for their unconditional support, inspiration and suggestions during the time of hard work and particularly, in the difficult moments.

# Abstract

This research is inspired by mathematical modelling of railcar dynamics and deals with developing a methodology for estimating the impact loads acting on freight cars using measured acceleration data in order to determine their limiting magnitudes for the alarm generation.

The developed scheme consists of the following steps. First, artificial neural network technology (ANN) is adapted to predict longitudinal forces in freight cars. Impact tests data for accelerations and forces were used for training ANN. The issue related to the lack of experimental results for training the network is addressed. A possibility of alternative theoretical training using mathematical models is studied. A restricted scope of conventional mathematical models based on rigid body dynamics is discovered. In particular, these models ignore the effect of self-equilibrated loads and internal dissipation.

Next, an advanced perturbation model is derived, taking into account low frequency internal motion with inhomogeneous stiffness, density, and viscosity incorporated. The developed advanced model is applied to the evaluation of impact forces arising at coupled impact.

The aforementioned model follows from a low-frequency analysis of a viscoelastic inhomogeneous bar, subject to end loads. The longitudinal variation of the problem

parameters is taken into consideration. Explicit asymptotic corrections to the conventional equations of rigid body motion are derived in an integro-differential form. The refined equations incorporate the effect of an internal viscoelastic microstructure on the overall dynamic response. Comparison with the exact time-harmonic solutions for extension and bending of a bar demonstrates the efficiency of the developed approach.

KEY WORDS: Railcar dynamics, artificial neural network, viscoelastic, microstructure, perturbation, rigid body, low-frequency, bar, contact forces.

# List of Figures

3.1	McCulloch and Pitts' neuron model <sup>1</sup> . . . . .	25
3.2	Scheme of a multilayer perceptron network <sup>2</sup> . . . . .	26
3.3	Scheme of a radial basis function network <sup>3</sup> . . . . .	31
3.4	Impact viscoelastic Kelvin-Voigt model . . . . .	32
3.5	Impact viscoelastic Kelvin-Voigt model. Typical result (a) Acceleration $a_1$ vs time; (b) Force $F_2$ vs time . . . . .	34
3.6	Modified standard-linear impact model . . . . .	39
3.7	Modified standard-linear impact model with one nonlinear and two lin- ear springs . . . . .	42
3.8	Modified standard-linear impact model with one nonlinear and two lin- ear springs. Typical result (a) Acceleration $a_1$ vs time; (b) Force $F_2$ vs time . . . . .	45
3.9	Test setup (a) free to roll impact; (b) coupled impact . . . . .	46
3.10	Typical frequency-amplitude diagrams for (a) free to roll impact; (b) coupled impact . . . . .	46
3.11	Two masses elastic model . . . . .	47
3.12	Typical results of finding closing force for (a) analytical modeled data; (b) experimental data . . . . .	50

3.13	Typical results of training of the MLP ANN for Kelvin-Voigt model . . .	51
3.14	Typical results of training of the MLP ANN for Modified standard-linear model . . . . .	52
3.15	Comparison of maximal force simulated through ANN with experimental data for normalized acceleration . . . . .	53
3.16	Comparison of results of ANN with experimental data for acceleration subject to low pass filter . . . . .	54
3.17	Comparison of results of ANN with experimental data for the case of spectrum acceleration input . . . . .	55
4.1	Longitudinal vibration of the rod . . . . .	57
4.2	horizontal acceleration vs frequency (Real Part) . . . . .	80
4.3	horizontal acceleration vs frequency (Imaginary Part) . . . . .	80
4.4	Density variation . . . . .	81
4.5	horizontal acceleration vs frequency (Real Part) variable density . . . .	83
4.6	horizontal acceleration vs frequency (Imaginary Part) variable density .	84
4.7	Stiffness variation . . . . .	85
5.1	Perturbed rigid body motion of a beam . . . . .	88
5.2	Perturbed rigid body motion. a. overall, b. vertical, c. rotational . . .	90
5.3	Vertical acceleration vs frequency (Real Part) . . . . .	111
5.4	Vertical acceleration vs frequency (Imaginary Part) . . . . .	112
5.5	Rotation acceleration vs frequency (Real Part) . . . . .	113
5.6	Rotation acceleration vs frequency (Imaginary Part) . . . . .	113
6.1	Numerical illustrations for test 1 . . . . .	124

6.2	Numerical illustrations for test 3 . . . . .	125
6.3	Evidence of further investigation for test 3 . . . . .	126
6.4	Numerical illustration (test 2) . . . . .	127
6.5	Numerical illustration (test 4) . . . . .	127
6.6	Numerical illustration (test 5) . . . . .	127
6.7	Numerical illustration (test 6) . . . . .	127
6.8	Numerical illustration (test 7) . . . . .	128
6.9	Numerical illustration (test 8) . . . . .	128
6.10	Numerical illustration (test 9) . . . . .	128
6.11	Numerical illustration (test 10) . . . . .	128
6.12	Numerical illustration (test 11) . . . . .	128
6.13	Numerical illustration (test 12) . . . . .	128
6.14	Numerical illustration (test 13) . . . . .	129
6.15	Numerical illustration (test 14) . . . . .	129
6.16	Numerical illustration (test 15) . . . . .	129
6.17	Numerical illustration (test 16) . . . . .	129
6.18	Numerical illustration (test 17) . . . . .	129
6.19	Numerical illustration (test 18) . . . . .	129
6.20	Numerical illustration (test 19) . . . . .	130
B.1	Screenshot for module “Ideal Model” . . . . .	141
B.2	Screenshot for module “Damper Model” . . . . .	141
B.3	Screenshot for module “Experimental Data” . . . . .	142
B.4	Screenshot for ANN training . . . . .	142
B.5	Screenshot for loading ANN data . . . . .	143

B.6 Screenshot for Time Close Model . . . . . 144

# Contents

<b>1</b>	<b>Introduction</b>	<b>11</b>
<b>2</b>	<b>Brief literature review</b>	<b>17</b>
<b>3</b>	<b>Investigation of maximal forces using artificial neural networks (ANN)</b>	<b>22</b>
3.1	Theoretical background of ANN . . . . .	22
3.1.1	Basic neural network components. McCulloch and Pitts' neuron	23
3.1.2	Training of neural networks . . . . .	25
3.1.3	Multilayer perceptron . . . . .	26
3.1.4	Backpropagation learning of multilayer perceptron . . . . .	27
3.1.5	Radial basis function networks . . . . .	30
3.2	Basic analytical models of railcar interaction . . . . .	32
3.2.1	Viscoelastic Kelvin-Voigt impact model . . . . .	32
	Exact solution . . . . .	33
	Approximate solution . . . . .	35
3.2.2	Modified standard-linear impact model with a nonlinear spring .	38
	General nonlinearity . . . . .	38
	One nonlinear and two linear springs . . . . .	42
3.3	Evaluation of maximal contact forces using ANN . . . . .	45

3.3.1	Analysis of impact type . . . . .	45
3.3.2	Theoretical evaluation of closure forces . . . . .	47
	Phases and amplitudes of sinusoidal approximations . . . . .	48
3.3.3	Numerical results . . . . .	51
<b>4</b>	<b>Low - frequency perturbation of rigid body motion of a viscoelastic</b>	
	<b>inhomogeneous rod</b>	<b>56</b>
4.1	Statement of the problem . . . . .	56
4.2	Asymptotic analysis . . . . .	58
4.3	Particular cases . . . . .	65
4.3.1	An inhomogeneous viscoelastic rod of uniform density . . . . .	65
4.3.2	An inhomogeneous viscoelastic rod of uniform stiffness . . . . .	67
4.3.3	A homogeneous viscoelastic rod . . . . .	68
4.3.4	An inhomogeneous Voigt rod . . . . .	69
	Uniform density . . . . .	76
	Uniform stiffness and viscosity . . . . .	77
	Uniform density, stiffness and viscosity . . . . .	77
4.4	Numerical Results . . . . .	78
4.4.1	A homogeneous Voigt rod . . . . .	78
4.4.2	An inhomogeneous Voigt rod of variable density . . . . .	80
4.4.3	An inhomogeneous Voigt rod of variable stiffness . . . . .	84
<b>5</b>	<b>Low - frequency perturbation of rigid body motion of a viscoelastic</b>	
	<b>inhomogeneous beam</b>	<b>87</b>
5.1	Statement of the problem . . . . .	87
5.2	Vertical Motion and Rotation . . . . .	90

5.3	Asymptotic analysis . . . . .	91
5.4	Particular cases . . . . .	102
5.4.1	An inhomogeneous viscoelastic beam of uniform density . . . . .	102
5.4.2	An inhomogeneous viscoelastic beam of uniform stiffness and viscosity . . . . .	105
5.4.3	A homogeneous viscoelastic beam . . . . .	108
5.5	Numerical results . . . . .	110
<b>6</b>	<b>Application of the low-frequency model to a coupled impact</b>	<b>114</b>
6.1	A homogeneous elastic rod . . . . .	114
6.2	An inhomogeneous elastic rod of variable density . . . . .	118
6.3	Evaluation of impact forces from experimental data . . . . .	122
	<b>Appendices</b>	<b>133</b>
	<b>Appendix A Exact solutions for homogeneous rods and beams</b>	<b>134</b>
A.1	Horizontal motion . . . . .	135
A.2	Vertical motion . . . . .	136
A.3	Rotation . . . . .	137
	<b>Appendix B Brief description of the developed software</b>	<b>139</b>
B.1	Application 'Model' . . . . .	139
B.2	Application 'Time Close Model' . . . . .	143

# Chapter 1

## Introduction

The cargo and freight damage suffered in the process of railway transportation is an important economic and safety problem. The development of an advanced methodology for estimating, analysing and predicting forces, accelerations and other reactions occurring upon collisions is of obvious interest from a practical view. Most of the damage is attributed to the car-to-car end impacts from coupling [1]. The damage is usually caused by high car and load acceleration, or by the fault or wear of the coupling system, including couplers, cushioning units, draft stills and gear. Artificial neural networks, ANNs [2]-[6], seem to be a promising methodology for tackling the aforementioned problem which may also benefit greatly from making use of theoretical modelling. Rigid body dynamic models [7, 8] have been widely used for determination of the reaction forces. However, the power of the traditional formulation appears to be rather limited. In particular, they do not allow straightforward evaluation of the longitudinal forces in case of coupled impact for self-equilibrating loads ( $F_2 - F_1 = 0$ ) and usually do not take into consideration inhomogeneity of the car and internal dissipation of energy. On the other hand, general three dimensional continuum models,

e.g. [9], are too complicated for using with the industrial software and require much more information on the problem parameters including spatial geometry, as well as mass and stiffness variation. This motivates refining of the classical models by using low-frequency perturbations of rigid body motions, see e.g. for viscoelastic inhomogeneous rod in differential form [10], for viscoelastic inhomogeneous rod and beam in integro-differential form [11, 12] and practical implementation of the derived quasi-rigid body motion model [13]. Such an approach is consistent with modern trends in multi-scale modelling based on the concept of frequency-dependent mass within the classical Newton law, e.g. see [14]. The developed approach is applied to the evaluation of the impact forces in the case of a coupled impact.

As it has been already mentioned, most of the damage appears due to high forces in the connection and deterioration of the coupler appliance. The original problem is separated into two independent steps. The first step is to determine the reaction force and, the second one is to find out whether the coupler is broken. In Chapter 3 we investigate whether an artificial neural network can be effectively used for the prediction of problem parameters. The development of an optimal network model consisted of the following stages: collecting and processing experimental data; selection of the network topology, including the number of hidden layers and the number of neurons in each layer; choosing activation functions; and finally, training and testing of the aforementioned network for simulating the required parameters. The series of tests on the collision of cars are conducted with different impact types, including coupled and free to roll impacts. The impacts data, supplied by the industrial partner, include initial velocities, masses, accelerations and forces. Initial data processing involves either filtering, scaling or smoothing. A special network was designed for each type of the

collision. The problem of determining collision type is solved using spectral frequency analysis of accelerations [15]-[17]. In the case of a coupled impact there is no zero harmonic, otherwise the latter takes non-zero values, see Subsection 3.3.1. The developed technique is tested and analysed using experimental data and enables to achieve almost 100% accuracy. The problem of the wearing down of draft gear equipment is resolved by finding out a closing force and comparing it with the given value for a serviceable draft gear. The equipment is assumed to be in order, if the calculated force is equal or greater than the given one. The theoretical model for solving the formulated problem, see Subsection 3.3.2, is based on calculating an intersection point of the curve related to a smoothed experimental graph and float associated with a theoretical sinusoidal approximation. The second step is oriented to predict the maximum of the reaction force by using the ANN. Two types of the ANN, including Multilayer Perceptron (Subsection 3.1.3) and Radial Basic Function Network (Subsection 3.1.5), are used to determine an unknown relationship between input and output data. The goal of MLP is to create a model that correctly maps the input (acceleration) to the unknown output (reaction force) by using measured data so that the model can then produce a desired output. RBF comprises one of the most widely utilised network models for function interpolation and gives a greater scope over the range of nonlinear functions.

Several mathematical models were developed for training and testing the network. They allow to generate various data with different parameters including mass, stiffness, initial velocities as well as others. The first model is a two-degree of freedom system consisting of two masses connected with a linear spring and viscous damper system, see Subsection 3.2.1. The second developed model is a system of two masses connected

with 2 linear springs and viscous damper/spring system, see Subsection 3.2.2. Both of the mentioned ANN demonstrate exceptionally accurate results when applied to these models. The average error between predicted and experimental maximum forces is approximately 2%, see Subsection 3.3.3. Conversely, an acceptable agreement with experimental datasets can be an issue because of a limited number of available experiments and lack of the information about some of problem parameters. However, the accuracy of the ANN for real experiment data is not high enough for industrial application. It is around 11% for each type of the impact. To improve the performance of the ANN, a number of tests with different parameters, including stiffness, mass, velocity, dissipation coefficient and others, are required. Compared with impact tests, numerical simulation is a more economical and faster method for investigating the analysed phenomena. At the same time, all mathematical models based on rigid body dynamics do not take into account the viscoelastic material properties and are not fully adequate for investigations car collision, especially in the case of coupling cars. The above limitations motivate the development of a new model.

The rigid body dynamic models mostly ignore small deformations of the car as well as the internal inhomogeneity and dissipation of energy. In the Chapter 4 a pseudo-rigid body model based on the principles of linear elastodynamics is developed. We start by analysing low - frequency perturbations of rigid body motion of a viscoelastic inhomogeneous rod subject to edge loads. Governing integro-differential equations are studied. We adapt a well established mathematical asymptotic procedure [18]-[20]. The characteristic timescale is assumed to be much greater than the period of free vibrations of the rod. First, we determine a rigid body acceleration from the Newton's second law. Then, we calculate the leading order variation of the stress along the rod.

At the next stage, we evaluate the sought for correction to the rigid body acceleration. It is worth noting that the representation of the chosen constitutive relation with the strain in the left-hand side is essential for perturbing rigid body motion [12]. Also, an important quantity corresponding the low-frequency variation of the longitudinal force along the length is crucial for our derivation. The obtained formulae represent asymptotic corrections to the classical equations of rigid body dynamics incorporating the effect of internal inhomogeneity and dissipation on the overall dynamic response. The equations governing perturbed rigid body motion enable, in particular, the evaluation of low-frequency behaviour induced by self-equilibrated end loads. The derived equations take a simpler and easy to use form for the variety of the particular cases with different variation of the Young's modules, density, stiffness and viscosity functions, see Section 4.3. Finally, to demonstrate a high level of accuracy as well as other advantage of the suggested method, its implementation is compared with the exact solution for a Voigt homogeneous rod, see Section 4.4.

The Chapter 5 deals with perturbed rigid body motion of an inhomogeneous Euler-Bernoulli beam loaded by end shear forces and moments. The perturbation scheme for a rod, proposed in the previous chapter, is now extended to a more sophisticated configuration for an inhomogeneous viscoelastic beams. A typical timescale characterising viscous behaviour is assumed to be much greater than the period of bending vibrations of the ends. The consideration is restricted to a symmetry of problem parameters that enables separation of vertical, see Subsection 5.3, and rotational motions, see Subsection 5.3. As before, we determine a rigid body acceleration. Then, we calculate the leading order variation of the longitudinal force and bending moments along the beam. Next, we evaluate the sought for corrections to rigid body accelerations ex-

pressed in terms of the shear forces and bending moments. Again, the representation of the constitutive relations with the bending strain in the left-hand side is handy for perturbing rigid body motion. Several examples for an inhomogeneous beam illustrate the developed methodology. Comparison with the exact solutions for vertical and rotational motion of a Voigt material provides a proof of the asymptotic consistency of the proposed scheme, see Section 5.5.

The developed methodology is applied to the evaluation of the impact forces in the most sophisticated case of a coupled impact. Elastic rods with uniform and variable density are studied in Chapter 6. Analysis of the available experimental data and their comparison with theoretically predicted forces are discussed. The experimental and predicted time derivatives of the impact forces show a relatively good agreement.

The advantage of the perturbed rigid body dynamic model incorporating the effect of the internal car structure is proven by numerical results. There is a considerable potential for further development and implementation of the designed procedure taking into account more precise structural models of freight cars, in particular, incorporating micro-resonance phenomena. There is also a clear possibility to use a similar approach for evaluating impact forces in tanks, see [21].

The main results of the thesis were presented at 17th Workshop on Advances in Experimental Mechanics (IWAEM) 2013 [10], 9th International Conference on Structural Dynamics EURODYN-2014 [11], EUROMECH-Colloquium 574 [13] and also delivered at applied mathematics seminar at Keele University.

# Chapter 2

## Brief literature review

Recently, numerous identification approaches predicting dynamic behaviours of freight car have been developed. In the case of the considered problem they can be generally classified into two groups: mathematical model-based approaches and procedures based on artificial neural network (ANN) prediction.

ANN is a biologically inspired computational model which consists of a network architecture composed of artificial neurons [22]. The structure contains a set of parameters, which can be adjusted to perform certain tasks. Selecting and pre-processing the datasets is the first and one of the most important steps to develop the appropriate network topology [23, 24]. ANN may be separated into two classes depending on their learning principles - unsupervised networks and supervised networks. Supervised learning means the adaptation of network's behaviour to the given input-output relationship. Typical tasks for supervised networks are function regression, pattern recognition and time series prediction. This class includes networks such as Multi Layer Perceptron (MLP) and ADALINE (Adaptive Linear Neuron or later Adaptive Linear Element) [25], Radial Basis Function Network (RBF) [26], Support Vector Ma-

chines (SVM) [27] and Hopfield Network [28]. The unsupervised learning networks adapt their internal structure to the structural properties of the input. In other words, such networks have the ability to learn and organize information without generating an error signal to evaluate a potential scenario [29]. Examples of these networks include Self-Organizing Map (SOM) or Kohonen Map (SOFM) [30] and Restricted Boltzmann Machine (RBM) [31]. The mentioned networks are highly competitive for tackling of a variety of problems, such as noise reduction, compressing and interpolating data. The Multilayer Perceptron with the Back-Propagation training algorithm (BPNN) [32] network is seen to be highly important and well supported out of the range of the other neural networks. Traditionally, the learning problem for MLP is to minimize an error function of free parameters in order to fit the outputs to an input-target dataset [33]. In the framework of the proposed research, the neural network is used to determine an unknown relation between input (accelerations) and output (forces) data. The BPNN performs relatively well, but is affected by a slow convergence and strict adherence to local minima [34]. The above issue may be readdressed by using a better activation function [35], choosing a dynamic learning rate and momentum term [36],[34] or modifying the optimization strategy and/or employing adaptation rules other than the gradient descent [22]. The RBF network is one of the most widely used networks for function interpolation and gives a broader scope over the range of nonlinear functions [37]. The output of this network is a linear combination of the radial basis functions depending on the inputs and neuron parameters. They have a tendency to require more data than a MLP [38] due to the locally acting nature of RBFs. Both of the mentioned ANN demonstrate exceptionally accurate results when applied to analytical models. At the same time an acceptable agreement with experimental datasets can be

an issue due to a limited number of available experiments and lack of the information on several problem parameters. A substantial amount of tests with different parameters, including stiffness, mass, velocity, dissipation coefficient and others are required to improve the performance of the ANN.

Compared with impact tests, numerical simulation is a more economical and faster method for investigating the analysed phenomena. Computational procedures for predicting longitudinal forces in railway dynamics, e.g. see recent contributions [1, 40] and references therein, are based on the traditional equations of rigid body motion. Basically, it is a multiple degree of freedom vibrating system [41] for which the equation of motion can be written down using Lagrange-D'Alembert's principle of dynamics equilibrium [42]. Analysis within the framework of the multibody dynamic has been carried out in the papers [43, 44] for rigid bodies system, [45] for system of rigid with deformable components and adaptation of a multibody dynamical formalism for satellite dynamics [46]-[48]. Various formulations have also been developed to determine the impact force during the contact period starting from the co-called "continuous analysis" [49]-[52]. The continuous contact force models deal with the forces applied to spring-damper elements, which can be linear, such as the Kelvin-Voigt viscoelastic model [53, 54], Maxwell model [55], Standard-Linear and Burger models, or non-linear, such as the Hunt and Crossley model [56]. However, the linear models are not always very accurate since they do not incorporate the overall nonlinear nature of the impact. The aforementioned nonlinear model in [56] is effective and accurate predominantly for long time impacts. A more suitable model for the impact force is based on the modification of a nonlinear Hertz force-displacement law model in conjunction with a hysteresis damping function representing the energy-dissipation [57, 58]. The math-

emational models, derived in [59], show clearly the influence of longitudinal forces on cargo. The numerical methods, such as Runge-Kutta fourth-order [60], Euler tangent [61] and Newmark- $\beta$  method [62], are widely applied in implementation of all of the abovementioned models. The rigid multi-body models ignore the effect of self-equilibrated loads and internal dissipation. In particular, evaluation of the longitudinal forces for the case of a coupled impact could be an issue for this type of model.

Mathematical modelling of an internal microstructure, aimed to extend the range of validity of the traditional equations of rigid body dynamics, is of an obvious interest for various industrial applications. For example, they may benefit from taking into account the absorption of vibration energy by transported loads including raw materials. Amongst the publications on the subject, we mention [63]-[65], which suggest a general methodology within the framework of linear anisotropic elasticity leading to a sort of 'macroscale' Newton's second law with a frequency-dependent mass. This methodology was earlier explored by [66] for modified Newtonian dynamics. We also cite here related publications [67] dealing with homogenisation of viscoelastic periodic media, such as composite elastic medium [68, 69], heterogeneous thermally conducting medium [70], two-phase conducting composites, an anisotropic fibres and isotropic material [71], composite material constituted of solid fibers and of a solidifying matrix [72] and random media [73]. This thesis is concerned with a low-frequency analysis of an inhomogeneous viscoelastic microstructure. A similar methodology was earlier exploited both for periodic and thin functionally graded structures, e.g. see [75]-[77] and references therein. The proposed perturbation scheme is developed for an inhomogeneous viscoelastic bar governed by the conventional integro-differential constitutive relations in linear viscoelasticity with strains on the left side. In-plane horizontal, vertical and

rotational motions induced by prescribed end forces and moments are studied starting from the classical one-dimensional theories for bar extension and bending. In the case of bending, only the symmetry of problem parameters is considered, allowing for the the separation of vertical and rotational motions. A typical timescale characterising viscous behaviour is assumed to be much greater than the time elastic waves take to propagate the distance between the ends of the bar [12].

Explicit low-frequency corrections to the equations of rigid body motion are constructed in Chapter 4 and Chapter 5. They are given in the form of integro-differential operators acting on a longitudinal force or bending moment. An example of a homogeneous bar is presented in Sections 4.3.4 and 5.4.3. Comparison with the exact solutions of the original time-harmonic problems for the extension and bending of a bar (see Sections 4.4 and 5.5) demonstrates the advantages of the proposed approach. Numerical data are calculated for a Voigt rod and beam. The developed methodology is tested and analysed on the experimental data in the most sophisticated case of a coupled impact. Second contact force derivatives were predicted. The comparison of experimental and predicted derivatives of the force shows relatively good agreement between them.

# Chapter 3

## Investigation of maximal forces using artificial neural networks (ANN)

### 3.1 Theoretical background of ANN

Artificial Neural Network (ANN) - is a series of algorithms that attempt to identify the relationships in a set of data by using a process that imitates the way the human brain operates. There are many different types of ANN depending on the problem which has to be solved (recognizing patterns, classification, data mining and predictions) and the training data, representing the task to be learnt [78, 79] . The most common to all of those components can be abstracted in the following way:

- a set of input and output units;
- a pattern of connectivity - assign the relations between the units set (weight value);

- a set of rules for propagating signals through the network (controlling when units can be updated), combining input signals (summarizing the weight values of the units) and calculating an output signal (determine the output units by using the activation function);
- a weight adaption rule (error-correcting rule to adapt the weight).

Depending on the training algorithms the Neural Networks (NN) are commonly classified to unsupervised networks and supervised networks. Supervised learning occurs when each sample in the training sets specifies all inputs as well as the outputs (for example, regression and classification tasks, time series prediction). In case of the the unsupervised learning the only collection of the sample inputs presented (for example, associative memory, grammatical induction and noise filtering tasks).

First step for design the optimal and appropriate network solution is to select [80] and preprocess the data sets [81]. Initial preprocessing data can be a rather simple procedure such as scaling, smoothing, normalization, as well as a complicated one involving advanced statistical methods [82]. The second step is to choose the appropriate network model, depending on task to be solved, then experimentally specify a network topology (number of units, connections) and, finally, set up the learning parameters [83].

### **3.1.1 Basic neural network components. McCulloch and Pitts' neuron**

The most common neuron model (neuron and a networked interconnection structure) has been developed by McCulloch and Pitts [38], see Figure 3.1.

Each neuron consists of a net and an activation functions. The net function determines how the network inputs  $x_i$ ,  $1 \leq i \leq N$  are combined inside the neuron. The most commonly used activation function:

$$net_j = \sum_{i=1}^N w_{ij}x_i + \theta, \quad (3.1)$$

where  $w_{ij}$ ,  $1 \leq i \leq N$  are weights, and  $\theta$  is bias (or threshold). The output of the neuron, which is denoted by  $o_j$  in Figure 3.1, is related to the network input  $net_j$  through the activation function:

$$o_j = f(net_j). \quad (3.2)$$

The other commonly used activation functions are

- $f(net) = (1 + e^{-\beta net})^{-1}$  - sigmoid
- $f(net) = \tanh(\beta net)$  - hyperbolic tangent
- $f(net) = a net + b$  - linear
- $f(net) = \frac{1}{\sqrt{2\pi\sigma}} e^{-\frac{(net-\mu)^2}{2\sigma^2}}$  - Gaussian
- $f(net) = \begin{cases} -1 & \text{if } net < 0 \\ 1 & \text{if } net \geq 0 \end{cases}$  - step

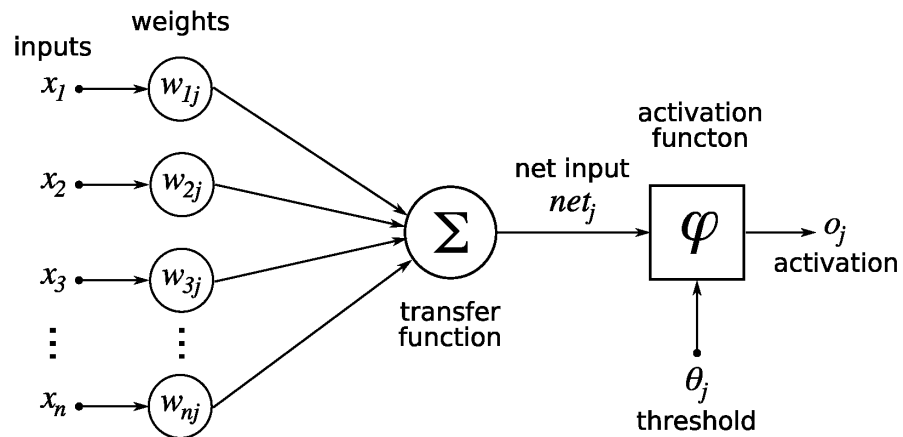


Figure 3.1: McCulloch and Pitts' neuron model<sup>1</sup>

### 3.1.2 Training of neural networks

A training algorithm is to set up the network's weights and thresholds to minimize the prediction error made by the network. On the first iteration the weight value is initiated with some small random parameters. The error of a particular configuration of the network can be determined by running all the training cases through the network, comparing the actual output generated with the desired or target outputs. The differences are combined together by an error function to give the network error [84]. The most common error functions are the least mean squared error (LMS), proposed by Widrow and Marcian Hoff in 1960, usually used for regression problems, and the cross entropy functions [85], usually used for maximum likelihood classification.

<sup>1</sup>The picture is taken from Wikipedia

### 3.1.3 Multilayer perceptron

A multilayer perceptron (MLP) neural network model firstly was proposed by Rosenblatt [87]. More recent variation of MLP consists of a feed-forward, layered network of McCulloch and Pitts' neurons with a nonlinear, continuously differentiable activation function. Every node in a layer is connected to every other node in the neighboring layer [34]. A typical MLP configuration is illustrated in Figure 3.2.

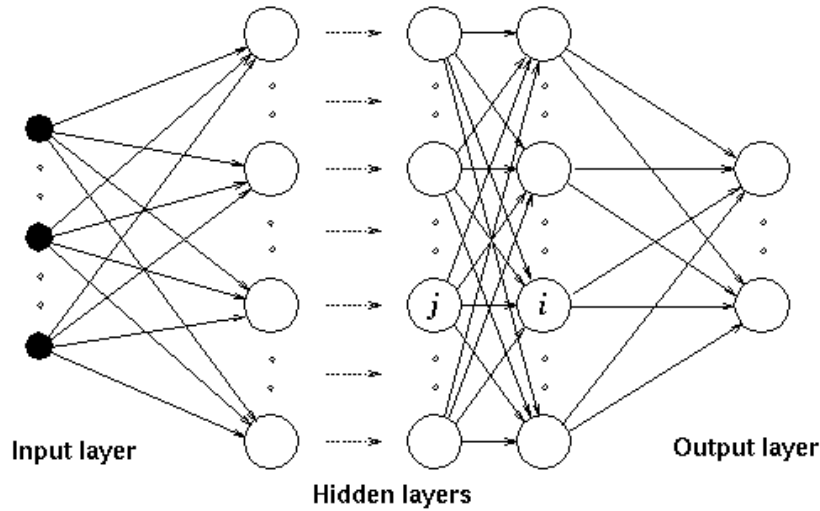


Figure 3.2: Scheme of a multilayer perceptron network<sup>2</sup>

The MLP is commonly used in regression problems, where the objective is to estimate the value of a continuous output variable, given the known input variables. In other words MLP is applied for approximating a real valued target functions. Moreover, in view of the Kolmogorov theorem any continuous function can be implemented by the Multilayer Perceptron with at least one hidden level. Also in [88] were derived the hidden units numbers depending on the estimating function properties and on the accuracy of its approximation. Common training algorithms for the MLP are backpropagation [25] and conjugate gradient [89, 94].

<sup>2</sup>The picture is taken from ecee.colorado.edu website

### 3.1.4 Backpropagation learning of multilayer perceptron

The BPNN learning algorithm is based on calculating the output layer errors to find out the errors in the hidden layers. An appropriate choice of the weight matrices is a key step in applying the MLP. The weight is feeding into each layer of neurons from a weight matrix of that layer (the input layer does not have a weight matrix as it contains no neurons) [25]. The values of these weights are found using the error back-propagation training method [22]. BPNN learning algorithm defines two sweeps: forward sweep propagates the input vectors through the network to provide outputs at the output layer and backward sweep propagates back the error values through the network to determine how the weight should be changed during the training.

The error  $E_p$  for the pattern  $p$  can be defined as

$$E_p = \frac{1}{2} \sum_{j=1}^N (t_j - o_j)^2, \quad (3.3)$$

where  $t_j$  denotes desired output and  $o_j$  the actual output and the overall error  $E = \sum E_p$ .

The derivative of the error is given by

$$\frac{\partial E}{\partial w_{ij}} = \frac{\partial E}{\partial o_j} \frac{\partial o_j}{\partial net_j} \frac{\partial net_j}{\partial w_{ij}} \quad (3.4)$$

We now define  $\delta_j$  by

$$\delta_j = -\frac{\partial E}{\partial net_j} \quad (3.5)$$

On the other hand we notice that  $\delta_j = -\frac{\partial E}{\partial o_j}$ , therefore

$$\delta_j = -\frac{\partial E}{\partial o_j} \frac{\partial o_j}{\partial net_j} \quad (3.6)$$

By using the definition of the overall error, we have

$$\frac{\partial E}{\partial o_j} = -(t_j - o_j). \quad (3.7)$$

For activation function the output  $o_j$  is

$$o_j = f(net) \quad (3.8)$$

and so the derivative  $f'$  is given by

$$\frac{\partial o_j}{\partial net_j} = f'(net_j). \quad (3.9)$$

Hence, we deduce that

$$\delta_j = (t_j - o_j)f'(net_j) \quad (3.10)$$

After substituting the product of each derivative into (3.4), we obtain

$$\frac{\partial E}{\partial w_{ij}} = -(t_j - o_j)f'(net_j)x_i \quad (3.11)$$

Therefore the weight change for a unit may be written as

$$\Delta w_{ij} = \eta \delta_j x_i \quad (3.12)$$

where  $x_i$  is the output unit  $i$  and  $\eta$  is the learning rate. For a hidden unit the error is given by

$$\delta_j = f'(net_j) \sum_k \delta_k w_{kj} \quad (3.13)$$

where index  $k$  stands for the sending back error layer.

Therefore, the weight update formula is given by

$$w_j(k+1) = w_j(k) + \eta \sum_{k=1}^N \delta_k x_{kj} \quad (3.14)$$

In order to reduce the effect of the weight changes oscillating the momentum term  $\alpha$  is added in the previous formula of the weight change

$$\Delta w_{ij}(k+1) = \eta(\delta_j o_i) + \alpha \Delta w_{ij}(k) \quad (3.15)$$

MLPs have several significant advantages over conventional approximation. First, MLP hidden unit output change adaptively during training, making it unnecessary for the user to choose them beforehand. Second, the number of free parameters can be increased by simply increasing the number of hidden units. Third, MLP basic functions are bounded, making round-off and overflow errors unlikely [38].

Among the disadvantages of the MLP compared to conventional approximations we note its rather long training time, sensitivity to initial weight values and the problem of "local minima". In addition, determination of the optimal amount of training epoch is difficult and the common solution to stop the training, when the validation error starts to increase, does not guarantee the optimal performance. Proposed approaches for addressing network mostly based on modification of the learning rate and momentum, using adaptive momentum coefficient instead of fixed, e.g., see [90, 91], or adaptive

learning rate coefficient [92], activation function, using combination of polynomial, periodic, sigmoidal functions [93], or learning algorithm, e.g. see references in [34].

### 3.1.5 Radial basis function networks

A radial basis function network (RBF) is another neural network used for classification and general function fitting. It is a feed forward neural network using the radial basis activation function.

RBF network in its simplest form is a three-layer network (see Figure 3.3) with the usual input layer to distribute a pattern to the first layer of weight, a hidden layer and output layer [38]. For each hidden unit there is a function  $\varphi$ . The typically used radial basis functions are

- $\varphi(r) = e^{-(\varepsilon r)^2}$  - Gaussian
- $\varphi(r) = \sqrt{1 + (\varepsilon r)^2}$  - multiquadric
- $\varphi(r) = \frac{1}{1 + (\varepsilon r)^2}$  - inverse quadratic
- $\varphi(r) = \frac{1}{\sqrt{1 + (\varepsilon r)^2}}$  - inverse multiquadric

where  $r = \|x - x_i\|$ .

The collective activations of all the hidden units define the vector to which the input vector has been mapped:

$$\varphi(x) = [\varphi(x_1), \varphi(x_2), \dots, \varphi(x_N)] \quad (3.16)$$

where  $N$  is the number of hidden units and  $x$  is the input vector.

---

<sup>3</sup>The picture is taken from bio.felk.cvut.cz website

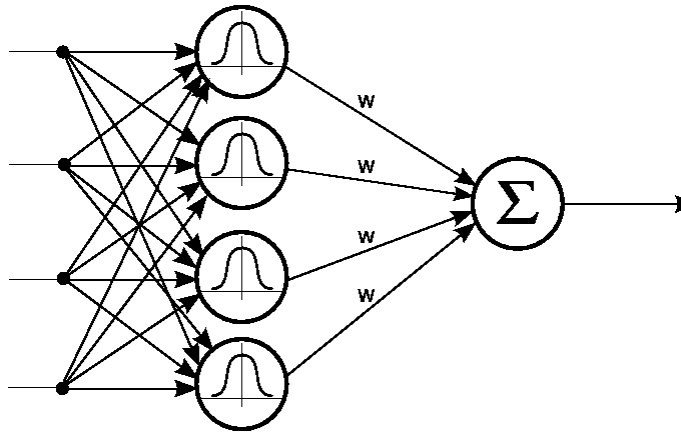


Figure 3.3: Scheme of a radial basis function network<sup>3</sup>

The weight connecting to a hidden unit define the center of the radial basis function for that hidden unit. The input to a unit is in a form:

$$net_j = \| x - w_i \| = \sqrt{\sum_{i=1}^n (x_i - w_{ij})^2} \quad (3.17)$$

where  $n$  is the number of input units.

First layer of weights are the chosen centers of the radial basis functions, second layer simply performs a linear addition of the outputs from the hidden layer. By using the Widrow-Hoff learning law the adjustment to be made is:

$$\Delta w = \eta \delta net \quad (3.18)$$

RBF networks can provide a fast and accurate means of approximating a nonlinear mapping based on observed data. Due to the locally acting nature of RBFs, they have a tendency to require more sufficient data that represents all aspects of the problem being solved.

Thus, the advantages of application of the ANN for the purpose of identification the reaction between the input and output parameters, are the network learning ability, solving the problem without finding and describing method, ability for generalization, easier implementation in any application. The disadvantages are requirement of high processing time, sufficient number of data, and inability to make changes when the network is trained.

## 3.2 Basic analytical models of railcar interaction

Here we present some elementary analytical models for railcar interaction, which were used for generating data for training of the ANN in the first part of the project.

### 3.2.1 Viscoelastic Kelvin-Voigt impact model

Consider a two-degree of freedom system of two masses connected together by a coupler with linear spring and a viscous damper elements, see Figure 3.4.

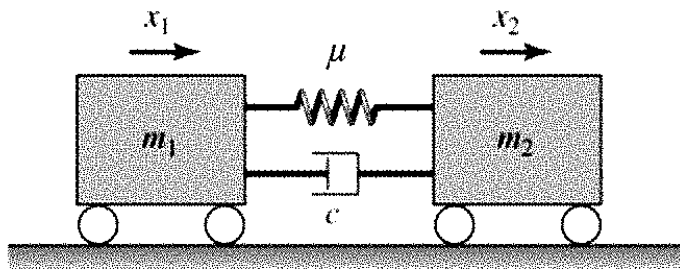


Figure 3.4: Impact viscoelastic Kelvin-Voigt model

According to Newton's second law the differential equations of motion for the spring-

mass system are written as

$$m_1 x_{1tt} = c(x_2 - x_1) + \mu(x_{2t} - x_{1t}) \quad (3.19)$$

$$m_2 x_{2tt} = c(x_1 - x_2) + \mu(x_{1t} - x_{2t})$$

where  $m_i$ ,  $i = 1, 2$  are masses,  $x_i$  are displacements, and  $\mu$  and  $c$  denote viscosity and stiffness, respectively.

The initial conditions for the (3.19) are as follows

$$x_i(0) = 0, \quad i = 1, 2 \quad \text{and} \quad x_{1t} = v, \quad x_{2t} = 0 \quad (3.20)$$

On introducing  $x = x_2 - x_1$  and  $m = (m_1 + m_2)/m_1 m_2$ , we get from the equations (3.19)

$$x_{tt} + cmx + \mu mx_t = 0. \quad (3.21)$$

### Exact solution

The solution of the 2nd order differential equation (3.21) is given by

$$x(t) = e^{\alpha t} (M \cos \beta t + N \sin \beta t) \quad (3.22)$$

where

$$\begin{aligned} \alpha &= -\frac{\mu}{2m} \\ \beta &= \frac{1}{2} \sqrt{\mu^2 m^2 - 4cm} \end{aligned} \quad (3.23)$$

Making use of the initial conditions (3.20) we deduce

$$M = 0 \quad \text{and} \quad N = -\frac{v}{\beta} \quad (3.24)$$

The accelerations for the masses 1 and 2 are expressed in the form

$$a_1(t) = -\frac{e^{\alpha t}}{m_1} \left[ c \left( v \cos \beta t + \frac{v\alpha}{\beta} \sin \beta t \right) + \mu \left( v\alpha \cos \beta t + \frac{v(\alpha^2 - \beta^2)}{\beta} \sin \beta t \right) \right] \quad (3.25)$$

$$a_2(t) = \frac{e^{\alpha t}}{m_2} \left[ c \left( v \cos \beta t + \frac{v\alpha}{\beta} \sin \beta t \right) + \mu \left( v\alpha \cos \beta t + \frac{v(\alpha^2 - \beta^2)}{\beta} \sin \beta t \right) \right] \quad (3.26)$$

An illustration of the developed model presented in the Figure 3.5. The curves related to the initial velocities  $v = 2, 4, 6 \text{ m/s}$  are drawn in a different line type.

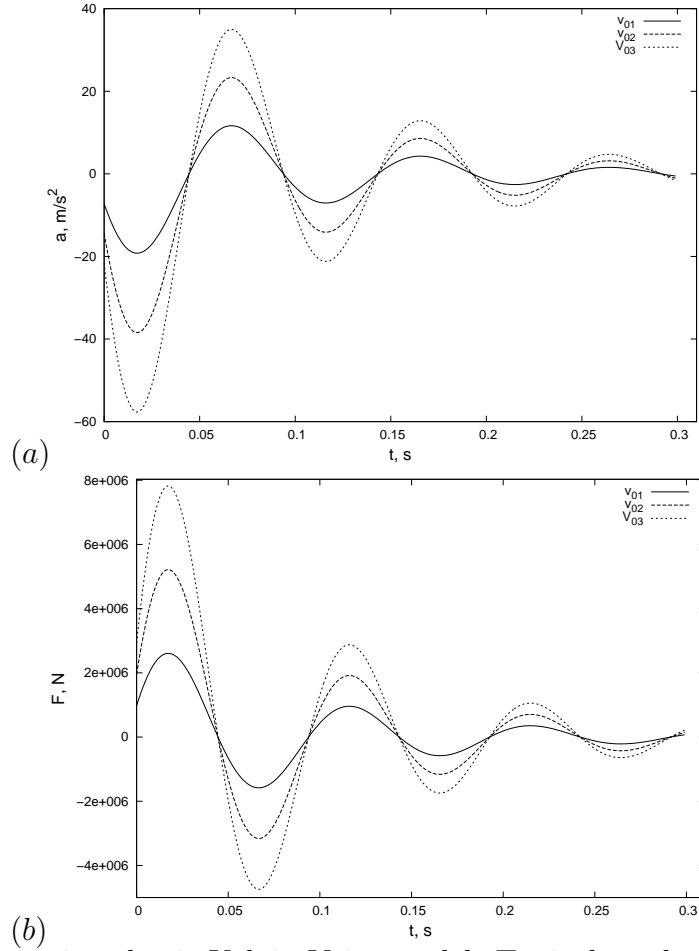


Figure 3.5: Impact viscoelastic Kelvin-Voigt model. Typical result (a) Acceleration  $a_1$  vs time; (b) Force  $F_2$  vs time

## Approximate solution

Let us introduce a dimensionless time

$$t = \tau \sqrt{\frac{m}{c}} \quad (3.27)$$

along with the small parameter

$$\varepsilon = \frac{\mu}{\sqrt{cm}} \ll 1 \quad (3.28)$$

Then the problem (3.19) and (3.20) may be formulated as

$$x_{\tau\tau} + x + \varepsilon x_{\tau} = 0 \quad (3.29)$$

with the following initial conditions

$$x(0) = 0 \quad \text{and} \quad x_{\tau} = -v^* \quad (3.30)$$

where

$$v^* = v \sqrt{\frac{m}{c}} \quad (3.31)$$

The solutions of (3.29) and (3.30) are sought in the form

$$x_* = x_{*0} + \varepsilon x_{*1} + \varepsilon^2 x_{*2} + \dots \quad (3.32)$$

At leading  $\varepsilon^{(0)}$  order

$$x_{*0\tau\tau} + x_{*0} = 0 \quad (3.33)$$

with the initial conditions

$$x_{*0}(0) = 0 \quad \text{and} \quad x_{*0\tau} = -v^* \quad (3.34)$$

Then

$$x_{*0} = A \cos \tau + B \sin \tau \quad (3.35)$$

Satisfying the initial conditions (3.34) we have

$$x_{*0} = -v^* \sin \tau \quad (3.36)$$

At next order  $\varepsilon^{(1)}$

$$x_{*1\tau\tau} + x_{*1} = -x_{*0} \quad (3.37)$$

with the homogeneous initial conditions  $x_{*1}(0) = x_{*1\tau} = 0$ . On solving the equation (3.36) along with the associated initial conditions we obtain

$$x_{*1} = \frac{v^*}{2} \sin \tau - \frac{v^* \tau}{2} \cos \tau \quad (3.38)$$

Similarly at order  $\varepsilon^{(2)}$

$$x_{*2} = -\frac{3v^*}{8} \sin \tau + \frac{3v^* \tau}{8} \cos \tau + \frac{v^* \tau^2}{8} \sin \tau \quad (3.39)$$

The solution at order  $(\varepsilon^3)$  is

$$x_{*3} = \frac{5v^*}{16} \sin \tau - \frac{5v^* \tau}{16} \cos \tau + \frac{v^* \tau^2}{8} \sin \tau + \frac{v^* \tau^3}{48} \cos \tau \quad (3.40)$$

Thus, the general solution is in a form

$$\begin{aligned}
x_* = v^* & \left[ -\sin \tau + \varepsilon \left( \frac{1}{2} \sin \tau - \frac{\tau}{2} \cos \tau \right) + \varepsilon^2 \left( -\frac{3}{8} \sin \tau + \frac{3\tau}{8} \cos \tau + \frac{\tau^2}{8} \sin \tau \right) + \right. \\
& \left. \varepsilon^3 \left( \frac{5v^*}{16} \sin \tau - \frac{5v^*\tau}{16} \cos \tau + \frac{v^*\tau^2}{8} \sin \tau + \frac{v^*\tau^3}{48} \cos \tau \right) + \dots \right] \quad (3.41)
\end{aligned}$$

therefore,

$$\begin{aligned}
x_{*\tau\tau} = v^* & \left[ \sin \tau + \varepsilon \left( \frac{1}{2} \sin \tau + \frac{1\tau}{2} \cos \tau \right) + \varepsilon^2 \left( -\frac{1}{8} \sin \tau + \frac{\tau}{8} \cos \tau - \frac{\tau^2}{8} \sin \tau \right) + \right. \\
& \left. \varepsilon^3 \left( \frac{9}{16} \sin \tau + \frac{15\tau}{16} \cos \tau - \frac{\tau^2}{4} \sin \tau - \frac{\tau^3}{48} \cos \tau \right) + \dots \right] \quad (3.42)
\end{aligned}$$

For simplicity, let us  $c_m = \sqrt{c/m}$ , then the accelerations may be re-cast in original variables as

$$\begin{aligned}
a = x_{tt} = v c_m & \left[ \sin c_m t + \frac{\mu}{\sqrt{c m}} \left( \frac{1}{2} \sin c_m t + \frac{1}{2} c_m t \cos c_m t \right) + \right. \\
& \frac{\mu^2}{c m} \left( -\frac{1}{8} c_m t \sin c_m t + \frac{1}{8} \cos c_m t - \frac{1}{8} c_m^3 t^2 \sin c_m t \right) + \\
& \frac{\mu^3}{\sqrt{(c m)^3}} \left( \frac{9}{16} \sin c_m t + \frac{15}{16} c_m t \cos c_m t - \frac{1}{4} \frac{c}{m} t^2 \sin c_m t - \right. \\
& \left. \left. \frac{1}{48} c_m^3 t^3 \cos c_m t \right) + \dots \right] \quad (3.43)
\end{aligned}$$

and the acceleration for the mass 1 and mass 2:

$$\begin{aligned}
a_1 = x_{1tt} &= \frac{1}{m_1} (cx + \mu x_t) = \frac{1}{m_1} \left\{ v\sqrt{mc} \left[ -\sin c_m t + \frac{\mu}{\sqrt{cm}} \left( \frac{1}{2} \sin c_m t - \right. \right. \right. \\
&\left. \left. \frac{1}{2} c_m t \cos c_m t \right) + \frac{\mu^2}{cm} \left( -\frac{3}{8} \sin c_m t + \frac{3}{8} c_m t \cos c_m t + \frac{1}{8} c_m^2 t^2 \sin c_m t \right) + \right. \\
&\left. \left. \frac{\mu^3}{\sqrt{(cm)^3}} \left( \frac{5}{16} \sin c_m t - \frac{5\tau}{16} \cos c_m t + \frac{1}{8} c_m^2 t^2 \sin c_m t + \frac{1}{48} c_m^3 t^3 \cos c_m t \right) + \dots \right] + \right. \\
&\mu c_m v \left[ -\cos c_m t + \frac{\mu}{\sqrt{cm}} \frac{1}{2} c_m t \sin c_m t + \frac{\mu^2}{cm} \left( -\frac{1}{8} c_m t \sin \sqrt{\frac{c}{m}} t + \right. \right. \\
&\left. \left. \frac{1}{8} c_m^2 t \cos \sqrt{\frac{c}{m}} t \right) + \frac{\mu^3}{\sqrt{(cm)^3}} \left( \frac{9}{16} c_m t \sin c_m t + \frac{3}{16} c_m^2 t^2 \cos c_m t - \right. \right. \\
&\left. \left. \frac{1}{48} c_m^3 t^3 \sin c_m t \right) + \dots \right] \left. \right\}
\end{aligned} \tag{3.44}$$

$$\begin{aligned}
a_2 = x_{2tt} &= -\frac{1}{m_2} (cx + \mu x_t) = -\frac{1}{m_2} \left\{ v\sqrt{mc} \left[ -\sin c_m t + \frac{\mu}{\sqrt{cm}} \left( \frac{1}{2} \sin c_m t - \right. \right. \right. \\
&\left. \left. \frac{1}{2} c_m t \cos c_m t \right) + \frac{\mu^2}{cm} \left( -\frac{3}{8} \sin c_m t + \frac{3}{8} c_m t \cos c_m t + \frac{1}{8} c_m^2 t^2 \sin c_m t \right) + \right. \\
&\left. \left. \frac{\mu^3}{\sqrt{(cm)^3}} \left( \frac{5}{16} \sin c_m t - \frac{5\tau}{16} \cos c_m t + \frac{1}{8} c_m^2 t^2 \sin c_m t + \frac{1}{48} c_m^3 t^3 \cos c_m t \right) + \dots \right] + \right. \\
&\mu c_m v \left[ -\cos c_m t + \frac{\mu}{\sqrt{cm}} \frac{1}{2} c_m t \sin c_m t + \frac{\mu^2}{cm} \left( -\frac{1}{8} c_m t \sin c_m t + \right. \right. \\
&\left. \left. \frac{1}{8} c_m^2 t \cos c_m t \right) + \frac{\mu^3}{\sqrt{(cm)^3}} \left( \frac{9}{16} c_m t \sin c_m t + \frac{3}{16} c_m^2 t^2 \cos c_m t - \right. \right. \\
&\left. \left. \frac{1}{48} c_m^3 t^3 \sin c_m t \right) + \dots \right] \left. \right\}
\end{aligned} \tag{3.45}$$

### 3.2.2 Modified standard-linear impact model with a nonlinear spring

#### General nonlinearity

Consider a two-degree of freedom system of two masses connected together with the nonlinear springs and viscous/spring damper.

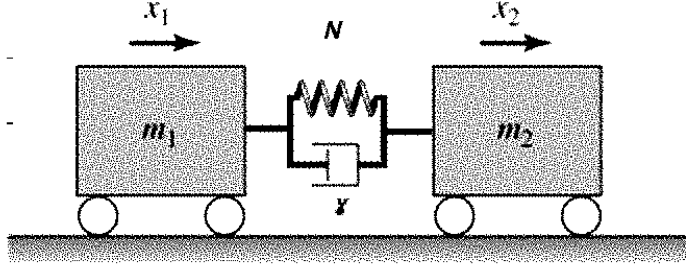


Figure 3.6: Modified standard-linear impact model

The equations of motion for spring-mass system (see Figure 3.6) are written as

$$\begin{aligned} m_1 x_{1tt} &= N(x) + \gamma(x)(x_{2t} - x_{1t}) \\ m_2 x_{2tt} &= -N(x) - \gamma(x)(x_{2t} - x_{1t}) \end{aligned} \quad (3.46)$$

where  $m_i$ ,  $i = 1, 2$  is mass,  $x_i$ ,  $i = 1, 2$  is the displacement,  $\gamma(x)$  is gear and damper characteristic function and  $N$  is force in the connection. Usually, the equation of the power characteristic damper appliance can be written as

$$N(x) = cx^n + N_0, \quad n \in \mathbb{N} \quad (3.47)$$

where  $c$  is stiffness,  $N_0$  is the initial tightening force and  $n$  is a power depended on the appliance's construction.

The initial conditions are

$$x_{1t}(0) = v, x_{2t}(0) = 0 \quad (3.48)$$

Let us  $x = x_2 - x_1$  and  $x_t = x_{2t} - x_{1t}$ , then from the equations (3.46) we get

$$x_{tt} = -\left(\frac{1}{m_1} + \frac{1}{m_2}\right) N(x) - \left(\frac{1}{m_1} + \frac{1}{m_2}\right) \gamma(x)x_t \quad (3.49)$$

or

$$mx_{tt} = -N(x) - \gamma(x)x_t \quad (3.50)$$

where  $m$  is in the form  $m = m_1 m_2 / (m_1 + m_2)$ .

By multiplying both part of the equation (3.46) by the  $\dot{x}$  and integrating by time  $t$ , we get

$$\frac{mx_t^2}{2} = \frac{mv^2}{2} - \int_{x_0}^x N(x)dx - \int_{x_0}^x \gamma(x)x_t dx \quad (3.51)$$

or

$$\frac{mx_t^2}{2} = \frac{mv^2}{2} - E_p - \int_{x_0}^x \gamma(x)x_t dx \quad (3.52)$$

where  $E_p = \int_{x_0}^x N(x)dx$  is elastic potential energy of compression damper appliance.

Let us  $\gamma(x) = \varepsilon\gamma_0(x)$ , where  $\varepsilon$  is a small parameter. Then, the equation (3.52) will be in the form

$$\frac{mx_t^2}{2} = \frac{mv^2}{2} - E_p - \varepsilon \int_{x_0}^x \gamma_0(x)x_t dx \quad (3.53)$$

We are looking for the solution of (3.53) in the form

$$x_t = x_{0t} + \varepsilon x_{1t} + \varepsilon^2 x_{2t} + \dots \quad (3.54)$$

At the leading order  $\varepsilon^{(0)}$

$$x_{0t} = \sqrt{v^2 - \frac{2E_p}{m}} \quad (3.55)$$

At next order  $\varepsilon^{(1)}$

$$x_{1t} = -\frac{\int_{x_0}^x \gamma_0(x)x_{0t} dx}{mx_{0t}} = -\left( \int_{x_0}^x \gamma_0(x) \sqrt{v^2 - \frac{2E_p}{m}} dx \right) / \left( m \sqrt{v^2 - \frac{2E_p}{m}} \right) \quad (3.56)$$

Similarly at order  $\varepsilon^{(2)}$  we have

$$x_{2t} = - \left( \int_{x_0}^x \gamma_0(x) x_{1t} dx + \frac{m x_{1t}^2}{2} \right) / m x_{0t} \quad (3.57)$$

next, at order  $\varepsilon^{(3)}$

$$x_{3t} = - \left( \int_{x_0}^x \gamma_0(x) x_{2t} dx + m x_{1t} x_{2t} \right) / m x_{0t} \quad (3.58)$$

and finally, at order  $\varepsilon^{(4)}$

$$x_{4t} = - \left( \int_{x_0}^x \gamma_0(x) x_{3t} dx + m x_{1t} x_{2t} + \frac{m v^2}{2} \right) / m x_{0t} \quad (3.59)$$

thus, the obtained formulae for accelerations mass 1 and mass 2 are in the form:

$$a_1 = x_{1tt} = \frac{1}{m_1} (N(x) + \gamma(x) x_t) = \frac{1}{m_1} \left[ N(x) + \sqrt{v^2 - \frac{2E_p}{m}} - \left( \int_{x_0}^x \gamma_0(x) \sqrt{v^2 - \frac{2E_p}{m}} dx \right) / \left( m \sqrt{v^2 - \frac{2E_p}{m}} \right) + \dots \right] \quad (3.60)$$

and

$$a_2 = x_{2tt} = - \frac{1}{m_2} (N(x) + \gamma(x) x_t) = - \frac{1}{m_2} \left[ N(x) + \sqrt{v^2 - \frac{2E_p}{m}} - \left( \int_{x_0}^x \gamma_0(x) \sqrt{v^2 - \frac{2E_p}{m}} dx \right) / \left( m \sqrt{v^2 - \frac{2E_p}{m}} \right) + \dots \right] \quad (3.61)$$

## One nonlinear and two linear springs

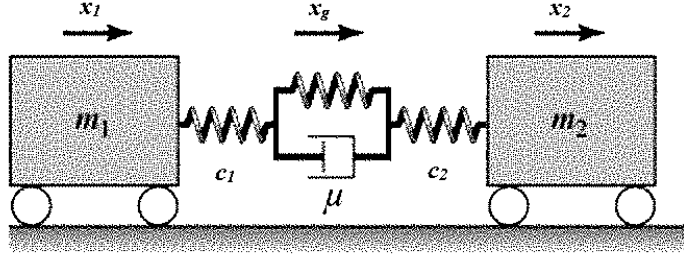


Figure 3.7: Modified standard-linear impact model with one nonlinear and two linear springs

Consider a system of two masses  $m_1$  and  $m_2$  connected together with the two linear springs of significant stiffness, a nonlinear spring/damper system. The equations of motion for spring-mass system (see Figure 3.7) are given by

$$\begin{aligned}
 m_1 x_{1tt} &= -F_g - \mu x_{gt} \\
 m_2 x_{2tt} &= F_g + \mu x_{gt} \\
 x_{gtt} &= \frac{1}{\mu} \left( x_{1t} - \frac{x_{2t}}{D} - x_{gt} \left( K_g + \frac{1}{D} \right) \right)
 \end{aligned} \tag{3.62}$$

where  $x_i, i = 1, 2, x_g$  are the displacements,  $\mu$  is viscosity,  $c_i, i = 1, 2$  are stiffness values,  $F_g$  is force, created by damper with spring, and

$$D = \frac{1}{c_1} + \frac{1}{c_2} \tag{3.63}$$

If the compression of the spring is greater than the gear stroke, the draft gears closes and force  $F_g$  is of the form

$$F_g = \begin{cases} cx_g & \text{if } |x_g| \leq Str \\ c_*x_g + (c - c_*)Str & \text{otherwise} \end{cases} \quad (3.64)$$

$$K_g = \begin{cases} c & \text{if } |x_g| \leq Str \\ c_* & \text{otherwise} \end{cases} \quad (3.65)$$

Let us denote vector of the initial conditions:

$$y = \begin{cases} x_1 \\ x_{1t} \\ x_2 \\ x_{2t} \\ x_g \\ x_{gt} \end{cases} \quad (3.66)$$

Then the vector of the corresponding derivatives is

$$D(y) = \begin{cases} x_{1t} \\ -\frac{1}{m_1} (F_g(x_g + \mu x_{gt})) \\ x_{2t} \\ \frac{1}{m_2} (F_g(x_g + \mu x_{gt})) \\ x_{gt} \\ \frac{1}{\mu} (x_{1t} - \frac{x_{2t}}{D} - x_{gt} (K_g + \frac{1}{D})) \end{cases} \quad (3.67)$$

Numerical solution of the system (3.67) can be obtained by the Runge-Kutta fourth-order method [95, 96].

The numerical results of the developed model presented in the Figure 3.8. The curves related to the initial velocities  $v = 2, 4, 6 \text{ m/s}$  are drawn in a different line type.

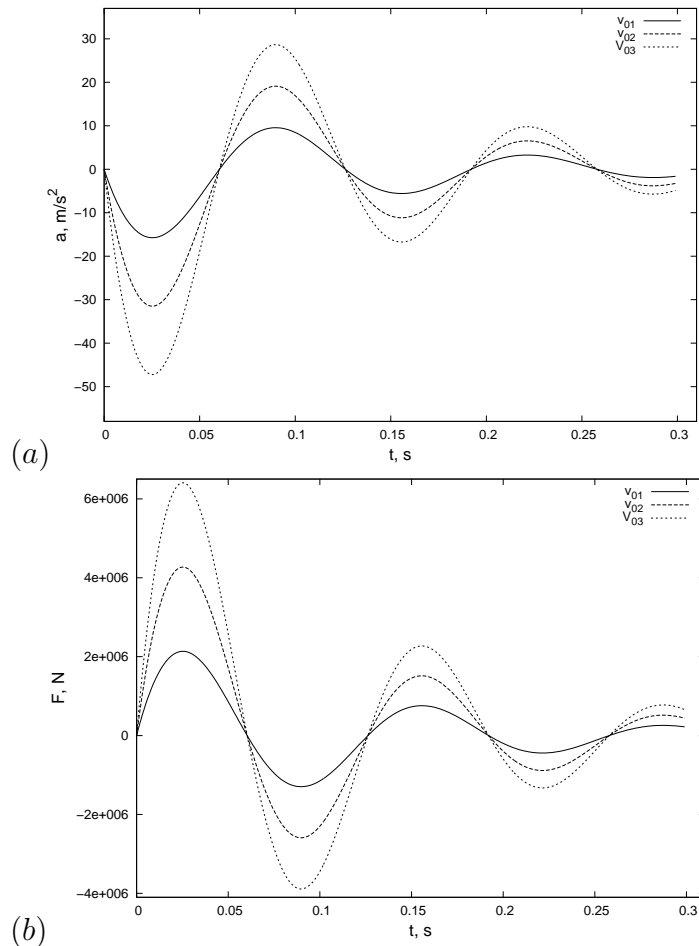


Figure 3.8: Modified standard-linear impact model with one nonlinear and two linear springs. Typical result (a) Acceleration  $a_1$  vs time; (b) Force  $F_2$  vs time

### 3.3 Evaluation of maximal contact forces using ANN

#### 3.3.1 Analysis of impact type

At the initial stage of the project the inverse problem of car-to-car interaction was tackled. Using the spectral frequency analysis (through fast Fourier transform, see, e.g. [97, 98]) it was first determined whether the specified data of accelerometers corresponds to free to roll or coupled impacts, see Figures 3.9. A series of impact tests were carried out to assess the spectral frequency response of the accelerations. The developed methodology is based on the analysis of the first frequency, there is no zero harmonic in the case of the coupled impact, otherwise the latter takes non-zero values.

The approach leads to a sufficiently accurate classification between impact types. Some typical diagrams, corresponding to these cases are shown on Figures 3.10 (a) and (b).



Figure 3.9: Test setup (a) free to roll impact; (b) coupled impact

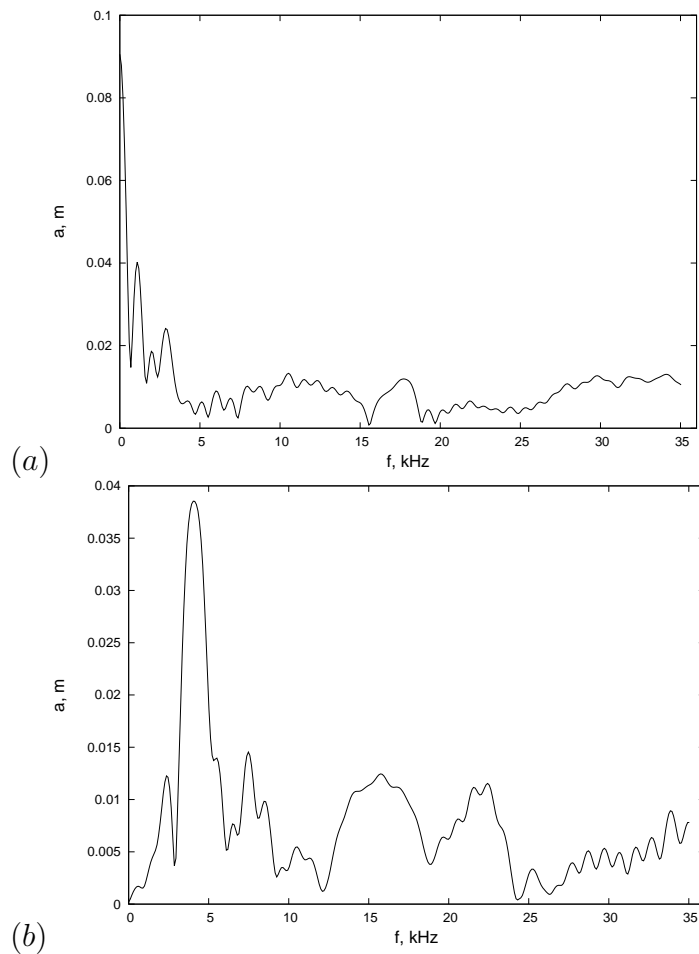


Figure 3.10: Typical frequency-amplitude diagrams for (a) free to roll impact; (b) coupled impact

The developed technique has been tested using some experimental data including two types of railcars (for details see Table 1)

Table 1.

Parameter	Hammer Car	Anvil Car
Car Type	Covered Hopper	Covered Hopper
Car Info	KREX 20	KREX 17
Car Weight	263,000 lbs	220,000 lbs
Cushioning Unit	MK 50	MK 50

A series of 19 tests for free to roll and 23 coupled impacts have been performed, demonstrating 100% success of the developed technique.

### 3.3.2 Theoretical evaluation of closure forces

The next preparatory step of the project is to determine the wearing condition of draft gear equipment. Identification the instant force when the friction device grasps and comparing with benchmark one allows to establish the wearing degree.

Consider a system of two masses coupled together by the linear elastic spring (see Figure 3.11).

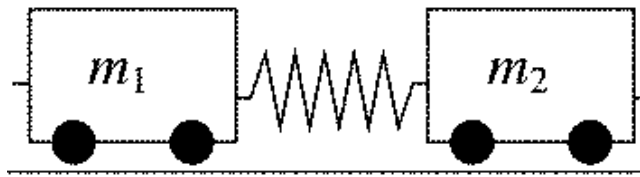


Figure 3.11: Two masses elastic model

The equations of motion for spring-mass system is written as

$$\begin{aligned}
 m_1 a_1 &= m_1 x_{1tt} = c(x_2 - x_1) \\
 m_2 a_2 &= m_2 x_{2tt} = -c(x_2 - x_1)
 \end{aligned}
 \tag{3.68}$$

where  $m_i$ ,  $i = 1, 2$  is mass,  $x_i$ ,  $i = 1, 2$  is the coordinate and  $c$  is stiffness.

Let us  $x = x_2 - x_1$  and  $m = 1/m_1 + 1/m_2$ , then from the equations (3.68) we obtain

$$x_{tt} = -cmx \quad (3.69)$$

The solution of the 2nd order differential equation (3.69) is

$$x(t) = A \sin kt + B \cos kt \quad (3.70)$$

Where  $k^2 = cm$ .

The contact force and acceleration after closure of the friction clutch draft gear assembly increasing rapidly and can be represented as a part of the sin function with some amplitude and phase. To calculate the closure force, the data were smoothed by using a Gaussian Kernel Method [99], an Adaptive Method [100] and passed through low pass filter data. We approximate the force/acceleration with sin function near max Force. Closure force is defined as an intersection point of sin and interpolated/filtered data. The best result for the data with noises gives Adaptive Method of interpolation function.

### **Phases and amplitudes of sinusoidal approximations**

The amplitude and phase for the sinusoidal approximation function can be found from the aforementioned trigonometric equation

$$y(x) = a \sin(bx + c) \quad (3.71)$$

The derivative in the maximum point is equal to zero, so

$$\frac{dy}{dx}\Big|_{x=x_{max}} = ab \cos(bx_{max} + c) = 0 \quad (3.72)$$

from the equation (3.72) we deduce

$$a = y_{max} \quad (3.73)$$

$$b = \frac{\frac{\pi}{2} - c}{x_{max}} \quad (3.74)$$

and

$$y_n = a \sin(bx_n + c) \quad (3.75)$$

Thus,

$$c = \frac{-\pi \frac{x_n}{2} + x_{max} y_{max} \sin\left(\frac{y_n}{y_{max}}\right)}{x_{max} - x_n} \quad (3.76)$$

$$b = \left( \frac{\pi}{2} - \frac{-\pi \frac{x_n}{2} + x_{max} y_{max} \sin\left(\frac{y_n}{y_{max}}\right)}{x_{max} - x_n} \right) \frac{1}{x_{max}} \quad (3.77)$$

Then

$$y(x) = y_{max} \sin \left[ \left( \frac{\pi}{2} - \frac{-\pi \frac{x_n}{2} + x_{max} y_{max} \sin\left(\frac{y_n}{y_{max}}\right)}{x_{max} - x_n} \right) \frac{x}{x_{max}} + \frac{-\pi \frac{x_n}{2} + x_{max} y_{max} \sin\left(\frac{y_n}{y_{max}}\right)}{x_{max} - x_n} \right] \quad (3.78)$$

Expressed in the terms of force, acceleration and time the equation (3.78) will be in the form of

$$F_{sin}(t) = F_{max} \sin \left[ \left( \frac{\pi}{2} - \frac{-\pi \frac{t_n}{2} + t_{max} F_{max} \sin \left( \frac{F_n}{F_{max}} \right)}{t_{max} - t_n} \right) \frac{t}{t_{max}} + \frac{-\pi \frac{t_n}{2} + t_{max} F_{max} \sin \left( \frac{F_n}{F_{max}} \right)}{t_{max} - t_n} \right] \quad (3.79)$$

where  $t$  - time,  $n$  is a random point closed to maximum force, which can be found experimentally.

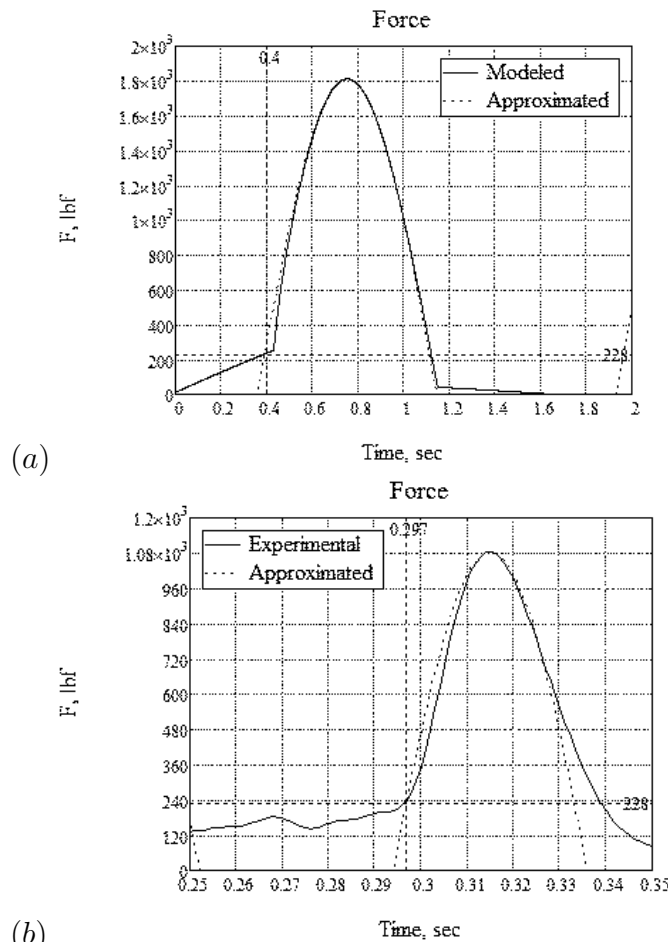


Figure 3.12: Typical results of finding closing force for (a) analytical modeled data; (b) experimental data

The suggested method to rate the force closure was tested on the data, generated by the analytical model, see Figure 3.12 (a), which allowed generation of any amount

of data with different model characteristics such as stiffness, mass, velocity, and dissipation coefficient and on the real experiment data, see Figure 3.12 (b).

### 3.3.3 Numerical results

Preliminary training of the ANN was based on the quantities calculated from the elementary analytical models developed in Section 3.2. For the data, generated by both models, the Multilayer Perceptron (MLP) neural network was trained using the supervised learning algorithm back propagation with decoupled momentum. The performance of the network configuration was estimated by calculating the difference between the generated output and real test data. The average error for specified range of parameters is around 2%. Some typical comparison of the ideal data with computed results of the ANN are presented in Figures 3.13 (a) and (b) for Kelvin-Voigt and Modified standard-linear models, respectively. It is showing variation of scaled maximal force for a set of tests (40 tests performed).

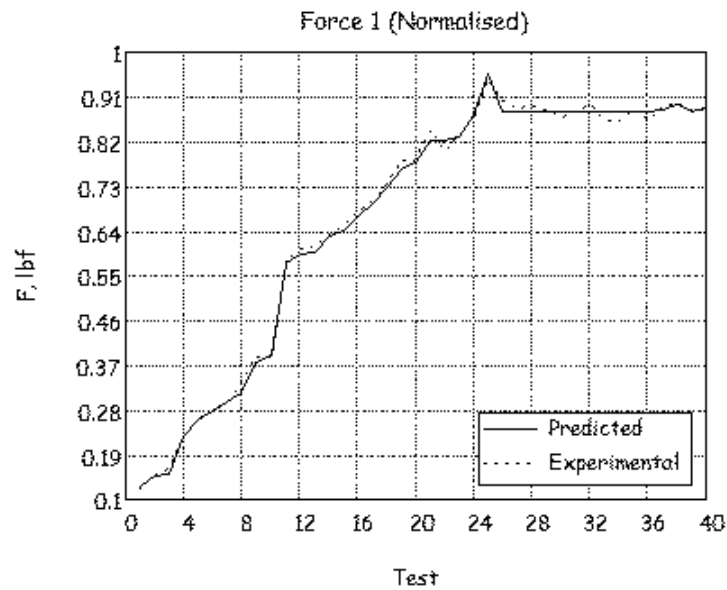


Figure 3.13: Typical results of training of the MLP ANN for Kelvin-Voigt model

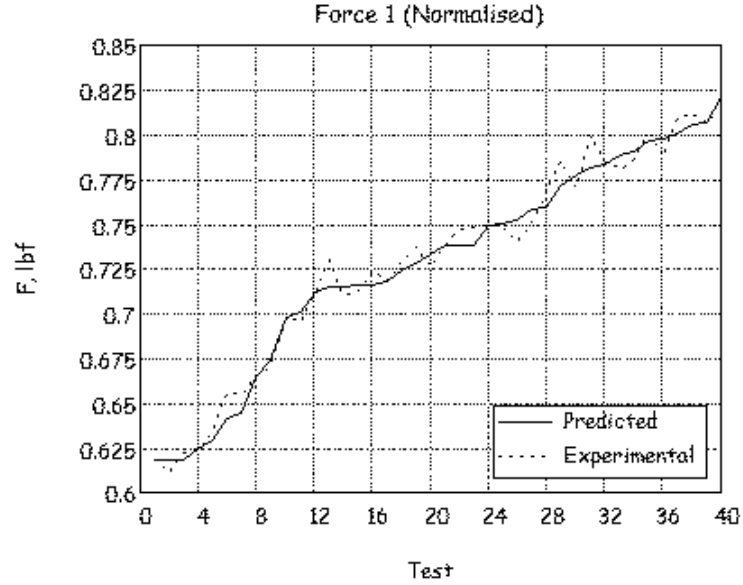


Figure 3.14: Typical results of training of the MLP ANN for Modified standard-linear model

The illustrations on Figures 3.13, 3.14 are performed for ANN of the configuration "input-hidden-output", with activation functions of the hidden and output layers adopted in "Sigmoid" form and the numbers of hidden layers as "200-21-1" and "200-18-1", respectively. The corresponding ANN performance was measured as 1.9%, and 2.5%.

However, when using results of real-life experiments, the precision of the ANN became lower, especially for higher speeds. Some typical graphs of maximal force are presented below for a series of 23 tests.

The first illustration is presented in Figure 3.15 for the normalized acceleration (performance 11.73%). The configuration of the ANN in this Figure is "300-70-5-1" with activation functions of "Tanh/Tanh/Log". An attempt was performed to filter acceleration from noise, which provided an improvement, see Figure 3.16, with accuracy rising to 5.20%. Here the ANN configuration of the ANN is "256-55-5-1" with activation functions of "Sigmoid/Tanh/Log". One more approach was tried through spectrum of

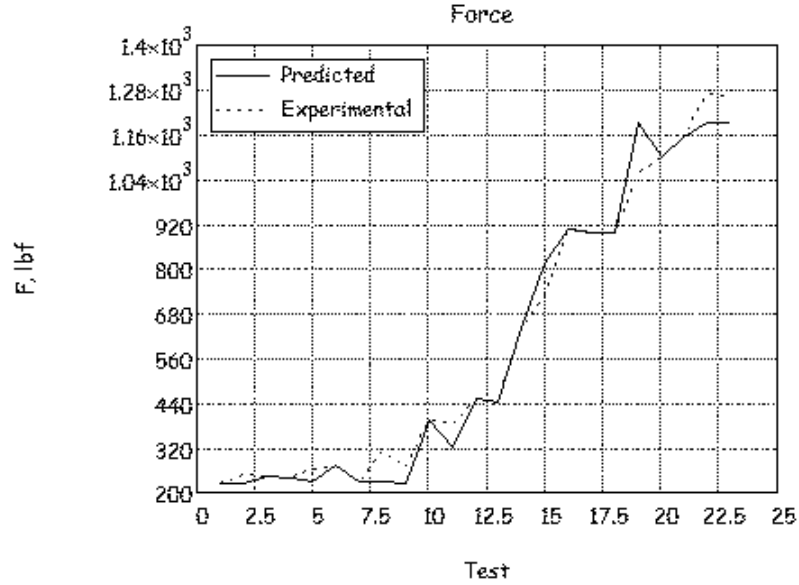


Figure 3.15: Comparison of maximal force simulated through ANN with experimental data for normalized acceleration

acceleration, however the results did not seem promising, see Figure 3.17. Here the structure of the layers is "50-17-4-1", with activation functions of "Tanh/Sigmoid/Log".

It may be suggested that the difference of the outcome of ANN for training data of the simple analytical data and real experimental data is significant due to the fact that both models do not incorporate the internal structure of the cars, therefore it is not straightforward to set up proper parameters with the asymptotic coverage of the real experiment data.

Thus, the project was started from the problem of determination of maximal force in the draft gear using the test data of accelerations of the railcars. This is a standard regression problem, therefore application of the ANN is justified. In order to perform training of the ANN two analytical models involving a simple linear spring and a slightly less trivial nonlinear spring, have been developed. These models allowed generation of sufficient data on impact for specified initial data of mass, velocity, stiffness and viscosity for training of the ANN. The results of tests proved to be excellent

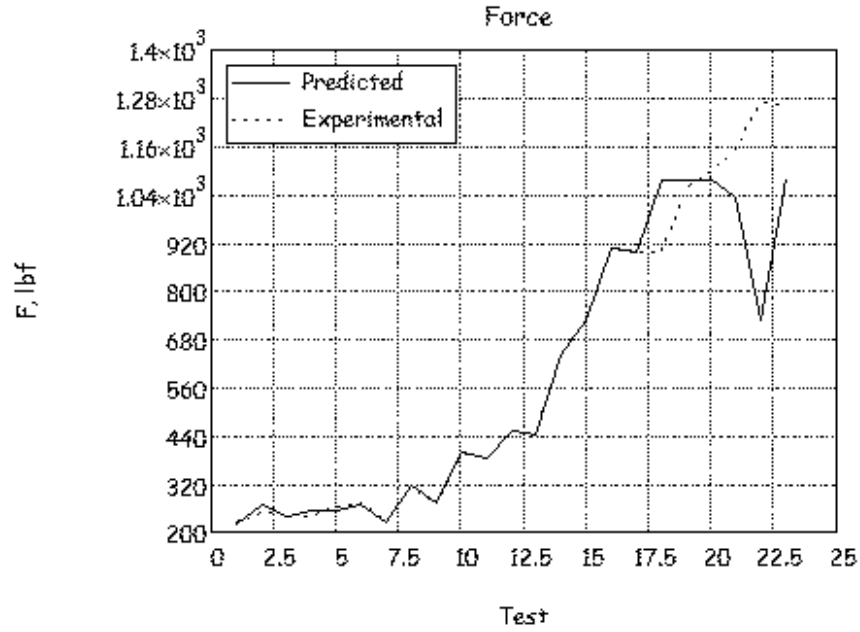


Figure 3.16: Comparison of results of ANN with experimental data for acceleration subject to low pass filter

for training data, however, comparison of ANN simulations versus experimental test data stimulated some further research.

On the one hand, performing sufficient number of real experiments for training of the ANN for a wide variety of parameters is rather expensive, whereas on the other hand use of simplified analytical models does not allow more precise mathematical modelling of train dynamics. Therefore, a more advanced mathematical model has been developed, taking into account viscous behavior of the draft gear. The results seem to be of both theoretical and practical interest.

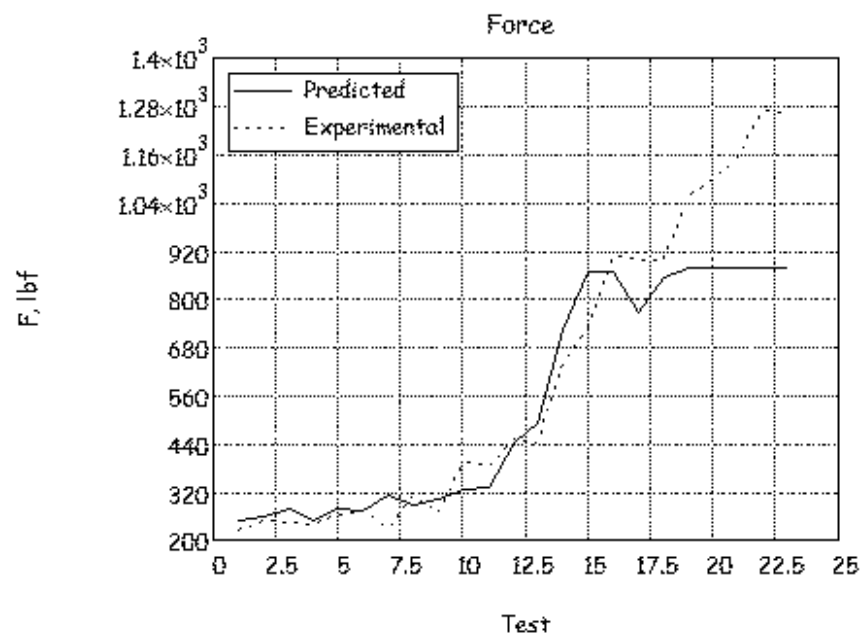


Figure 3.17: Comparison of results of ANN with experimental data for the case of spectrum acceleration input

# Chapter 4

## Low - frequency perturbation of rigid body motion of a viscoelastic inhomogeneous rod

In this Chapter we develop a new pseudo rigid body dynamic model based on the principles of the linear elastodynamic. Mathematical modeling of the effect of an internal microstructure allow to increase the level of accuracy and to extend the range of validity of the traditional equations of rigid body dynamics. We start by analysing low - frequency perturbations of rigid body motion of a viscoelastic inhomogeneous rod subject to edge loads.

### 4.1 Statement of the problem

Consider a viscoelastic inhomogeneous rod of length  $2l$  subject to end longitudinal forces, see Figure 4.1. The 1D equation of motion [111] is written as



Figure 4.1: Longitudinal vibration of the rod

$$F_x = m(x)u_{tt} \quad (4.1)$$

where  $x$  is the longitudinal coordinate,  $t$  is time,  $u$  is longitudinal displacement,  $F$  is longitudinal force, and  $m(x)$  is mass per unit length.

Linear viscoelastic behavior within the classical theory of extension can be described by the following integral relation, see, e.g. [101, 102]:

$$e(x, t) = \frac{1}{E(x)A(x)} \left( F(x, t) - \int_0^t K(\gamma(x)(t - t_1)) \frac{\partial F(x, t_1)}{\partial t_1} dt_1 \right) \quad (4.2)$$

where  $e = u_x$  is the longitudinal strain. We also use the notation:  $E(x)$  is the Young's modulus,  $A(x)$  is cross-sectional area,  $K(\gamma(x)t)$  is creep kernel depending on function  $\gamma(x)$ . For example, for the Voigt model

$$K(\gamma(x)t) = e^{-\gamma(x)t} \quad (4.3)$$

with  $\gamma(x) = \frac{E(x)}{\mu(x)}$ , where  $\mu(x)$  denotes viscosity. In this case the equation (4.2) can be rewritten in a differential form as

$$F(x, t) = A(x) [E(x)e(x, t) + \mu(x)e_t(x, t)] \quad (4.4)$$

The boundary conditions corresponding to the end forces shown in Figure 4.1 are

$$F(-l, t) = F_1(t), \quad F(l, t) = F_2(t) \quad (4.5)$$

Let us denote typical values of the variable quantities  $m(x)$ ,  $E(x)$ ,  $A(x)$  and  $\gamma(x)$  by  $m_0$ ,  $E_0$ ,  $A_0$  and  $\gamma_0$ , respectively. In what follows we assume that a typical time scale of viscous behavior  $\gamma_0^{-1}$  is much greater than a characteristic time that elastic waves take to propagate the distance between the ends of the rod, i.e.,

$$\gamma_0^{-1} \gg l \sqrt{\frac{m_0}{E_0 A_0}} \quad (4.6)$$

We also suppose that  $K(\gamma(x)t) \sim K(\gamma(\xi)\tau) \sim 1$ , i.e. viscous phenomena can not be neglected at leading order.

## 4.2 Asymptotic analysis

Consider the problem of (4.1) and (4.2) under the asymptotic assumption (4.6). We introduce dimensionless variables and dimensionless displacement and force by the formulae

$$x = \xi l \quad \text{and} \quad t = \tau \gamma_0^{-1} \quad (4.7)$$

and

$$u = l u_* \quad \text{and} \quad F = \varepsilon A_0 E_0 F_* \quad (4.8)$$

where

$$\varepsilon = \frac{l^2 \gamma_0^2 m_0}{E_0 A_0} \ll 1 \quad (4.9)$$

is a small parameter related to (4.6).

Then we get

$$F_{*\xi} = m_*(\xi)u_{*\tau\tau} \quad (4.10)$$

and

$$u_{*\xi} = \frac{\varepsilon}{E_*(\xi)A_*(\xi)} \left( F_* - \int_0^\tau K(\gamma_*(\xi)(\tau - \tau_1))F_{*\tau_1} d\tau_1 \right) \quad (4.11)$$

with

$$F_*(-1, \tau) = F_{1*}(t) \quad \text{and} \quad F_*(1, \tau) = F_{2*}(t) \quad (4.12)$$

where

$$A_*(\xi) = \frac{A(\xi)}{A_0}, \quad E_*(\xi) = \frac{E(\xi)}{E_0}, \quad m_*(\xi) = \frac{m(\xi)}{m_0} \quad \text{and} \quad \gamma_*(\xi) = \frac{\gamma(\xi)}{\gamma_0} \quad (4.13)$$

and

$$F_i = \varepsilon A_0 E_0 F_{i*}, \quad i = 1, 2 \quad (4.14)$$

Here and below we assume that the integral term in the right hand side of (4.11) is of order  $F_*$ .

We are looking for the solution of (4.10) - (4.12) in the form

$$u_* = u_0 + \varepsilon u_1 + \dots \quad \text{and} \quad F_* = f_0 + \varepsilon f_1 + \dots \quad (4.15)$$

At leading order

$$f_{0\xi} = m_*(\xi)u_{0\tau\tau} \quad \text{and} \quad u_{0\xi} = 0 \quad (4.16)$$

subject to the boundary conditions

$$f_0(-1, \tau) = F_{1*}(\tau) \quad \text{and} \quad f_0(1, \tau) = F_{2*}(\tau) \quad (4.17)$$

Immediately, we get from the second equation (4.16)

$$u_0(\xi, \tau) = v_0(\tau) \quad (4.18)$$

i.e. at leading order we observe horizontal rigid body motion. Next, we have from the first equation (4.16) taking into account the imposed boundary conditions (4.17)

$$v_{0\tau\tau} \int_{-1}^1 m_*(\xi) d\xi = F_{2*} - F_{1*} \quad (4.19)$$

At the same time

$$f_0 = v_{0\tau\tau} \int_{-1}^{\xi} m_*(\xi_1) d\xi_1 + F_{1*} \quad (4.20)$$

or

$$f_0 = \frac{(F_{2*} - F_{1*}) \int_{-1}^{\xi} m_*(\xi_1) d\xi_1}{\int_{-1}^1 m_*(\xi) d\xi} + F_{1*} \quad (4.21)$$

At next order

$$f_{1\xi} = m_*(\xi) u_{1\tau\tau} \quad \text{and} \quad u_{1\xi} = \frac{1}{E_*(\xi) A_*(\xi)} \left( f_0 - \int_0^{\tau} K(\gamma_*(\xi)(\tau - \tau_1)) f_{0\tau_1} d\tau_1 \right) \quad (4.22)$$

with the homogeneous boundary conditions  $f_1(\pm 1, \tau) = 0$ . By integrating the second

equation (4.22) we have

$$u_1 = \int_0^\xi \frac{1}{E_*(\xi_1)A_*(\xi_1)} \left( f_0(\xi_1, \tau) - \int_0^\tau K(\gamma_*(\xi_1)(\tau - \tau_1)) f_{0\tau_1}(\xi_1, \tau_1) d\tau_1 \right) d\xi_1 + v_1 \quad (4.23)$$

where  $v_1(\tau)$  is a low-frequency correction to the center displacement. The first derivative of (4.23) in the dimensionless time is

$$u_{1\tau} = \int_0^\xi \frac{1}{E_*(\xi_1)A_*(\xi_1)} \left( f_{0\tau}(\xi_1, \tau)(1 - K(0)) - \int_0^\tau K_\tau(\gamma_*(\xi_1)(\tau - \tau_1)) f_{0\tau_1}(\xi_1, \tau_1) d\tau_1 \right) d\xi_1 + v_{1\tau} \quad (4.24)$$

The second derivative of (4.23) is

$$u_{1\tau\tau} = \int_0^\xi \frac{1}{E_*(\xi_1)A_*(\xi_1)} \left( f_{0\tau\tau}(\xi_1, \tau)(1 - K(0)) - f_{0\tau}(\xi_1, \tau)K_\tau(0) - \int_0^\tau K_{\tau\tau}(\gamma_*(\xi_1)(\tau - \tau_1)) f_{0\tau_1}(\xi_1, \tau_1) d\tau_1 \right) d\xi_1 + v_{1\tau\tau} \quad (4.25)$$

We also get from the first equation (4.22) and the homogeneous boundary conditions above that

$$v_{1\tau\tau} = -\frac{1}{\int_{-1}^1 m_*(\xi) d\xi} \int_{-1}^1 m_*(\xi) \left[ \int_0^\xi \frac{1}{E_*(\xi_1)A_*(\xi_1)} \left( f_{0\tau\tau}(\xi_1, \tau)(1 - K(0)) - f_{0\tau}(\xi_1, \tau)K_\tau(0) - \int_0^\tau K_{\tau\tau}(\gamma_*(\xi_1)(\tau - \tau_1)) f_{0\tau_1}(\xi_1, \tau_1) d\tau_1 \right) d\xi_1 \right] d\xi \quad (4.26)$$

We obtain the acceleration of the rod  $u_{*\tau\tau} = u_{0\tau\tau} + \varepsilon u_{1\tau\tau} + \dots$

The acceleration of the left end of the rod

$$\begin{aligned}
u_{\tau\tau}|_{\xi=-1} &= \frac{F_{2*} - F_{1*}}{\int_{-1}^1 m_*(\xi) d\xi} - \varepsilon \left( \int_{-1}^0 \frac{1}{E_*(\xi)A_*(\xi)} \left( f_{0\tau\tau}(\xi, \tau)(1 - K(0)) - \right. \right. \\
& f_{0\tau}(\xi, \tau)K_\tau(0) - \int_0^\tau K_{\tau\tau}(\gamma_*(\xi)(\tau - \tau_1))f_{0\tau_1}(\xi, \tau_1)d\tau_1 \Big) d\xi + \frac{1}{\int_{-1}^1 m_*(\xi) d\xi} \times \\
& \left. \int_{-1}^1 m_*(\xi) \left[ \int_0^\xi \frac{1}{E_*(\xi_1)A_*(\xi_1)} \left( f_{0\tau\tau}(\xi_1, \tau)(1 - K(0)) - f_{0\tau}(\xi_1, \tau)K_\tau(0) - \right. \right. \right. \\
& \left. \left. \left. \int_0^\tau K_{\tau\tau}(\gamma_*(\xi_1)(\tau - \tau_1))f_{0\tau_1}(\xi_1, \tau_1)d\tau_1 \right) d\xi_1 \right] d\xi \right)
\end{aligned} \tag{4.27}$$

Similarly, the acceleration of the right end of the rod

$$\begin{aligned}
u_{\tau\tau}|_{\xi=1} &= \frac{F_{2*} - F_{1*}}{\int_{-1}^1 m_*(\xi) d\xi} + \varepsilon \left( \int_0^1 \frac{1}{E_*(\xi)A_*(\xi)} \left( f_{0\tau\tau}(\xi, \tau)(1 - K(0)) - \right. \right. \\
& f_{0\tau}(\xi, \tau)K_\tau(0) - \int_0^\tau K_{\tau\tau}(\gamma_*(\xi)(\tau - \tau_1))f_{0\tau_1}(\xi, \tau_1)d\tau_1 \Big) d\xi - \\
& \frac{1}{\int_{-1}^1 m_*(\xi) d\xi} \int_{-1}^1 m_*(\xi) \left[ \int_0^\xi \frac{1}{E_*(\xi_1)A_*(\xi_1)} \left( f_{0\tau\tau}(\xi_1, \tau)(1 - K(0)) - \right. \right. \\
& \left. \left. \left. f_{0\tau}(\xi_1, \tau)K_\tau(0) - \int_0^\tau K_{\tau\tau}(\gamma_*(\xi_1)(\tau - \tau_1))f_{0\tau_1}(\xi_1, \tau_1)d\tau_1 \right) d\xi_1 \right] d\xi \right)
\end{aligned} \tag{4.28}$$

Finally, we obtain for the acceleration of the center

$$\begin{aligned}
u_{\tau\tau}|_{\xi=0} &= \frac{F_{2*} - F_{1*}}{\int_{-1}^1 m_*(\xi) d\xi} - \varepsilon \frac{1}{\int_{-1}^1 m_*(\xi) d\xi} \int_{-1}^1 m_*(\xi) \left[ \int_0^\xi \frac{1}{E_*(\xi_1)A_*(\xi_1)} \times \right. \\
&\left. \left( f_{0\tau\tau}(\xi_1, \tau)(1 - K(0)) - f_{0\tau}(\xi_1, \tau)K_\tau(0) - \right. \right. \\
&\left. \left. \int_0^\tau K_{\tau\tau}(\gamma_*(\xi_1)(\tau - \tau_1)) f_{0\tau_1}(\xi_1, \tau_1) d\tau_1 \right) d\xi_1 \right] d\xi
\end{aligned} \tag{4.29}$$

or in the original variables

$$\begin{aligned}
Ma_h|_{x=-l} &= F_2 - F_1 - (1 - K(0)) \times \\
&\left[ M \int_{-l}^0 \frac{F_{0tt}(x, t)}{E(x)A(x)} dx + \int_{-l}^l m(x) \left( \int_0^x \frac{F_{0tt}(x_1, t)}{E(x_1)A(x_1)} dx_1 \right) dx \right] + \\
K_t(0) &\left[ M \int_{-l}^0 \frac{F_{0tt}(x, t)}{E(x)A(x)} dx + \int_{-l}^l m(x) \left( \int_0^x \frac{F_{0t}(x_1, t)}{E(x_1)A(x_1)} dx_1 \right) dx \right] + \\
M &\left[ \int_{-l}^0 \frac{1}{E(x_1)A(x_1)} \left( \int_0^t K_{tt}(\gamma(x_1)(t - t_1)) F_{0t_1}(x_1, t_1) dt_1 \right) dx_1 \right] + \\
&\int_{-l}^l m(x) \left[ \int_0^x \frac{1}{E(x_1)A(x_1)} \left( \int_0^t K_{tt}(\gamma(x_1)(t - t_1)) F_{0t_1}(x_1, t_1) dt_1 \right) dx_1 \right] dx
\end{aligned} \tag{4.30}$$

$$\begin{aligned}
Ma_h|_{x=l} &= F_2 - F_1 + (1 - K(0)) \times \\
&\left[ M \int_0^l \frac{F_{0tt}(x, t)}{E(x)A(x)} dx - \int_{-l}^l m(x) \left( \int_0^x \frac{F_{0tt}(x_1, t)}{E(x_1)A(x_1)} dx_1 \right) dx \right] - \\
K_t(0) &\left[ M \int_0^l \frac{F_{0tt}(x, t)}{E(x)A(x)} dx - \int_{-l}^l m(x) \left( \int_0^x \frac{F_{0t}(x_1, t)}{E(x_1)A(x_1)} dx_1 \right) dx \right] - \\
M &\left[ \int_0^l \frac{1}{E(x_1)A(x_1)} \left( \int_0^t K_{tt}(\gamma(x_1)(t - t_1)) F_{0t_1}(x_1, t_1) dt_1 \right) dx_1 \right] - \\
&\int_{-l}^l m(x) \left[ \int_0^x \frac{1}{E(x_1)A(x_1)} \left( \int_0^t K_{tt}(\gamma(x_1)(t - t_1)) F_{0t_1}(x_1, t_1) dt_1 \right) dx_1 \right] dx
\end{aligned} \tag{4.31}$$

$$\begin{aligned}
Ma_h|_{x=0} &= F_2 - F_1 - (1 - K(0)) \int_{-l}^l m(x) \left( \int_0^x \frac{F_{0tt}(x_1, t)}{E(x_1)A(x_1)} dx_1 \right) dx + \\
K_t(0) &\int_{-l}^l m(x) \left( \int_0^x \frac{F_{0t}(x_1, t)}{E(x_1)A(x_1)} dx_1 \right) dx + \\
&\int_{-l}^l m(x) \left[ \int_0^x \frac{1}{E(x_1)A(x_1)} \left( \int_0^t K_{tt}(\gamma(x_1)(t - t_1)) F_{0t_1}(x_1, t_1) dt_1 \right) dx_1 \right] dx
\end{aligned} \tag{4.32}$$

where  $a_h(t) = lv_{tt}(t)$  and  $M = \int_{-l}^l m(x) dx$  denote acceleration and mass respectively, and

$$F_0 = \frac{F_2 - F_1}{M} \int_{-l}^x m(x_1) dx_1 + F_1 \tag{4.33}$$

The derived formulae (4.30)-(4.32) contain in the right hand side a low-frequency correction to the classical equation of rigid body motion  $Ma_h = F_2 - F_1$ . The above mentioned correction incorporates the effect of viscoelasticity of an inhomogeneous rod and makes possible calculating dynamic responds caused by self-equilibrated loads, i.e.,  $F_1 = F_2$ . Obviously, a similar formulae can be established for any point of the structure ( $|x| \ll l$ ) starting from the equations in this section. The quantity (4.33) is crucial for the obtained correction. It corresponds to the low-frequency variation of

the longitudinal force along the length.

## 4.3 Particular cases

### 4.3.1 An inhomogeneous viscoelastic rod of uniform density

The equations (4.30)- (4.32) take a simpler form for a homogeneous viscoelastic rod

$$m(x) = m.$$

$$\begin{aligned}
Ma_h|_{x=-l} &= F_2 - F_1 - (1 - K(0)) \times \\
&\left[ l \int_{-l}^0 \frac{F_{0tt}(x, t)}{E(x)A(x)} dx + \int_{-l}^l \left( \int_0^x \frac{F_{0tt}(x_1, t)}{E(x_1)A(x_1)} dx_1 \right) dx \right] + \\
K_t(0) &\left[ l \int_{-l}^0 \frac{F_{0t}(x, t)}{E(x)A(x)} dx + m \int_{-l}^l \left( \int_0^x \frac{F_{0t}(x_1, t)}{E(x_1)A(x_1)} dx_1 \right) dx \right] + \\
l &\left[ \int_{-l}^0 \frac{1}{E(x_1)A(x_1)} \left( \int_0^t K_{tt}(\gamma(x_1)(t - t_1)) F_{0t_1}(x_1, t_1) dt_1 \right) dx_1 \right] + \\
&\int_{-l}^l \left[ \int_0^x \frac{1}{E(x_1)A(x_1)} \left( \int_0^t K_{tt}(\gamma(x_1)(t - t_1)) F_{0t_1}(x_1, t_1) dt_1 \right) dx_1 \right] dx
\end{aligned} \tag{4.34}$$

$$\begin{aligned}
Ma_h|_{x=l} &= F_2 - F_1 + (1 - K(0)) \times \\
&\left[ l \int_0^l \frac{F_{0tt}(x, t)}{E(x)A(x)} dx - \int_{-l}^l \left( \int_0^x \frac{F_{0tt}(x_1, t)}{E(x_1)A(x_1)} dx_1 \right) dx \right] - \\
K_t(0) &\left[ l \int_0^l \frac{F_{0t}(x, t)}{E(x)A(x)} dx - \int_{-l}^l \left( \int_0^x \frac{F_{0t}(x_1, t)}{E(x_1)A(x_1)} dx_1 \right) dx \right] - \\
&l \left[ \int_0^l \frac{1}{E(x_1)A(x_1)} \left( \int_0^t K_{tt}(\gamma(x_1)(t - t_1)) F_{0t_1}(x_1, t_1) dt_1 \right) dx_1 \right] - \\
&\int_{-l}^l \left[ \int_0^x \frac{1}{E(x_1)A(x_1)} \left( \int_0^t K_{tt}(\gamma(x_1)(t - t_1)) F_{0t_1}(x_1, t_1) dt_1 \right) dx_1 \right] dx
\end{aligned} \tag{4.35}$$

and

$$\begin{aligned}
Ma_h|_{x=0} &= F_2 - F_1 - (1 - K(0)) \int_{-l}^l \left( \int_0^x \frac{F_{0tt}(x_1, t)}{E(x_1)A(x_1)} dx_1 \right) dx + \\
K_t(0) &\int_{-l}^l \left( \int_0^x \frac{F_{0t}(x_1, t)}{E(x_1)A(x_1)} dx_1 \right) dx + \\
&\int_{-l}^l \left[ \int_0^x \frac{1}{E(x_1)A(x_1)} \left( \int_0^t K_{tt}(\gamma(x_1)(t - t_1)) F_{0t_1}(x_1, t_1) dt_1 \right) dx_1 \right] dx
\end{aligned} \tag{4.36}$$

where  $a_h(t) = lv_{tt}(t)$  denote acceleration and  $F_0 = \frac{1}{2l} (x(F_2 - F_1) + l(F_2 + F_1))$ .

### 4.3.2 An inhomogeneous viscoelastic rod of uniform stiffness

In the case of an inhomogeneous rod of uniform stiffness the equations (4.30)- (4.32) take the form:

$$\begin{aligned}
Ma_h|_{x=-l} = & F_2 - F_1 - \frac{1}{EA} [(1 - K(0)) \times \\
& \left( M \int_{-l}^0 F_{0tt}(x, t) dx + \int_{-l}^l m(x) \int_0^x F_{0tt}(x_1, t) dx_1 dx \right) + \\
& K_t(0) \left( M \int_{-l}^0 F_{0tt}(x, t) dx + \int_{-l}^l m(x) \int_0^x F_{0t}(x_1, t) dx_1 dx \right) + \\
& M \int_{-l}^0 \int_0^t K_{tt}(\gamma(x_1)(t - t_1)) F_{0t_1}(x_1, t_1) dt_1 dx_1 \left. + \right. \\
& \left. \int_{-l}^l m(x) \int_0^x \int_0^t K_{tt}(\gamma(x_1)(t - t_1)) F_{0t_1}(x_1, t_1) dt_1 dx_1 dx \right]
\end{aligned} \tag{4.37}$$

$$\begin{aligned}
Ma_h|_{x=l} = & F_2 - F_1 + \frac{1}{EA} [(1 - K(0)) \times \\
& \left( M \int_0^l F_{0tt}(x, t) dx - \int_{-l}^l m(x) \int_0^x F_{0tt}(x_1, t) dx_1 dx \right) - \\
& K_t(0) \left( M \int_0^l F_{0tt}(x, t) dx - \int_{-l}^l m(x) \int_0^x F_{0t}(x_1, t) dx_1 dx \right) - \\
& M \int_0^l \int_0^t K_{tt}(\gamma(x_1)(t - t_1)) F_{0t_1}(x_1, t_1) dt_1 dx_1 \left. - \right. \\
& \left. \int_{-l}^l m(x) \int_0^x \int_0^t K_{tt}(\gamma(x_1)(t - t_1)) F_{0t_1}(x_1, t_1) dt_1 dx_1 dx \right]
\end{aligned} \tag{4.38}$$

and

$$\begin{aligned}
Ma_h|_{x=0} = F_2 - F_1 - \frac{1}{EA} & \left[ (1 - K(0)) \int_{-l}^l m(x) \int_0^x F_{0tt}(x_1, t) dx_1 dx + \right. \\
K_t(0) \int_{-l}^l m(x) \int_0^x & F_{0t}(x_1, t) dx_1 dx + \\
\left. \int_{-l}^l m(x) \int_0^x \int_0^t & K_{tt}(\gamma(x_1)(t - t_1)) F_{0t_1}(x_1, t_1) dt_1 dx_1 dx \right] \quad (4.39)
\end{aligned}$$

where acceleration and mass are  $a_h(t) = lv_{tt}(t)$  and  $M = \int_{-l}^l m(x) dx$  and  $F_0$  is in the form (4.33)

### 4.3.3 A homogeneous viscoelastic rod

And finally, the derived equations (4.30)- (4.32) take a simpler form for perturbed rigid body motion of a homogeneous viscoelastic rod of uniform stiffness, density and viscosity. In this case  $m(x) = m, E(x) = E, A(x) = A$  and  $\gamma(x) = \gamma$  with the quantity  $F_0$  in the form (4.28). For the center of the rod, we get respectively

$$Ma_h|_{x=0} = F_2 - F_1 - \frac{ml^2}{6EA} \left( \dot{F}_{0tt}(1 - K(0)) + \dot{F}_{0t}K_t(0) + \int_0^t K_{tt}(\gamma(t - t_1)) \dot{F}_{0t_1} dt_1 \right) \quad (4.40)$$

and for the left end of the rod

$$Ma_h|_{x=-l} = F_2 - F_1 - \frac{ml^2}{6EA} \left( \dot{F}_{0tt}^{(l)}(1 - K(0)) + \dot{F}_{0t}^{(l)}K_t(0) + \int_0^t K_{tt}(\gamma(t - t_1)) \dot{F}_{0t_1}^{(l)} dt_1 \right) \quad (4.41)$$

finally, for the right end of the rod

$$Ma_h|_{x=1} = F_2 - F_1 + \frac{ml^2}{6EA} \left( \dot{F}_{0tt}^{(r)} (1 - K(0)) - \dot{F}_{0t}^{(r)} K_t(0) - \int_0^t K_{tt}(\gamma(t-t_1)) \dot{F}_{0t_1}^{(r)} dt_1 \right) \quad (4.42)$$

where  $M = 2ml$ ,  $\dot{F}_0^{(l)} = 7F_2 + 11F_1$ ,  $\dot{F}_0^{(r)} = 5F_2 + F_1$  and  $\dot{F}_0 = F_2 - F_1$ .

#### 4.3.4 An inhomogeneous Voigt rod

Consider the problem of (4.1) and (4.2) under the asymptotic assumption (4.6) for an inhomogeneous viscoelastic Voigt rod. The creep kernel is in the form (4.3)

$$K(\gamma(x)t) = e^{-\frac{E(x)}{\mu(x)}t} \quad (4.43)$$

The Volterra equation in a differential form is in a form of

$$F(x, t) = A(x) [E(x)u_x(x, t) + \mu(x)u_{xt}(x, t)] \quad (4.44)$$

The boundary conditions (4.5) are

$$F(-l, t) = F_1(t), \quad F(l, t) = F_2(t)$$

After substituting dimensionless variables and dimensionless displacement (4.7) and (4.8) with a small parameter  $\varepsilon$  in the form (4.9), we get

$$F_{*\xi} = m_*(\xi)u_{*\tau\tau} \quad (4.45)$$

and

$$\varepsilon F_* = A_*(\xi) [E_*(\xi)u_{*\xi} + \beta\mu_*(\xi)u_{*\xi\tau}] \quad (4.46)$$

with boundary conditions in the form (4.12)

$$F_*(-1, \tau) = F_{1*}(t) \quad \text{and} \quad F_*(1, \tau) = F_{2*}(t)$$

where  $A_*(\xi)$ ,  $E_*(\xi)$ ,  $m_*(\xi)$  are represented in (4.13),  $F_i$ ,  $i = 1, 2$  is in (4.14) and

$$\mu_*(\xi) = \frac{\mu(\xi)}{\mu_0} \quad (4.47)$$

We are looking for the solution of (4.45), (4.46) and (4.12) in the form (4.15)

$$u_* = u_0 + \varepsilon u_1 + \dots \quad \text{and} \quad F_* = f_0 + \varepsilon f_1 + \dots$$

At leading order

$$f_{0\xi} = m_*(\xi)u_{0\tau\tau} \quad \text{and} \quad E_*(\xi)u_{*\xi} + \beta\mu_*(\xi)u_{*\xi\tau} = 0 \quad (4.48)$$

subject to the boundary conditions

$$f_0(-1, \tau) = F_{1*}(\tau) \quad \text{and} \quad f_0(1, \tau) = F_{2*}(\tau) \quad (4.49)$$

We get from the second equation (4.48)

$$u_0(\xi, \tau) = v_0(\tau) \quad (4.50)$$

Next, we have from the first equation (4.48) taking into account the imposed boundary conditions (4.49)

$$v_{0\tau\tau} \int_{-1}^1 m_*(\xi) d\xi = F_{2*} - F_{1*} \quad (4.51)$$

At the same time

$$f_0 = v_{0\tau\tau} \int_{-1}^{\xi} m_*(\xi_1) d\xi_1 + F_{1*} \quad (4.52)$$

or

$$f_0 = \frac{(F_{2*} - F_{1*}) \int_{-1}^{\xi} m_*(\xi_1) d\xi_1}{\int_{-1}^1 m_*(\xi) d\xi} + F_{1*} \quad (4.53)$$

At next order

$$f_{1\xi} = m_*(\xi) u_{1\tau\tau} \quad \text{and} \quad f_0 = A_*(\xi) [E_*(\xi) u_{1\xi} + \beta \mu_*(\xi) u_{1\xi\tau}] \quad (4.54)$$

with the homogeneous boundary conditions  $f_1(\pm 1, \tau) = 0$ .

We are looking for the solution of the first equation (4.54) in the form:

$$u_{1\xi} = C(\xi, \tau) e^{-\frac{\tau E_*(\xi)}{\mu_*(\xi)\beta}} \quad (4.55)$$

then

$$u_{1\xi\tau} = C_\tau(\tau, \xi) e^{-\frac{\tau E_*(\xi)}{\mu_*(\xi)\beta}} - \frac{E_*(\xi)}{\mu_*(\xi)\beta} C(\tau, \xi) e^{-\frac{\tau E_*(\xi)}{\mu_*(\xi)\beta}} \quad (4.56)$$

after substituting (4.55) and (4.56) into second equation (4.54), we get

$$f_0 = \beta \mu_*(\xi) A_*(\xi) C_\tau(\tau, \xi) e^{-\frac{\tau E_*(\xi)}{\mu_*(\xi)\beta}} \quad (4.57)$$

then

$$C_\tau(\tau, \xi) = \frac{1}{\beta \mu_*(\xi) A_*(\xi)} f_0 e^{\frac{\tau E_*(\xi)}{\mu_*(\xi) \beta}} \quad (4.58)$$

and

$$C(\tau, \xi) = \frac{1}{\beta \mu_*(\xi) A_*(\xi)} \int_0^\tau f_0 e^{\frac{\tau_1 E_*(\xi)}{\mu_*(\xi) \beta}} d\tau_1 \quad (4.59)$$

thus

$$u_{1\xi} = \frac{1}{\beta \mu_*(\xi) A_*(\xi)} \int_0^\tau f_0 e^{-\frac{E_*(\xi)}{\mu_*(\xi) \beta}(\tau-\tau_1)} d\tau_1 \quad (4.60)$$

finally,

$$u_1 = \frac{1}{\beta} \int_0^\xi \frac{1}{\mu_*(\xi_1) A_*(\xi_1)} \int_0^\tau f_0(\xi_1, \tau_1) e^{-\frac{E_*(\xi_1)}{\mu_*(\xi_1) \beta}(\tau-\tau_1)} d\tau_1 d\xi_1 + v_1 \quad (4.61)$$

The first derivative of (4.61) in the dimensionless time is

$$u_{1\tau} = \frac{1}{\beta} \int_0^\xi \frac{1}{\mu(\xi_1) A_*(\xi_1)} \left( f_0(\xi_1, \tau) - \frac{E_*(\xi_1)}{\mu_*(\xi_1) \beta} \int_0^\tau f_0(\xi_1, \tau_1) e^{-\frac{E_*(\xi_1)}{\mu_*(\xi_1) \beta}(\tau-\tau_1)} d\tau_1 \right) d\xi_1 + v_{1\tau} \quad (4.62)$$

$$u_{1\tau\tau} = \frac{1}{\beta} \int_0^\xi \frac{1}{\mu(\xi_1) A_*(\xi_1)} \left( f_{0\tau_1}(\xi_1, \tau) - \frac{E_*(\xi_1)}{\mu_*(\xi_1) \beta} f_0(\xi_1, \tau) + \frac{E_*^2(\xi_1)}{\mu_*^2(\xi_1) \beta^2} \times \int_0^\tau f_0(\xi_1, \tau_1) e^{-\frac{E_*(\xi_1)}{\mu_*(\xi_1) \beta}(\tau-\tau_1)} d\tau_1 \right) d\xi_1 + v_{1\tau\tau} \quad (4.63)$$

from the first equation (4.54) we get

$$f_1 = \int_{-1}^\xi \frac{m_*(\xi_1)}{\beta} \int_0^{\xi_1} \frac{1}{\mu(\xi_2) A_*(\xi_2)} \left( f_{0\tau_1}(\xi_2, \tau) - \frac{E_*(\xi_2)}{\mu_*(\xi_2) \beta} f_0(\xi_2, \tau) + \frac{E_*^2(\xi_2)}{\mu_*^2(\xi_2) \beta^2} \times \int_0^\tau f_0(\xi_2, \tau_1) e^{-\frac{E_*(\xi_2)}{\mu_*(\xi_2) \beta}(\tau-\tau_1)} d\tau_1 \right) d\xi_2 d\xi_1 + \int_{-1}^\xi m_*(\xi_1) v_{1\tau\tau} d\xi_1 \quad (4.64)$$

we get after using homogeneous boundary conditions

$$\begin{aligned}
v_{1\tau\tau} = & -\frac{1}{\int_{-1}^1 m_*(\xi_1) d\xi_{1-1}} \int_{-1}^1 \frac{m_*(\xi)}{\beta} \int_0^\xi \frac{1}{\mu(\xi_1) A_*(\xi_1)} (f_{0\tau_1}(\xi_1, \tau) - \\
& \left. \frac{E_*(\xi_1)}{\mu_*(\xi_1)\beta} f_0(\xi_1, \tau) + \frac{E_*^2(\xi_1)}{\mu_*^2(\xi_1)\beta^2} \int_0^\tau f_0(\xi_1, \tau_1) e^{-\frac{E_*(\xi_1)}{\mu_*(\xi_1)\beta}(\tau-\tau_1)} d\tau_1 \right) d\xi_1 d\xi
\end{aligned} \tag{4.65}$$

We obtain the acceleration of the rod  $u_{*\tau\tau} = u_{0\tau\tau} + \varepsilon u_{1\tau\tau} + \dots$

The acceleration of the left end of the rod

$$\begin{aligned}
u_{\tau\tau}|_{\xi=-1} = & \frac{F_{2*} - F_{1*}}{\int_{-1}^1 m_*(\xi) d\xi} - \frac{\varepsilon}{\beta} \left[ \int_{-1}^0 \frac{1}{\mu(\xi_1) A_*(\xi_1)} (f_{0\tau_1}(\xi_1, \tau) - \right. \\
& \left. \frac{E_*(\xi_1)}{\mu_*(\xi_1)\beta} f_0(\xi_1, \tau) + \frac{E_*^2(\xi_1)}{\mu_*^2(\xi_1)\beta^2} \int_0^\tau f_0(\xi_1, \tau_1) e^{-\frac{E_*(\xi_1)}{\mu_*(\xi_1)\beta}(\tau-\tau_1)} d\tau_1 \right) d\xi_1 + \\
& \frac{1}{\int_{-1}^1 m_*(\xi_1) d\xi_{1-1}} \int_{-1}^1 m_*(\xi) \int_0^\xi \frac{1}{\mu(\xi_1) A_*(\xi_1)} (f_{0\tau_1}(\xi_1, \tau) - \\
& \left. \frac{E_*(\xi_1)}{\mu_*(\xi_1)\beta} f_0(\xi_1, \tau) + \frac{E_*^2(\xi_1)}{\mu_*^2(\xi_1)\beta^2} \int_0^\tau f_0(\xi_1, \tau_1) e^{-\frac{E_*(\xi_1)}{\mu_*(\xi_1)\beta}(\tau-\tau_1)} d\tau_1 \right) d\xi_1 d\xi \Big]
\end{aligned} \tag{4.66}$$

Similarly, the acceleration of the right end of the rod

$$\begin{aligned}
u_{\tau\tau}|_{\xi=1} = & \frac{F_{2*} - F_{1*}}{\int_{-1}^1 m_*(\xi) d\xi} + \frac{\varepsilon}{\beta} \left[ \int_0^1 \frac{1}{\mu(\xi_1)A_*(\xi_1)} (f_{0\tau_1}(\xi_1, \tau) - \right. \\
& \left. \frac{E_*(\xi_1)}{\mu_*(\xi_1)\beta} f_0(\xi_1, \tau) + \frac{E_*^2(\xi_1)}{\mu_*^2(\xi_1)\beta^2} \int_0^\tau f_0(\xi_1, \tau_1) e^{-\frac{E_*(\xi_1)}{\mu_*(\xi_1)\beta}(\tau-\tau_1)} d\tau_1 \right) d\xi_1 - \\
& \frac{1}{\int_{-1}^1 m_*(\xi_1) d\xi_1} \int_{-1}^1 m_*(\xi) \int_0^\xi \frac{1}{\mu(\xi_1)A_*(\xi_1)} (f_{0\tau_1}(\xi_1, \tau) - \\
& \left. \frac{E_*(\xi_1)}{\mu_*(\xi_1)\beta} f_0(\xi_1, \tau) + \frac{E_*^2(\xi_1)}{\mu_*^2(\xi_1)\beta^2} \int_0^\tau f_0(\xi_1, \tau_1) e^{-\frac{E_*(\xi_1)}{\mu_*(\xi_1)\beta}(\tau-\tau_1)} d\tau_1 \right) d\xi_1 d\xi \Big]
\end{aligned} \tag{4.67}$$

Finally, we obtain for the acceleration of the center

$$\begin{aligned}
u_{\tau\tau}|_{\xi=0} = & \frac{F_{2*} - F_{1*}}{\int_{-1}^1 m_*(\xi) d\xi} - \frac{\varepsilon}{\beta} \frac{1}{\int_{-1}^1 m_*(\xi_1) d\xi_1} \int_{-1}^1 m_*(\xi) \int_0^\xi \frac{1}{\mu(\xi_1)A_*(\xi_1)} \left( f_{0\tau_1}(\xi_1, \tau) - \right. \\
& \left. \frac{E_*(\xi_1)}{\mu_*(\xi_1)\beta} f_0(\xi_1, \tau) + \frac{E_*^2(\xi_1)}{\mu_*^2(\xi_1)\beta^2} \int_0^\tau f_0(\xi_1, \tau_1) e^{-\frac{E_*(\xi_1)}{\mu_*(\xi_1)\beta}(\tau-\tau_1)} d\tau_1 \right) d\xi_1 d\xi
\end{aligned} \tag{4.68}$$

or in the original variables

$$\begin{aligned}
Mah|_{x=-l} = & F_2 - F_1 - M \int_{-l}^0 \frac{1}{\mu(x)A(x)} \left( F_{0t}(x, t) - \frac{E(x)}{\mu(x)} F_0(x_1, t) + \right. \\
& \left. \frac{E^2(x)}{\mu^2(x)} \int_0^t f_0(x_1, t_1) e^{-\frac{E(x_1)}{\mu(x_1)}(t-t_1)} dt_1 \right) dx_1 - \\
& \int_{-l}^l m(x) \int_0^x \frac{1}{\mu(x_1)A(x_1)} \left( F_{0t_1}(x_1, t) - \frac{E(x_1)}{\mu(x_1)} F_0(x_1, t) + \right. \\
& \left. \frac{E^2(x_1)}{\mu^2(x_1)} \int_0^t F_0(x_1, t_1) e^{-\frac{E(x_1)}{\mu(x_1)}(t-t_1)} dt_1 \right) dx_1 dx
\end{aligned} \tag{4.69}$$

$$\begin{aligned}
Ma_h|_{x=l} &= F_2 - F_1 + M \int_{-l}^0 \frac{1}{\mu(x)A(x)} \left( F_{0t}(x, t) - \frac{E(x)}{\mu(x)} F_0(x_1, t) + \right. \\
&\quad \left. \frac{E^2(x)}{\mu^2(x)} \int_0^t f_0(x_1, t_1) e^{-\frac{E(x_1)}{\mu(x_1)}(t-t_1)} dt_1 \right) dx_1 - \\
&\quad \int_{-l}^l m(x) \int_0^x \frac{1}{\mu(x_1)A(x_1)} \left( F_{0t_1}(x_1, t) - \frac{E(x_1)}{\mu(x_1)} F_0(x_1, t) + \right. \\
&\quad \left. \frac{E^2(x_1)}{\mu^2(x_1)} \int_0^t F_0(x_1, t_1) e^{-\frac{E(x_1)}{\mu(x_1)}(t-t_1)} dt_1 \right) dx_1 dx
\end{aligned} \tag{4.70}$$

and

$$\begin{aligned}
Ma_h|_{x=0} &= F_2 - F_1 - \int_{-l}^l m(x) \int_0^x \frac{1}{\mu(x_1)A(x_1)} (F_{0t_1}(x_1, t) - \\
&\quad \frac{E(x_1)}{\mu(x_1)} F_0(x_1, t) + \frac{E^2(x_1)}{\mu^2(x_1)} \int_0^t F_0(x_1, t_1) e^{-\frac{E(x_1)}{\mu(x_1)}(t-t_1)} dt_1) dx_1 dx \Big]
\end{aligned} \tag{4.71}$$

The results (4.69)-(4.71) can be get from the equation (4.29)-(4.31) by substituting the creep kernel in the form (4.3)

$$\begin{aligned}
Ma_h|_{x=-l} &= F_2 - F_1 - \frac{E(x)}{\mu(x)} \left( M \int_{-l}^0 \frac{F_{0t}(x, t)}{E(x)A(x)} dx + \int_{-l}^l m(x) \int_0^x \frac{F_{0t}(x_1, t)}{E(x_1)A(x_1)} dx_1 dx \right) + \\
&\quad M \int_{-l}^0 \frac{E(x)}{A(x)\mu^2(x)} \int_0^t e^{-\frac{E(x)}{\mu(x)}(t-t_1)} F_{0t_1}(x, t_1) dt_1 dx + \\
&\quad \int_{-l}^l m(x) \int_0^x \frac{E(x_1)}{A(x_1)\mu^2(x_1)} \int_0^t e^{-\frac{E(x_1)}{\mu(x_1)}(t-t_1)} F_{0t_1} dt_1 dx_1 dx
\end{aligned} \tag{4.72}$$

$$\begin{aligned}
Ma_h|_{x=l} &= F_2 - F_1 + \frac{E(x)}{\mu(x)} \left( M \int_{-l}^0 \frac{F_{0t}(x, t)}{E(x)A(x)} dx - \int_{-l}^l m(x) \int_0^x \frac{F_{0t}(x_1, t)}{E(x_1)A(x_1)} dx_1 dx \right) - \\
&\quad M \int_{-l}^0 \frac{E(x)}{A(x)\mu^2(x)} \int_0^t e^{-\frac{E(x)}{\mu(x)}(t-t_1)} F_{0t_1}(x, t_1) dt_1 dx - \\
&\quad \int_{-l}^l m(x) \int_0^x \frac{E(x_1)}{A(x_1)\mu^2(x_1)} \int_0^t e^{-\frac{E(x_1)}{\mu(x_1)}(t-t_1)} F_{0t_1} dt_1 dx_1 dx
\end{aligned} \tag{4.73}$$

and

$$\begin{aligned}
Ma_h|_{x=0} &= F_2 - F_1 - \frac{E(x)}{\mu(x)} \int_{-l}^l m(x) \int_0^x \frac{F_{0t}(x_1, t)}{E(x_1)A(x_1)} dx_1 dx + \\
&\int_{-l}^l m(x) \int_0^x \frac{E(x_1)}{A(x_1)\mu^2(x_1)} \int_0^t e^{-\frac{E(x_1)}{\mu(x_1)}(t-t_1)} F_{ot_1} dt_1 dx_1 dx
\end{aligned} \tag{4.74}$$

### Uniform density

The equation (4.72) - (4.74) in the case of uniform density take the following form

$$\begin{aligned}
Ma_h|_{x=-l} &= F_2 - F_1 - \frac{E(x)}{\mu(x)} \left( M \int_{-l}^0 \frac{F_{0t}(x, t)}{E(x)A(x)} dx + m \int_{-l}^l \int_0^x \frac{F_{0t}(x_1, t)}{E(x_1)A(x_1)} dx_1 dx \right) + \\
2ml \int_{-l}^0 \frac{E(x)}{A(x)\mu^2(x)} \int_0^t e^{-\frac{E(x)}{\mu(x)}(t-t_1)} F_{ot_1}(x, t_1) dt_1 dx + \\
m \int_{-l}^l \int_0^x \frac{E(x_1)}{A(x_1)\mu^2(x_1)} \int_0^t e^{-\frac{E(x_1)}{\mu(x_1)}(t-t_1)} F_{ot_1} dt_1 dx_1 dx
\end{aligned} \tag{4.75}$$

$$\begin{aligned}
Ma_h|_{x=l} &= F_2 - F_1 + \frac{E(x)}{\mu(x)} \left( M \int_{-l}^0 \frac{F_{0t}(x, t)}{E(x)A(x)} dx - m \int_{-l}^l \int_0^x \frac{F_{0t}(x_1, t)}{E(x_1)A(x_1)} dx_1 dx \right) - \\
2ml \int_{-l}^0 \frac{E(x)}{A(x)\mu^2(x)} \int_0^t e^{-\frac{E(x)}{\mu(x)}(t-t_1)} F_{ot_1}(x, t_1) dt_1 dx - \\
m \int_{-l}^l \int_0^x \frac{E(x_1)}{A(x_1)\mu^2(x_1)} \int_0^t e^{-\frac{E(x_1)}{\mu(x_1)}(t-t_1)} F_{ot_1} dt_1 dx_1 dx
\end{aligned} \tag{4.76}$$

and

$$\begin{aligned}
Ma_h|_{x=0} &= F_2 - F_1 - \frac{E(x)m}{\mu(x)} \int_{-l}^l \int_0^x \frac{F_{0t}(x_1, t)}{E(x_1)A(x_1)} dx_1 dx + \\
m \int_{-l}^l \int_0^x \frac{E(x_1)}{A(x_1)\mu^2(x_1)} \int_0^t e^{-\frac{E(x_1)}{\mu(x_1)}(t-t_1)} F_{ot_1} dt_1 dx_1 dx
\end{aligned} \tag{4.77}$$

### Uniform stiffness and viscosity

$$\begin{aligned}
 Ma_h|_{x=-l} &= F_2 - F_1 - \frac{1}{\mu A} \left( M \int_{-l}^0 F_{0t}(x, t) dx + \frac{1}{EA} \int_{-l}^l m(x) \int_0^x F_{0t}(x_1, t) dx_1 dx \right) + \\
 & \frac{M}{EA} \int_{-l}^0 \int_0^t e^{-\frac{E}{\mu}(t-t_1)} F_{ot_1}(x, t_1) dt_1 dx + \frac{E}{A\mu^2} \int_{-l}^l m(x) \int_0^x \int_0^t e^{-\frac{E}{\mu}(t-t_1)} F_{ot_1} dt_1 dx_1 dx
 \end{aligned} \tag{4.78}$$

$$\begin{aligned}
 Ma_h|_{x=l} &= F_2 - F_1 + \frac{1}{\mu A} \left( M \int_{-l}^0 F_{0t}(x, t) dx - \frac{F_{0t}(x_1, t)}{E(x_1)A(x_1)} \int_{-l}^l m(x) \int_0^x \frac{1}{EA} dx_1 dx \right) - \\
 & \frac{ME}{A\mu^2} \int_{-l}^0 \int_0^t e^{-\frac{E}{\mu}(t-t_1)} F_{ot_1}(x, t_1) dt_1 dx - \frac{E}{A\mu^2} \int_{-l}^l m(x) \int_0^x \int_0^t e^{-\frac{E}{\mu}(t-t_1)} F_{ot_1} dt_1 dx_1 dx
 \end{aligned} \tag{4.79}$$

and

$$\begin{aligned}
 Ma_h|_{x=0} &= F_2 - F_1 - \frac{1}{\mu A} \int_{-l}^l m(x) \int_0^x F_{0t}(x_1, t) dx_1 dx + \\
 & \frac{E}{A\mu^2} \int_{-l}^l m(x) \int_0^x \int_0^t e^{-\frac{E}{\mu}(t-t_1)} F_{ot_1} dt_1 dx_1 dx
 \end{aligned} \tag{4.80}$$

where  $F_0$  is in the form of (4.33).

As an illustration, we specify these formulae for a Voigt rod with linear density function  $m(x) = ax + b$ , where  $a, b$  are given constant. It become

$$\begin{aligned}
 Ma_h|_{x=0} &= F_2 - F_1 - \frac{l^2(a^2l^2 + 5abl + 5b^2)}{15(2b + al)} \frac{1}{A\mu} \left( F_{2t} - F_{1t} + \right. \\
 & \left. \frac{E}{\mu} \int_0^t e^{-\frac{E}{\mu}t_1} (F_{2t_1} - F_{1t_1}) dt_1 \right) - \frac{l^2(2al + 3b)}{6} \frac{1}{A\mu} \left( F_{2t} + \frac{E}{\mu} \int_0^t e^{-\frac{E}{\mu}t_1} F_{2t_1} dt_1 \right)
 \end{aligned} \tag{4.81}$$

### Uniform density, stiffness and viscosity

Finally, we write down an easy to use formulae for a homogeneous Voigt rod with uniform density, stiffness and viscosity  $m(x) = m, A(x) = A, E(x) = E$  and  $\mu(x) = \mu$ .

The acceleration for the center of the rod

$$Ma_h|_{x=0} = F_1 - F_2 + \frac{ml^2}{6A\mu} (F_{2t} - F_{1t}) - \frac{ml^2 E}{6A\mu^2} \int_0^t e^{-\frac{E}{\mu}(t-t_1)} (F_{2t_1} - F_{1t_1}) dt_1 \quad (4.82)$$

and for the left end of the rod

$$Ma_h|_{x=l} = F_1 - F_2 + \frac{ml^2}{6A\mu} (7F_{2t} + 11F_{1t}) - \frac{ml^2 E}{6A\mu^2} \int_0^t e^{-\frac{E}{\mu}(t-t_1)} (7F_{2t_1} + 11F_{1t_1}) dt_1 \quad (4.83)$$

finally, for the right end of the rod

$$Ma_h|_{x=l} = F_1 - F_2 + \frac{ml^2}{6A\mu} (5F_{2t} + F_{1t}) - \frac{ml^2 E}{6A\mu^2} \int_0^t e^{-\frac{E}{\mu}(t-t_1)} (5F_{2t_1} + F_{1t_1}) dt_1 \quad (4.84)$$

## 4.4 Numerical Results

### 4.4.1 A homogeneous Voigt rod

As an example, consider time-harmonic motion of a homogeneous viscoelastic rod studied in the previous section. In this case the constitutive relation (4.2) become

$$e = \frac{F}{EA} (1 + i\delta) \quad (4.85)$$

with

$$\delta = \int_0^\infty K \left( \frac{\gamma}{\omega} z \right) e^{iz} dz \quad (4.86)$$

where  $\omega$  is circular frequency. Here and below the factor  $e^{-i\omega t}$  is separated.

Let first horizontal motion of the bar be induced by a force applied to its right end, i.e.  $F(-l) = 0$  and  $F(l) = F_2$ , see Figure 4.1. Then, we get from the equation

(4.32)

$$Ma_h = F_2 \left[ 1 + \frac{\lambda_h^2}{6} (1 + i\delta) \right] \quad (4.87)$$

where

$$\lambda_h = \omega l \sqrt{\frac{m}{EA}} \quad (4.88)$$

This formula coincides with a two-term low-frequency expansion of the exact solution of the associated problem, see (A.10).

It is worth mentioning that in line with the dynamic homogenisation procedure developed for three-dimensional anisotropic elastic solids [14], this result can be presented in the form of a generalised Newton's second law with a frequency dependent complex mass given by

$$M_*(\lambda_h) = \frac{M}{1 + \frac{\lambda_h^2}{6} (1 + i\delta)} \quad (4.89)$$

Numerical data are presented in Figures 4.2 and 4.3 , where  $a_h^* = Ma/F_2$  is the normalised acceleration of the center of the rod plotted versus the dimensionless frequency  $\lambda_h$ . A Voigt material is studied. In this case

$$\delta = \frac{\lambda_h \beta}{1 - i\lambda_h \beta} \quad (4.90)$$

with

$$\beta = \frac{\mu}{l} \sqrt{\frac{A}{mE}}$$

The solid and dashed lines correspond to the exact solution, see A.1, and the asymptotic formulae (4.43), respectively. The curves related to the values  $\beta = 0.1, 1.0, 5.0$  are marked with the numbers 1, 2 and 3. Numerical comparison presented in these figures demonstrates the advantage of the developed methodology.

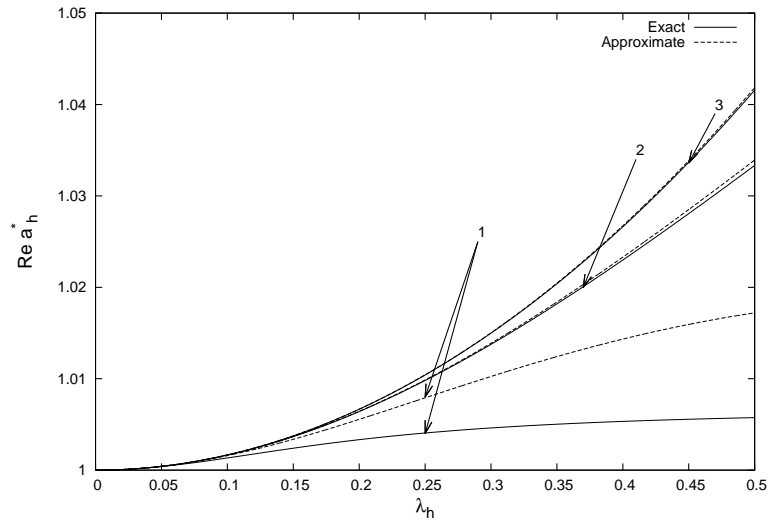


Figure 4.2: horizontal acceleration vs frequency (Real Part)

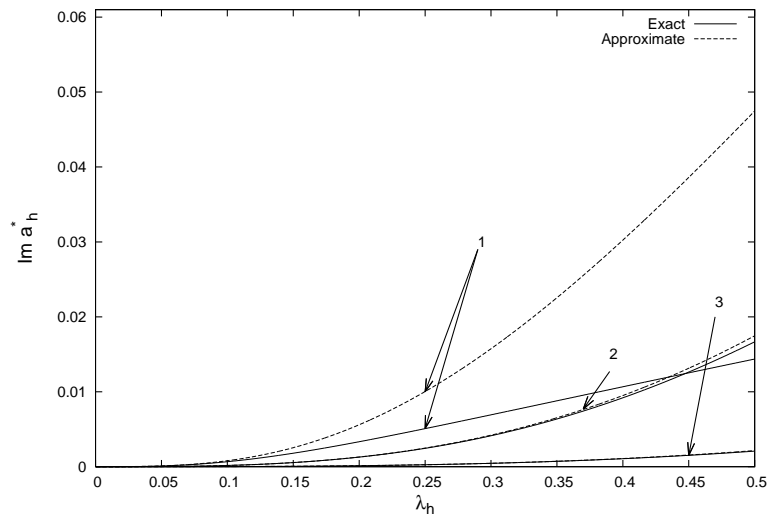


Figure 4.3: horizontal acceleration vs frequency (Imaginary Part)

#### 4.4.2 An inhomogeneous Voigt rod of variable density

Consider a viscoelastic inhomogeneous Voigt rod of length  $2l$  with density function given as  $m_1 + m_2 = 2m$  and  $M = 2ml$ , with  $0 \leq m_1 \leq m$

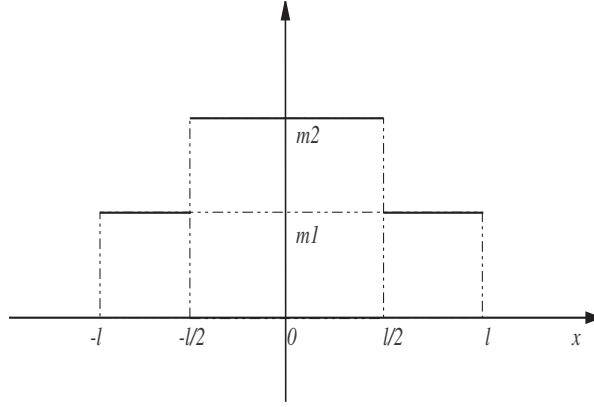


Figure 4.4: Density variation

The acceleration for the center of the rod is in the form

$$\begin{aligned}
 Ma_h|_{x=0} &= F_2 - F_1 - \frac{1}{\mu A} \int_{-l}^l m(x) \int_0^x F_{0t}(x_1, t) dx_1 dx + \\
 &\frac{E}{A\mu^2} \int_{-l}^l m(x) \int_0^x \int_0^t e^{-\frac{E}{\mu}(t-t_1)} F_{ot_1} dt_1 dx_1 dx
 \end{aligned} \tag{4.91}$$

where

$$F_0 = \frac{F_2 - F_1}{M} \int_{-l}^x m(x_1) dx_1 + F_1$$

Let us rewrite the formulae (4.91) as a sum of integrals for each interval with constant

viscosity

$$\begin{aligned}
Ma_h = & F_2 - F_1 - \frac{1}{\mu A} \left[ \int_{-l}^{-\frac{l}{2}} m_1 \int_0^x F_{0t}(x_1, t) dx_1 dx + \int_{-\frac{l}{2}}^{\frac{l}{2}} m_2 \int_0^x F_{0t}(x_1, t) dx_1 dx + \right. \\
& \left. \int_{\frac{l}{2}}^l m_1 \int_0^x F_{0t}(x_1, t) dx_1 dx \right] + \frac{E}{A\mu^2} \int_0^t e^{-\frac{E}{\mu}(t-t_1)} \left[ \int_{-l}^{-\frac{l}{2}} m_1 \int_0^x F_{ot_1} dx_1 dx + \right. \\
& \left. \int_{-\frac{l}{2}}^{\frac{l}{2}} m_2 \int_0^x F_{ot_1} dx_1 dx + \int_{\frac{l}{2}}^l m_1 \int_0^x F_{ot_1} dx_1 dx \right] dt_1 = \\
& F_2 - F_1 - \frac{1}{\mu A} \left[ \int_{-l}^{-\frac{l}{2}} m_1 \int_0^x \left( \frac{F_{2t} - F_{1t}}{2ml} \int_{-l}^{x_1} m_1 dx_2 + F_{1t} \right) dx_1 dx + \right. \\
& \int_{-\frac{l}{2}}^{\frac{l}{2}} m_2 \int_0^x \left( \frac{F_{2t} - F_{1t}}{2ml} \int_{-l}^{x_1} m_2 dx_2 + F_{1t} \right) dx_1 dx + \\
& \left. \int_{\frac{l}{2}}^l m_1 \int_0^x \left( \frac{F_{2t} - F_{1t}}{2ml} \int_{-l}^{x_1} m_1 dx_2 + F_{1t} \right) dx_1 dx \right] + \\
& \frac{E}{A\mu^2} \int_0^t e^{-\frac{E}{\mu}(t-t_1)} \left[ \int_{-l}^{-\frac{l}{2}} m_1 \int_0^x \left( \frac{F_{2t_1} - F_{1t_1}}{2ml} \int_{-l}^{x_1} m_1 dx_2 + F_{1t_1} \right) dx_1 dx + \right. \\
& \int_{-\frac{l}{2}}^{\frac{l}{2}} m_2 \int_0^x \left( \frac{F_{2t_1} - F_{1t_1}}{2ml} \int_{-l}^{x_1} m_2 dx_2 + F_{1t_1} \right) dx_1 dx + \\
& \left. \int_{\frac{l}{2}}^l m_1 \int_0^x \left( \frac{F_{2t_1} - F_{1t_1}}{2ml} \int_{-l}^{x_1} m_1 dx_2 + F_{1t_1} \right) dx_1 dx \right] dt_1
\end{aligned} \tag{4.92}$$

thus

$$Ma_h = F_2 - F_1 + \frac{l^2(7m_1^2 + m_2^2)}{48A\mu m} \left( - (F_{2t} - F_{1t}) + \frac{E}{\mu} \int_0^t e^{-\frac{E}{\mu}(t-t_1)} (F_{2t_1} - F_{1t_1}) dt_1 \right) \tag{4.93}$$

We study time-harmonic motion separating the factor  $e^{-i\omega t}$  ( $\omega$  is circular frequency)

in what follows. In this case (4.93) is in the form

$$Ma_h = (F_2 - F_1) \left( 1 + \frac{l^2(7m_1^2 + m_2^2)\omega^2}{48AE m (1 - i\omega\frac{\mu}{E})} \right) \quad (4.94)$$

Let us

$$\lambda_h = \omega l \sqrt{\frac{m}{EA}} \quad (4.95)$$

and

$$\beta = \frac{\mu}{l} \sqrt{\frac{A}{Em}} \quad (4.96)$$

then

$$Ma_h = (F_2 - F_1) \left( 1 + \frac{l^2(7m_1^2 + m_2^2)\lambda_h^2}{48m^2(1 - i\lambda_h\beta)} \right) \quad (4.97)$$

As a result, the normalised acceleration is

$$a_h^* = 1 + \frac{\left( 7 + \left( \frac{m_2}{m_1} \right)^2 \right) \lambda_h^2}{12 \left( 1 + \frac{m_2}{m_1} \right)^2 (1 - i\lambda_h\beta)} \quad (4.98)$$

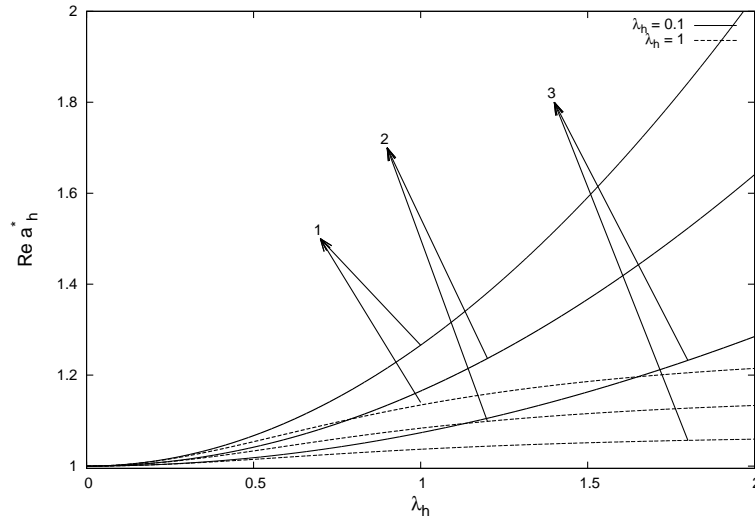


Figure 4.5: horizontal acceleration vs frequency (Real Part) variable density

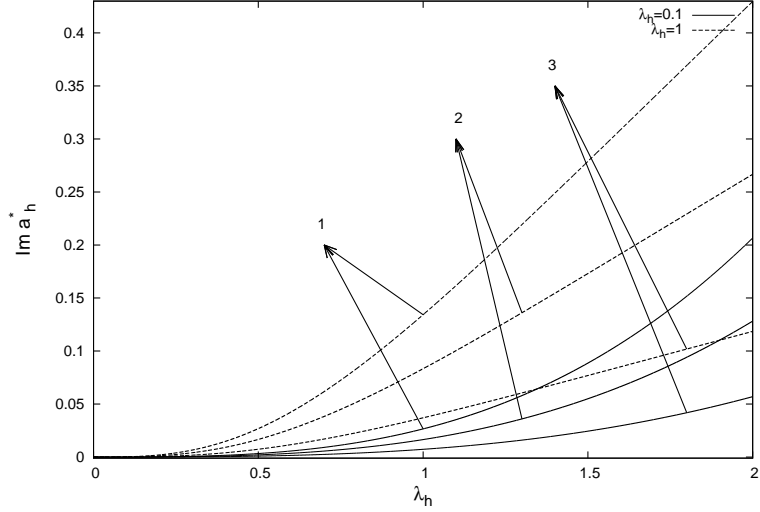


Figure 4.6: horizontal acceleration vs frequency (Imaginary Part) variable density

The solid and dashed lines in Figures 4.5 and 4.6 correspond to the asymptotic formulae (4.98) related to the values  $\beta = 0.1, 1.0$ , where  $a_h^* = Ma/(F_2 - F_1)$  is the normalised acceleration plotted versus the dimensionless frequency  $\lambda_h$ . The curves associated to the values  $m_2/m_1 = 0.1, 1.0, 5.0$  are marked with the numbers 1, 2 and 3.

### 4.4.3 An inhomogeneous Voigt rod of variable stiffness

Consider a viscoelastic inhomogeneous Voigt rod of length  $2l$  with stiffness function given as  $\mu(x) = \mu_1$  for  $|x| \geq \frac{l}{2}$  and  $\mu(x) = \mu_2$  for  $|x| \leq \frac{l}{2}$  (see Figure 4.7). Let first horizontal motion of the rod be inducted by a force applied to its right end, i.e.  $F(-l) = 0$  and  $F(l) = F_2$ .

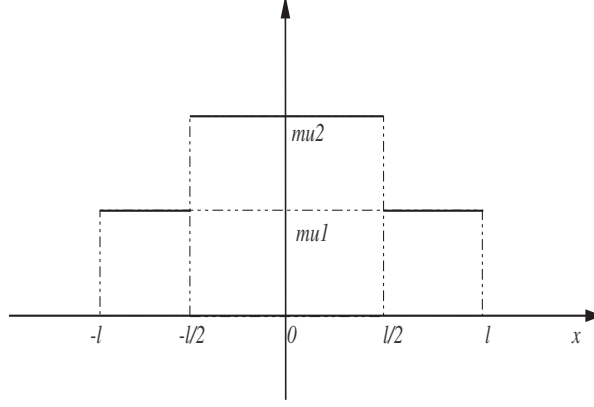


Figure 4.7: Stiffness variation

The acceleration for the center of the rod is in the form

$$\begin{aligned}
 Ma_h = F_2 - F_1 - \frac{m}{\mu(x)A} \int_{-l}^l \int_0^x F_{0t}(x_1, t) dx_1 dx + \\
 \frac{mE}{A} \int_{-l}^l \int_0^x \frac{1}{\mu^2(x_1)} \int_0^t e^{-\frac{E}{\mu(x_1)}(t-t_1)} F_{0t_1} dt_1 dx_1 dx
 \end{aligned} \tag{4.99}$$

where

$$F_0 = \frac{F_2(x+l)}{2l} \tag{4.100}$$

Let us rewrite the formula (4.99) as a sum of integrals for each interval with constant viscosity

$$\begin{aligned}
 Ma_h = F_2 - \frac{m}{\mu(x)A} \left[ \int_{-l}^{-\frac{l}{2}} \int_0^x \frac{F_{2t}(x_1+l)}{2ml} dx_1 dx + \int_{-\frac{l}{2}}^{\frac{l}{2}} \int_0^x \frac{F_{2t}(x_1+l)}{2ml} dx_1 dx + \right. \\
 \left. \int_{\frac{l}{2}}^l \int_0^x \frac{F_{2t}(x_1+l)}{2ml} dx_1 dx \right] + \frac{Em}{A} \int_0^t \left[ \frac{1}{\mu_1^2} e^{-\frac{E}{\mu_1}(t-t_1)} \int_{-l}^{-\frac{l}{2}} \int_0^x \frac{F_{2t}(x_1+l)}{2ml} dx_1 dx + \right. \\
 \left. \frac{1}{\mu_2^2} e^{-\frac{E}{\mu_2}(t-t_1)} \int_{-\frac{l}{2}}^{\frac{l}{2}} \int_0^x \frac{F_{2t}(x_1+l)}{2ml} dx_1 dx + \frac{1}{\mu_1^2} e^{-\frac{E}{\mu_1}(t-t_1)} \int_{\frac{l}{2}}^l \int_0^x \frac{F_{2t}(x_1+l)}{2ml} dx_1 dx \right] dt_1
 \end{aligned} \tag{4.101}$$

thus

$$\begin{aligned}
Ma_h = F_2 - \frac{ml^2}{48A} F_{2t} \left( \frac{7}{\mu_1} + \frac{1}{\mu_2} \right) + \frac{7l^2 E}{48A\mu_1^2} \int_0^t e^{-\frac{E}{\mu_1}(t-t_1)} F_{2t_1} dt_1 + \\
\frac{l^2 E}{48A\mu_2^2} \int_0^t e^{-\frac{E}{\mu_2}(t-t_1)} F_{2t_1} dt_1
\end{aligned} \tag{4.102}$$

We study time-harmonic motion separating the factor  $e^{-i\omega t}$  ( $\omega$  is circular frequency) in what follows. In this case (4.102) is in the form

$$Ma_h = F_2 \left( 1 + \frac{\omega^2 ml^2}{48AE} \left( \frac{7}{1 - \frac{i\omega\mu_1}{E}} + \frac{1}{1 - \frac{i\omega\mu_2}{E}} \right) \right) \tag{4.103}$$

Let us

$$\lambda = \omega l \sqrt{\frac{m}{EA}} \tag{4.104}$$

and

$$\beta_1 = \frac{\mu_1}{l} \sqrt{\frac{A}{Em}}, \quad \beta_2 = \frac{\mu_2}{l} \sqrt{\frac{A}{Em}} \tag{4.105}$$

then

$$Ma_h = F_2 \left( 1 + \frac{\lambda^2}{48} \left( \frac{7}{1 - i\lambda\beta_1} + \frac{1}{1 - i\lambda\beta_2} \right) \right) \tag{4.106}$$

As a result, the normalised acceleration is

$$a_h^* = 1 + \frac{\lambda^2}{48} \left( \frac{7}{1 - i\lambda\beta_1} + \frac{1}{1 - i\lambda\beta_2} \right) \tag{4.107}$$

# Chapter 5

## Low - frequency perturbation of rigid body motion of a viscoelastic inhomogeneous beam

### 5.1 Statement of the problem

In this chapter we consider a viscoelastic inhomogeneous beam of length  $2l$  subject to end transverse forces as well as end bending moments, see Figure 5.1. The 1D equations of motion are written as

$$N_x + m(x)w_{tt} = 0 \tag{5.1}$$

$$N = G_x \tag{5.2}$$

where  $x$  is the longitudinal coordinate,  $t$  is time,  $w$  is transverse displacement,

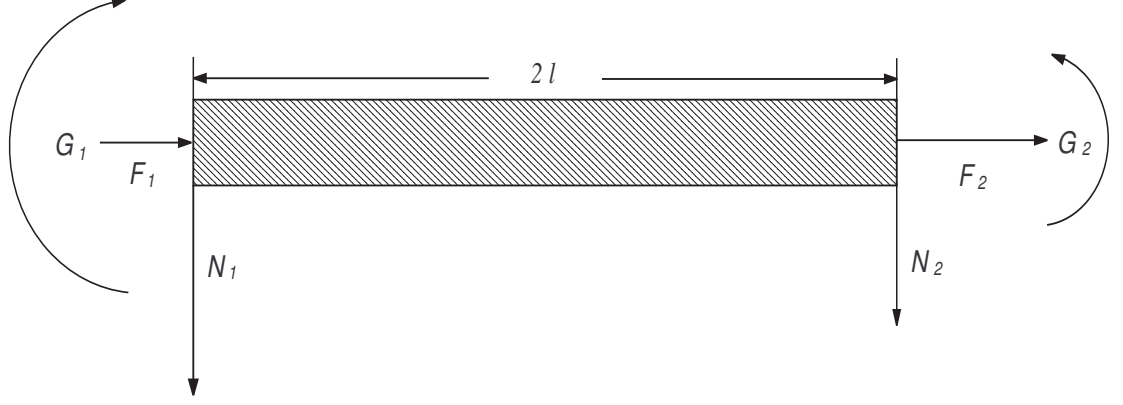


Figure 5.1: Perturbed rigid body motion of a beam

$G$  is bending moment,  $N$  is transverse force and  $m(x)$  is mass per unit length.

Linear viscoelastic behavior within the classical theories of extension and bending can be described by the following relations,

$$\kappa(x, t) = \frac{1}{E(x)I(x)} \left( G(x, t) - \int_0^t K(\gamma(x)(t - t_1)) \frac{\partial G(x, t_1)}{\partial t_1} dt_1 \right) \quad (5.3)$$

where  $\kappa = w_{xx}$  is curvature. We also use the notation:  $E(x)$  is the Young's modulus,  $I(x)$  is the second moment of inertia,  $K(\gamma(x)t)$  is creep kernel depending on function  $\gamma(x)$ . For example, for the Voigt model

$$K(\gamma(x)t) = e^{-\gamma(x)t} \quad (5.4)$$

with  $\gamma(x) = \frac{E(x)}{\mu(x)}$ , where  $\mu(x)$  denotes viscosity. In this case we get from (5.1) respectively

$$G(x, t) = I(x)[E(x)\kappa(x, t) + \mu(x)\kappa_t(x, t)] \quad (5.5)$$

The boundary conditions corresponding to the end moments shown in Figure 5.1 are

$$N(-l, t) = N_1(t), \quad N(l, t) = N_2(t) \quad \text{and} \quad G(-l, t) = G_1(t), \quad G(l, t) = G_2(t) \quad (5.6)$$

Consider the low-frequency motions starting from the governing equations above. Let us denote typical values of the variable quantities  $m(x), E(x), I(x)$  and  $\gamma(x)$  by  $m_0, E_0, I_0$  and  $\gamma_0$ , respectively. In what follows we assume that a typical time scale of viscous behavior  $\gamma_0^{-1}$  is much greater than a characteristic time that elastic waves take to propagate the distance between the ends of the bar, i.e.

$$\gamma_0^{-1} \gg l^2 \sqrt{\frac{m_0}{E_0 I_0}} \quad (5.7)$$

## 5.2 Vertical Motion and Rotation

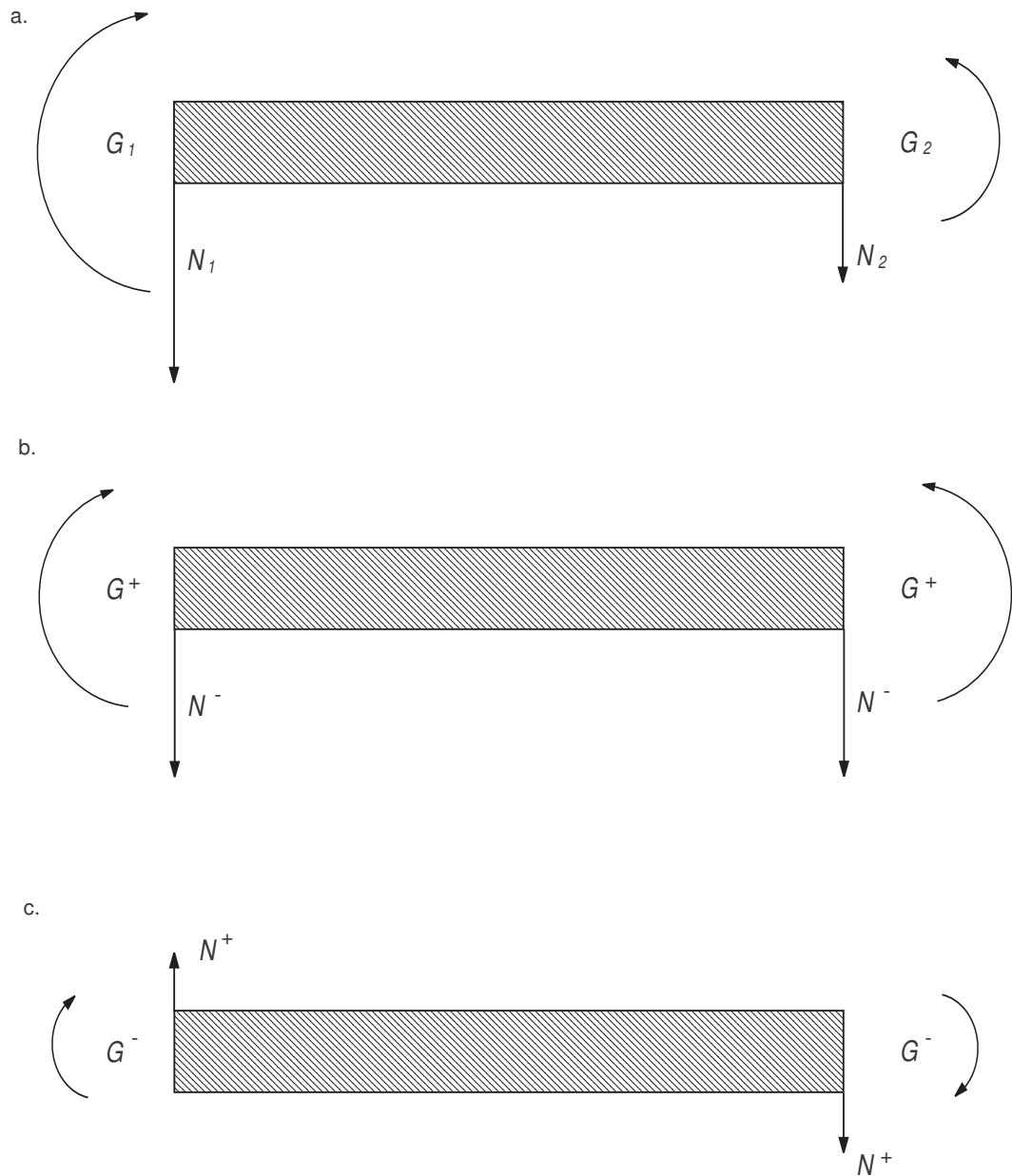


Figure 5.2: Perturbed rigid body motion. a. overall, b. vertical, c. rotational

For the sake of simplicity, we assume a symmetry of the problem parameters specified by even functions  $m(x)$ ,  $E(x)$ ,  $I(x)$  and  $\gamma(x)$ . In this case the boundary condition (5.6)

corresponding to the bending vibration can be separated into two parts

$$N(\mp l, t) = \pm N^-(t), \quad G(\mp l, t) = G^+(t) \quad (5.8)$$

and

$$N(\mp l, t) = N^+(t), \quad G(\mp l, t) = \pm G^-(t) \quad (5.9)$$

where

$$\begin{aligned} N^+(t) &= \frac{N_1(t) + N_2(t)}{2}, \quad N^-(t) = \frac{N_1(t) - N_2(t)}{2} \\ G^+(t) &= \frac{G_1(t) + G_2(t)}{2}, \quad G^-(t) = \frac{G_1(t) - G_2(t)}{2} \end{aligned} \quad (5.10)$$

In the low-frequency domain the boundary conditions (5.8) and (5.9) govern perturbed rigid body vertical motion and rotation, respectively, see Figure 5.2.

### 5.3 Asymptotic analysis

We introduce a small parameter

$$\varepsilon = l^4 \gamma_0^2 \frac{m_0}{E_0 I_0} \ll 1 \quad (5.11)$$

according to (2.12) and dimensionless quantities by the formulae

$$w = lw^*, \quad G = \frac{\varepsilon E_0 I_0}{l} G_*, \quad \text{and} \quad N = \frac{\varepsilon E_0 I_0}{l^2} N_* \quad (5.12)$$

Then, we get from (5.1), (5.2), (5.3), (5.8) and (5.9)

$$N_{*\xi} + m_*(\xi) w_{*\tau\tau} = 0 \quad (5.13)$$

$$N_* = G_{*\xi} \quad (5.14)$$

and

$$w_{*\xi\xi} = \frac{\varepsilon}{E_*(\xi)I_*(\xi)} \left( G_* - \int_0^\tau K(\gamma_*(\xi)(\tau - \tau_1)) G_{*\tau_1} d\tau_1 \right) \quad (5.15)$$

with

$$N_*(\mp 1, t) = \pm N_*^- \quad \text{and} \quad G_*(\mp 1, t) = G_*^+ \quad (5.16)$$

or

$$N_*(\mp 1, t) = N_*^+ \quad \text{and} \quad G_*(\mp 1, t) = \pm G_*^- \quad (5.17)$$

In the formulae above

$$I_*(\xi) = \frac{I(\xi)}{I_0}, \quad G^\pm = \frac{\varepsilon E_0 I_0}{l} G_*^\pm \quad \text{and} \quad N^\pm = \frac{\varepsilon E_0 I_0}{l^2} N_*^\pm \quad (5.18)$$

We express the sought for solution as

$$w_* = w_0 + \varepsilon w_1 + \dots, \quad N_* = n_0 + \varepsilon n_1 + \dots \quad \text{and} \quad G_* = g_0 + \varepsilon g_1 + \dots \quad (5.19)$$

At leading order

$$n_{0\xi} = -m_*(\xi)w_{0\tau\tau}, \quad w_{0\xi\xi} = 0 \quad \text{and} \quad n_0 = g_{0\xi} \quad (5.20)$$

subject to

$$n_0(\mp 1, \tau) = \pm N_*^- \quad \text{and} \quad g_0(\mp 1, \tau) = G_*^+ \quad (5.21)$$

or

$$n_0(\mp 1, \tau) = N_*^+ \quad \text{and} \quad g_0(\mp 1, \tau) = \pm G_*^- \quad (5.22)$$

## Vertical motion

First, consider vertical motion for which  $w_*(\xi, \tau)$  and  $G_*(\xi, \tau)$  are even functions of  $\xi$ , whereas  $N_*(\xi, \tau)$  is an odd function. In this case we get from the second equation

(5.19)

$$w_0(\xi, \tau) = v_0(\tau) \quad (5.23)$$

corresponding to vertical rigid body motion. We also get taking into account the boundary conditions (5.21) imposed on  $n_0$

$$v_{0\tau\tau} \int_{-1}^1 m_*(\xi) d\xi = 2N_*^- \quad (5.24)$$

and

$$n_0 = - \frac{2N_*^- \int_0^\xi m_*(\xi_1) d\xi_1}{\int_{-1}^1 m_*(\xi) d\xi} \quad (5.25)$$

Then, we derive from the last equation (5.19) by applying the boundary conditions (5.21) related to  $g_0$

$$g_0 = \frac{2N_*^-}{\int_{-1}^1 m_*(\xi) d\xi} \int_{\xi}^1 \int_0^{\xi_1} m_*(\xi_2) d\xi_2 d\xi_1 + G_*^+ \quad (5.26)$$

At next order

$$n_{1\xi} = -m_*(\xi)w_{1\tau\tau}, \quad n_1 = g_{1\xi} \quad (5.27)$$

and

$$w_{1\xi\xi} = \frac{1}{E_*(\xi)I_*(\xi)} \left( g_0 - \int_0^\tau K(\gamma_*(\xi)(\tau - \tau_1)) g_{0\tau_1}(\xi, \tau_1) d\tau_1 \right) \quad (5.28)$$

with the homogeneous boundary conditions  $n_1(\mp 1, \tau) = g_1(\mp 1, \tau) = 0$ , where  $g_0$  is given by (5.26). On integrating twice the last equation (5.27) we have

$$w_1 = \int_0^\xi \int_0^{\xi_1} \frac{1}{E_*(\xi_2)I_*(\xi_2)} \left( g_0(\xi_2, \tau) - \int_0^\tau K(\gamma_*(\xi_1)(\tau - \tau_1)) g_{0\tau_1}(\xi_2, \tau_1) d\tau_1 \right) d\xi_2 d\xi_1 + v_1 \quad (5.29)$$

leading to

$$w_{1\tau\tau} = \int_0^\xi \int_0^{\xi_1} \frac{1}{E_*(\xi_2)I_*(\xi_2)} \left( g_{0\tau\tau}(\xi_2, \tau)(1 - K(0)) - g_{0\tau}(\xi_2, \tau)K_\tau(0) - \int_0^\tau K_{\tau\tau}(\gamma_*(\xi_2)(\tau - \tau_1)) g_{0\tau_1}(\xi_2, \tau_1) d\tau_1 \right) d\xi_2 d\xi_1 + v_{1\tau\tau} \quad (5.30)$$

Then, from the first equation (5.27) and the homogeneous boundary conditions above

$$v_{1\tau\tau} = -\frac{1}{\int_{-1}^1 m_*(\xi) d\xi} \int_{-1}^1 m_*(\xi) \left[ \int_0^\xi \int_0^{\xi_1} \frac{1}{E_*(\xi_2)I_*(\xi_2)} \left( g_{0\tau\tau}(\xi_2, \tau) \times \right. \right. \quad (5.31)$$

$$\left. \left. (1 - K(0)) - g_{0\tau}(\xi_1, \tau)K_\tau(0) - \int_0^\tau K_{\tau\tau}(\gamma_*(\xi_2)(\tau - \tau_1)) g_{0\tau_1}(\xi_2, \tau_1) d\tau_1 \right) d\xi_2 d\xi_1 \right] d\xi$$

Finally, we obtain for the refined acceleration of the beam  $w_{\tau\tau} = w_{0\tau\tau} + \varepsilon w_{1\tau\tau} + \dots$

The acceleration of the left end of the beam  $\xi = -1$

$$\begin{aligned}
w_{\tau\tau} = & \frac{2N_*^-}{\int_{-1}^1 m_*(\xi) d\xi} - \varepsilon \left[ \int_{-1}^0 \int_0^\xi \frac{1}{E_*(\xi_1) I_*(\xi_1)} (g_{0\tau\tau}(\xi_1, \tau)(1 - K(0)) - \right. \\
& g_{0\tau}(\xi_2, \tau) K_\tau(0) - \int_0^\tau K_{\tau\tau}(\gamma_*(\xi_1)(\tau - \tau_1)) g_{0\tau_1}(\xi_1, \tau_1) d\tau_1) d\xi_1 d\xi + \\
& \left. \frac{1}{\int_{-1}^1 m_*(\xi) d\xi} \int_{-1}^1 m_*(\xi) \left( \int_0^\xi \frac{1}{E_*(\xi_1) I_*(\xi_1)} \left( g_{0\tau\tau}(\xi_1, \tau)(1 - K(0)) - g_{0\tau}(\xi_1, \tau) K_\tau(0) - \right. \right. \right. \\
& \left. \left. \left. \int_0^\tau K_{\tau\tau}(\gamma_*(\xi_1)(\tau - \tau_1)) g_{0\tau_1}(\xi_1, \tau_1) d\tau_1 \right) d\xi_1 \right) d\xi \right]
\end{aligned} \tag{5.32}$$

the acceleration of the right end of the beam  $\xi = 1$

$$\begin{aligned}
w_{\tau\tau} = & \frac{2N_*^-}{\int_{-1}^1 m_*(\xi) d\xi} - \varepsilon \left[ - \int_0^1 \int_0^\xi \frac{1}{E_*(\xi_1) I_*(\xi_1)} (g_{0\tau\tau}(\xi_1, \tau)(1 - K(0)) - \right. \\
& g_{0\tau}(\xi_2, \tau) K_\tau(0) - \int_0^\tau K_{\tau\tau}(\gamma_*(\xi_1)(\tau - \tau_1)) g_{0\tau_1}(\xi_1, \tau_1) d\tau_1) d\xi_1 d\xi + \\
& \left. \frac{1}{\int_{-1}^1 m_*(\xi) d\xi} \int_{-1}^1 m_*(\xi) \left( \int_0^\xi \frac{1}{E_*(\xi_1) I_*(\xi_1)} \left( g_{0\tau\tau}(\xi_1, \tau)(1 - K(0)) - g_{0\tau}(\xi_1, \tau) K_\tau(0) - \right. \right. \right. \\
& \left. \left. \left. \int_0^\tau K_{\tau\tau}(\gamma_*(\xi_1)(\tau - \tau_1)) g_{0\tau_1}(\xi_1, \tau_1) d\tau_1 \right) d\xi_1 \right) d\xi \right]
\end{aligned} \tag{5.33}$$

and the acceleration of the center of the beam  $\xi = 0$

$$\begin{aligned}
w_{\tau\tau} = & \frac{2N_*^-}{\int_{-1}^1 m_*(\xi) d\xi} - \varepsilon \left[ \frac{1}{\int_{-1}^1 m_*(\xi) d\xi} \int_{-1}^1 m_*(\xi) \left[ \int_0^\xi \frac{1}{E_*(\xi_1) I_*(\xi_1)} \times \right. \right. \\
& \left. \left. \left( g_{0\tau\tau}(\xi_1, \tau)(1 - K(0)) - g_{0\tau}(\xi_1, \tau) K_\tau(0) - \int_0^\tau K_{\tau\tau}(\gamma_*(\xi_1)(\tau - \tau_1)) g_{0\tau_1}(\xi_1, \tau_1) d\tau_1 \right) d\xi_1 \right] d\xi \right]
\end{aligned} \tag{5.34}$$

or in the original variables

$$\begin{aligned}
Ma_v|_{x=-l} &= N_1 - N_2 - (1 - K(0)) \left( M \int_{-l}^0 \int_0^x \frac{1}{E(x_1)I(x_1)} G_{0tt}(x_1, t) dx_1 dx + \right. \\
&\quad \left. \int_{-l}^l m(x) \int_0^x \int_0^{x_1} \frac{1}{E(x_2)I(x_2)} G_{0tt}(x_2, t) dx_2 dx_1 dx \right) + \\
&\quad K_t(0) \left( M \int_{-l}^0 \int_0^x \frac{1}{E(x_1)I(x_1)} G_{0t} dx_1 dx + \int_{-l}^l m(x) \int_0^x \int_0^{x_1} \frac{1}{E(x_2)I(x_2)} G_{0t}(x_2, t) dx_2 dx_1 dx \right) + \\
&\quad M \int_{-l}^0 \int_0^x \frac{1}{E(x_1)I(x_1)} \int_0^t K_{tt}(\gamma(t - t_1)) G_{0t_1}(x_1, t_1) dt_1 dx_1 dx + \\
&\quad \int_{-l}^l m(x) \int_0^x \int_0^{x_1} \frac{1}{E(x_2)I(x_2)} \int_0^t K_{tt}(\gamma(t - t_1)) G_{0t_1}(x_2, t_1) dt_1 dx_2 dx_1 dx
\end{aligned} \tag{5.35}$$

$$\begin{aligned}
Ma_v|_{x=l} &= N_1 - N_2 + (1 - K(0)) \left( M \int_0^l \int_0^x \frac{1}{E(x_1)I(x_1)} G_{0tt} * (x_1, t) dx_1 dx - \right. \\
&\quad \left. \int_{-l}^l m(x) \int_0^x \int_0^{x_1} \frac{1}{E(x_2)I(x_2)} G_{0tt}(x_2, t) dx_2 dx_1 dx \right) - \\
&\quad K_t(0) \left( M \int_0^l \int_0^x \frac{1}{E(x_1)I(x_1)} G_{0t} dx_1 dx - \int_{-l}^l m(x) \int_0^x \int_0^{x_1} \frac{1}{E(x_2)I(x_2)} G_{0t}(x_2, t) dx_2 dx_1 dx \right) - \\
&\quad M \int_0^l \int_0^x \frac{1}{E(x_1)I(x_1)} \int_0^t K_{tt}(\gamma(t - t_1)) G_{0t_1}(x_1, t_1) dt_1 dx_1 dx + \\
&\quad \int_{-l}^l m(x) \int_0^x \int_0^{x_1} \frac{1}{E(x_2)I(x_2)} \int_0^t K_{tt}(\gamma(t - t_1)) G_{0t_1}(x_2, t_1) dt_1 dx_2 dx_1 dx
\end{aligned} \tag{5.36}$$

$$\begin{aligned}
Ma_v|_{x=0} &= N_1 - N_2 - \int_{-l}^l m(x) \left[ \int_0^x \int_0^{x_1} \frac{1}{E(x_2)I(x_2)} ((1 - K(0)) G_{0tt}(x_2, t) - \right. \\
&\quad \left. K_t(0) G_{0t}(x_2, t) - \int_0^t K_{tt}(\gamma(t - t_1)) G_{0t_1}(x_2, t_1) dt_1) dx_2 dx_1 \right] dx
\end{aligned} \tag{5.37}$$

where  $a_v(t) = lw_{tt}(t)$ ,  $M = \int_{-l}^l m(x)dx$  and

$$G_0(x, t) = \frac{N_1 - N_2}{M} \int_x^l \int_0^{x_1} m(x_2) dx_2 dx_1 + \frac{G_1 + G_2}{2} \quad (5.38)$$

## Rotation

In case of perturbed rigid body rotation  $w_*(\xi, \tau)$  and  $G_*(\xi, \tau)$  are odd functions of  $\xi$ , while  $N_*(\xi, \tau)$  is an even function. Thus, we get from the second equation (5.20)

$$w_0(\xi, \tau) = \xi v_{0\tau}(\tau) \quad (5.39)$$

Now, multiply the first equation (5.20) by  $\xi$  having

$$\xi n_{0\xi} + \xi^2 m_*(\xi) v_{0\tau} = 0 \quad (5.40)$$

On integrating the latter over the length of the structure and taking into account the boundary conditions (5.22) along with the third equation (5.20) we have

$$v_{0\tau\tau} \int_{-1}^1 \xi^2 m_*(\xi) d\xi = -2(G_*^- + N_*^+) \quad (5.41)$$

We also deduce from (5.20), (5.22) and (5.36)

$$n_0 = -\frac{2(G_*^- + N_*^+) \int_{-1}^1 \xi_1 m_*(\xi_1) d\xi_1}{\int_{-1}^1 \xi^2 m_*(\xi) d\xi} + N_*^+ \quad (5.42)$$

and

$$g_0 = -2 (G_*^- + N_*^+) \frac{\int_0^\xi \int_0^{\xi_1} \xi_2 m_*(\xi_2) d\xi_2 d\xi_1}{\int_{-1}^1 \xi^2 m_*(\xi) d\xi} + \xi N_*^+ \quad (5.43)$$

Then, on integrating the third equation (5.27) we obtain

$$w_1 = \int_0^\xi \int_0^{\xi_1} \frac{1}{E_*(\xi_2) I_*(\xi_2)} \left( g_0(\xi_2, \tau) - \int_0^\tau K(\gamma_*(\xi_1)) (\tau - \tau_1) g_{0\tau_1}(\xi_2, \tau_1) d\tau_1 \right) d\xi_2 d\xi_1 + \xi v_1 \quad (5.44)$$

The second derivative of (5.43) in the dimensionless time is

$$w_{1\tau\tau} = \int_0^\xi \int_0^{\xi_1} \frac{1}{E_*(\xi_2) I_*(\xi_2)} \left( g_{0\tau\tau}(\xi_2, \tau) (1 - K(0)) - g_{0\tau}(\xi_2, \tau) \times \right. \\ \left. K_\tau(0) - \int_0^\tau K_{\tau\tau}(\gamma_*(\xi_2)) (\tau - \tau_1) g_{0\tau_1}(\xi_2, \tau_1) d\tau_1 \right) d\xi_2 d\xi_1 + \xi v_{1\tau\tau} \quad (5.45)$$

Finally,

$$v_{1\tau\tau} = - \frac{1}{\int_{-1}^1 \xi^2 m_*(\xi) d\xi} \int_{-1}^1 \xi m_*(\xi) \left[ \int_0^\xi \int_0^{\xi_1} \frac{1}{E_*(\xi_2) I_*(\xi_2)} \times \right. \\ \left. \left( g_{0\tau\tau}(\xi_2, \tau) (1 - K(0)) - g_{0\tau}(\xi_2, \tau) K_\tau(0) - \int_0^\tau K_{\tau\tau}(\gamma_*(\xi_2)) (\tau - \tau_1) g_{0\tau_1}(\xi_2, \tau_1) d\tau_1 \right) d\xi_2 d\xi_1 \right] d\xi \quad (5.46)$$

The obtained angular acceleration of the beam is

$$w_{\tau\tau} = w_{0\tau\tau} + \varepsilon w_{1\tau\tau} + \dots \quad (5.47)$$

The angular acceleration of the left end of the beam  $\xi = -1$

$$\begin{aligned}
w_{\tau\tau} = & -\frac{G_*^- + N_*^+}{\int_{-1}^1 \xi^2 m_*(\xi) d\xi} - \varepsilon \left[ \int_{-1}^0 \int_0^\xi \frac{1}{E_*(\xi_1) I_*(\xi_1)} \left( g_{0\tau\tau}(\xi_1, \tau) (1 - K(0)) - \right. \right. \\
& \left. \left. g_{0\tau}(\xi_1, \tau) K_\tau(0) - \int_0^\tau K_{\tau\tau}(\gamma_*(\xi_1) (\tau - \tau_1)) g_{0\tau_1}(\xi_1, \tau_1) d\tau_1 \right) d\xi_1 d\xi + \right. \\
& \left. \frac{1}{\int_{-1}^1 \xi^2 m_*(\xi) d\xi} \int_{-1}^1 \xi m_*(\xi) \left[ \int_0^\xi \int_0^{\xi_1} \frac{1}{E_*(\xi_2) I_*(\xi_2)} \left( g_{0\tau\tau}(\xi_2, \tau) (1 - K(0)) - \right. \right. \right. \\
& \left. \left. \left. g_{0\tau}(\xi_2, \tau) K_\tau(0) - \int_0^\tau K_{\tau\tau}(\gamma_*(\xi_2) (\tau - \tau_1)) g_{0\tau_1}(\xi_2, \tau_1) d\tau_1 \right) d\xi_2 d\xi_1 \right] d\xi \right]
\end{aligned} \tag{5.48}$$

the angular acceleration of the left end of the beam  $\xi = l$

$$\begin{aligned}
w_{\tau\tau} = & -\frac{G_*^- + N_*^+}{\int_{-1}^1 \xi^2 m_*(\xi) d\xi} + \varepsilon \left[ \int_0^1 \int_0^\xi \frac{1}{E_*(\xi_1) I_*(\xi_1)} \left( g_{0\tau\tau}(\xi_1, \tau) (1 - K(0)) - \right. \right. \\
& \left. \left. g_{0\tau}(\xi_1, \tau) K_\tau(0) - \int_0^\tau K_{\tau\tau}(\gamma_*(\xi_1) (\tau - \tau_1)) g_{0\tau_1}(\xi_1, \tau_1) d\tau_1 \right) d\xi_1 d\xi - \right. \\
& \left. \frac{1}{\int_{-1}^1 \xi^2 m_*(\xi) d\xi} \int_{-1}^1 \xi m_*(\xi) \left[ \int_0^\xi \int_0^{\xi_1} \frac{1}{E_*(\xi_2) I_*(\xi_2)} \left( g_{0\tau\tau}(\xi_2, \tau) (1 - K(0)) - \right. \right. \right. \\
& \left. \left. \left. g_{0\tau}(\xi_2, \tau) K_\tau(0) - \int_0^\tau K_{\tau\tau}(\gamma_*(\xi_2) (\tau - \tau_1)) g_{0\tau_1}(\xi_2, \tau_1) d\tau_1 \right) d\xi_2 d\xi_1 \right] d\xi \right]
\end{aligned} \tag{5.49}$$

and finally the angular acceleration of the center of the beam  $\xi = 0$

$$\begin{aligned}
w_{\tau\tau} = & -\frac{G_*^- + N_*^+}{\int_{-1}^1 \xi^2 m_*(\xi) d\xi} - \frac{1}{\int_{-1}^1 \xi^2 m_*(\xi) d\xi} \int_{-1}^1 \xi m_*(\xi) \left[ \int_0^\xi \int_0^{\xi_1} \frac{1}{E_*(\xi_2) I_*(\xi_2)} \times \right. \\
& \left. \left( g_{0\tau\tau}(\xi_2, \tau)(1 - K(0)) - g_{0\tau}(\xi_2, \tau) K_\tau(0) - \right. \right. \\
& \left. \left. \int_0^\tau K_{\tau\tau}(\gamma_*(\xi_2)(\tau - \tau_1)) g_{0t_1}(\xi_2, \tau_1) d\tau_1 \right) d\xi_2 d\xi_1 \right] d\xi
\end{aligned} \tag{5.50}$$

In the original variables the equation (5.46)-(5.50) take the form

$$\begin{aligned}
J\Omega|_{x=-l} = & G_2 - G_1 - l(N_1 + N_2) - (1 - K(0)) \left[ \frac{1}{l} \int_{-l}^l x^2 m(x) dx \times \right. \\
& \left. \int_{-l}^0 \int_0^x \frac{1}{E(x_1) I(x_1)} G_{0tt}(x_1, t) dx_1 dx + \int_{-l}^l x m(x) \int_0^x \int_0^{x_1} \frac{1}{E(x_2) I(x_2)} G_{0tt}(x_2, t) dx_2 dx_1 dx \right] + \\
& K_t(0) \left[ \frac{1}{l} \int_{-l}^l x^2 m(x) dx \int_{-l}^0 \int_0^x \frac{1}{E(x_1) I(x_1)} G_{0t}(x_1, t) dx_1 dx + \right. \\
& \left. \int_{-l}^l x m(x) \int_0^x \int_0^{x_1} \frac{1}{E(x_2) I(x_2)} G_{0t}(x_2, t) dx_2 dx_1 dx \right] + \\
& \frac{1}{l} \int_{-l}^l x^2 m(x) dx \int_{-l}^0 \int_0^x \frac{1}{E(x_1) I(x_1)} \int_0^t K_{tt}(\gamma(x_2)(t - t_1)) G_{0\tau_1}(x_2, t_1) dt_1 dx_1 dx + \\
& \int_{-l}^l x m(x) \int_0^x \int_0^{x_1} \frac{1}{E(x_2) I(x_2)} \int_0^t K_{tt}(\gamma(x_2)(t - t_1)) G_{0\tau_1}(x_2, t_1) dt_1 dx_2 dx_1 dx
\end{aligned} \tag{5.51}$$

$$\begin{aligned}
J\Omega|_{x=l} = & G_2 - G_1 - l(N_1 + N_2) + (1 - K(0)) \left[ \frac{1}{l} \int_{-l}^l x^2 m(x) dx \times \right. \\
& \left. \int_0^l \int_0^x \frac{1}{E(x_1)I(x_1)} G_{0tt}(x_1, t) dx_1 dx - \int_{-l}^l xm(x) \int_0^x \int_0^{x_1} \frac{1}{E(x_2)I(x_2)} G_{0tt}(x_2, t) dx_2 dx_1 dx \right] + \\
& K_t(0) \left[ \frac{1}{l} \int_{-l}^l x^2 m(x) dx \int_0^l \int_0^x \frac{1}{E(x_1)I(x_1)} G_{0t}(x_1, t) dx_1 dx - \right. \\
& \left. \int_{-l}^l xm(x) \int_0^x \int_0^{x_1} \frac{1}{E(x_2)I(x_2)} G_{0t}(x_2, t) dx_2 dx_1 dx \right] - \\
& \frac{1}{l} \int_{-l}^l x^2 m(x) dx \int_0^l \int_0^x \frac{1}{E(x_1)I(x_1)} \int_0^t K_{tt}(\gamma(x_2)(t - t_1)) G_{0\tau_1}(x_2, t_1) dt_1 dx_1 dx + \\
& \int_{-l}^l xm(x) \int_0^x \int_0^{x_1} \frac{1}{E(x_2)I(x_2)} \int_0^t K_{tt}(\gamma(x_2)(t - t_1)) G_{0\tau_1}(x_2, t_1) dt_1 dx_2 dx_1 dx
\end{aligned} \tag{5.52}$$

and

$$\begin{aligned}
J\Omega|_{x=0} = & G_2 - G_1 - l(N_1 + N_2) - \int_{-l}^l xm(x) \left[ \int_0^x \int_0^{x_1} \frac{1}{E(x_2)I(x_2)} \times \right. \\
& \left( (1 - K(0)) G_{0tt}(x_2, t) - K_t(0) G_{0t}(x_2, t) - \right. \\
& \left. \left. \int_0^t K_{tt}(\gamma(x_2)(t - t_1)) G_{0\tau_1}(x_2, t_1) dt_1 \right) dx_2 dx_1 \right] dx
\end{aligned} \tag{5.53}$$

where angular acceleration  $\Omega$  and moment of inertia  $J$  are given by  $\Omega = v_{tt}$  and  $J = \int_{-l}^l x^2 m(x) dx$ , whereas

$$G_0(x, t) = \frac{(G_2 - G_1 - l(N_1 + N_2)) \int_0^x \int_0^{x_1} x_2 m(x_2) dx_2 dx_1}{\int_{-l}^l x^2 m(x) dx} + \frac{x}{2} (N_1 + N_2) \tag{5.54}$$

The equations (5.33) and (5.43) contain low-frequency corrections to classical equa-

tion of rigid body dynamics  $Ma_v = N_1 - N_2$  and  $J\Omega = G_2 - G_1 - l(N_1 + N_2)$ . The quantities (5.34) and (5.44) are key for the established approximate formulae. They express the leading order low-frequency variation of the bending moment along the length of the structure.

## 5.4 Particular cases

### 5.4.1 An inhomogeneous viscoelastic beam of uniform density

The derived equations (5.33) and (5.43) take a simpler form for perturbed rigid body motion of a homogeneous viscoelastic beam ( $m(x) = m$ ). For vertical motion they become

$$\begin{aligned}
Ma_v|_{x=-l} &= N_1 - N_2 - (1 - K(0)) \left( l \int_{-l}^0 \int_0^x \frac{1}{E(x_1)I(x_1)} G_{0tt}(x_1, t) dx_1 dx + \right. \\
&\quad \left. \frac{1}{2} \int_{-l}^l m(x) \int_0^x \int_0^{x_1} \frac{1}{E(x_2)I(x_2)} G_{0tt}(x_2, t) dx_2 dx_1 dx \right) + \\
K_t(0) &\left( l \int_{-l}^0 \int_0^x \frac{1}{E(x_1)I(x_1)} G_{0t} dx_1 dx + \frac{1}{2} \int_{-l}^l \int_0^x \int_0^{x_1} \frac{1}{E(x_2)I(x_2)} G_{0t}(x_2, t) dx_2 dx_1 dx \right) + \quad (5.55) \\
&l \int_{-l}^0 \int_0^x \frac{1}{E(x_1)I(x_1)} \int_0^t K_{tt}(\gamma(t - t_1)) G_{0t_1}(x_1, t_1) dt_1 dx_1 dx + \\
&\frac{1}{2} \int_{-l}^l \int_0^x \int_0^{x_1} \frac{1}{E(x_2)I(x_2)} \int_0^t K_{tt}(\gamma(t - t_1)) G_{0t_1}(x_2, t_1) dt_1 dx_2 dx_1 dx
\end{aligned}$$

$$\begin{aligned}
Ma_v|_{x=l} = & N_1 - N_2 + (1 - K(0)) \left( l \int_0^l \int_0^x \frac{1}{E(x_1)I(x_1)} G_{0tt} * (x_1, t) dx_1 dx - \right. \\
& \left. \frac{1}{2} \int_{-l}^l \int_0^x \int_0^{x_1} \frac{1}{E(x_2)I(x_2)} G_{0tt}(x_2, t) dx_2 dx_1 dx \right) - \\
& K_t(0) \left( l \int_0^l \int_0^x \frac{1}{E(x_1)I(x_1)} G_{0t} dx_1 dx - \frac{1}{2} \int_{-l}^l \int_0^x \int_0^{x_1} \frac{1}{E(x_2)I(x_2)} G_{0t}(x_2, t) dx_2 dx_1 dx \right) - \quad (5.56) \\
& l \int_0^l \int_0^x \frac{1}{E(x_1)I(x_1)} \int_0^t K_{tt}(\gamma(t - t_1)) G_{0t_1}(x_1, t_1) dt_1 dx_1 dx + \\
& \frac{1}{2} \int_{-l}^l \int_0^x \int_0^{x_1} \frac{1}{E(x_2)I(x_2)} \int_0^t K_{tt}(\gamma(t - t_1)) G_{0t_1}(x_2, t_1) dt_1 dx_2 dx_1 dx
\end{aligned}$$

and

$$\begin{aligned}
Ma_v|_{x=0} = & N_1 - N_2 - \frac{1}{2} \int_{-l}^l \left[ \int_0^x \int_0^{x_1} \frac{1}{E(x_2)I(x_2)} ((1 - K(0)) G_{0tt}(x_2, t) - \right. \\
& \left. K_t(0) G_{0t}(x_2, t) - \int_0^t K_{tt}(\gamma(t - t_1)) G_{0t_1}(x_2, t_1) dt_1 \right) dx_2 dx_1 \Big] dx \quad (5.57)
\end{aligned}$$

where

$$G_0 = (l^2 - x^2)m \frac{N_1 - N_2}{2l} + \frac{m(G_1 + G_2)}{2} \quad (5.58)$$

and for rotation

$$\begin{aligned}
J\Omega|_{x=-l} &= G_2 - G_1 - l(N_1 + N_2) - (1 - K(0)) \left[ \frac{l^2}{3} \times \right. \\
&\quad \left. \int_{-l}^0 \int_0^x \frac{1}{E(x_1)I(x_1)} G_{0tt}(x_1, t) dx_1 dx + \frac{1}{2} \int_{-l}^l x \int_0^x \int_0^{x_1} \frac{1}{E(x_2)I(x_2)} G_{0tt}(x_2, t) dx_2 dx_1 dx \right] + \\
K_t(0) &\left[ \frac{l^2}{3} \int_{-l}^0 \int_0^x \frac{1}{E(x_1)I(x_1)} G_{0t}(x_1, t) dx_1 dx + \right. \\
&\quad \left. \frac{1}{2} \int_{-l}^l x \int_0^x \int_0^{x_1} \frac{1}{E(x_2)I(x_2)} G_{0t}(x_2, t) dx_2 dx_1 dx \right] + \\
&\quad \frac{l^2}{3} \int_{-l}^0 \int_0^x \frac{1}{E(x_1)I(x_1)} \int_0^t K_{tt}(\gamma(x_2)(t - t_1)) G_{0\tau_1}(x_2, t_1) dt_1 dx_1 dx + \\
&\quad \frac{1}{2} \int_{-l}^l x \int_0^x \int_0^{x_1} \frac{1}{E(x_2)I(x_2)} \int_0^t K_{tt}(\gamma(x_2)(t - t_1)) G_{0\tau_1}(x_2, t_1) dt_1 dx_2 dx_1 dx
\end{aligned} \tag{5.59}$$

$$\begin{aligned}
J\Omega|_{x=l} &= G_2 - G_1 - l(N_1 + N_2) + (1 - K(0)) \left[ \frac{l^2}{3} \times \right. \\
&\quad \left. \int_0^l \int_0^x \frac{1}{E(x_1)I(x_1)} G_{0tt}(x_1, t) dx_1 dx - \frac{1}{2} \int_{-l}^l x \int_0^x \int_0^{x_1} \frac{1}{E(x_2)I(x_2)} G_{0tt}(x_2, t) dx_2 dx_1 dx \right] + \\
K_t(0) &\left[ \frac{l^2}{3} \int_0^l \int_0^x \frac{1}{E(x_1)I(x_1)} G_{0t}(x_1, t) dx_1 dx - \right. \\
&\quad \left. \frac{1}{2} \int_{-l}^l x \int_0^x \int_0^{x_1} \frac{1}{E(x_2)I(x_2)} G_{0t}(x_2, t) dx_2 dx_1 dx \right] - \\
&\quad \frac{l^2}{3} \int_0^l \int_0^x \frac{1}{E(x_1)I(x_1)} \int_0^t K_{tt}(\gamma(x_2)(t - t_1)) G_{0\tau_1}(x_2, t_1) dt_1 dx_1 dx + \\
&\quad \frac{1}{2} \int_{-l}^l x \int_0^x \int_0^{x_1} \frac{1}{E(x_2)I(x_2)} \int_0^t K_{tt}(\gamma(x_2)(t - t_1)) G_{0\tau_1}(x_2, t_1) dt_1 dx_2 dx_1 dx
\end{aligned} \tag{5.60}$$

and

$$\begin{aligned}
J\Omega|_{x=0} = & G_2 - G_1 - l(N_1 + N_2) - \frac{1}{2} \int_{-l}^l x \left[ \int_0^x \int_0^{x_1} \frac{1}{E(x_2)I(x_2)} \times \right. \\
& \left. \left( (1 - K(0))G_{0tt}(x_2, t) - K_t(0)G_{0t}(x_2, t) - \right. \right. \\
& \left. \left. \int_0^t K_{tt}(\gamma(x_2)(t - t_1))G_{0t_1}(x_2, t_1)dt_1 \right) dx_2 dx_1 \right] dx
\end{aligned} \tag{5.61}$$

where

$$G_0 = xm \left( \frac{x^2}{l^2} - 1 \right) \frac{N_1 + N_2}{2} + xm(3l^2 - x^2) \frac{G_2 - G_1}{2l^3} \tag{5.62}$$

### 5.4.2 An inhomogeneous viscoelastic beam of uniform stiffness and viscosity

In the case of inhomogeneous viscoelastic beam with constant stiffness and viscosity ( $E(x) = E, I(x) = I, \mu(x) = \mu$  and  $\gamma(x) = \gamma$ ) the derived formulae (5.34) and (5.44) become

$$\begin{aligned}
Ma_v|_{x=-l} = & N_1 - N_2 - (1 - K(0)) \left( M \int_{-l}^0 \int_0^x G_{0tt}(x_1, t) dx_1 dx + \right. \\
& \left. \int_{-l}^l m(x) \int_0^x \int_0^{x_1} G_{0tt}(x_2, t) dx_2 dx_1 dx \right) + \\
& K_t(0) \left( M \int_{-l}^0 \int_0^x G_{0t} dx_1 dx + \int_{-l}^l m(x) \int_0^x \int_0^{x_1} G_{0t}(x_2, t) dx_2 dx_1 dx \right) + \\
& M \int_{-l}^0 \int_0^x \int_0^t K_{tt}(\gamma(t - t_1)) G_{0t_1}(x_1, t_1) dt_1 dx_1 dx + \\
& \int_{-l}^l m(x) \int_0^x \int_0^{x_1} \int_0^t K_{tt}(\gamma(t - t_1)) G_{0t_1}(x_2, t_1) dt_1 dx_2 dx_1 dx
\end{aligned} \tag{5.63}$$

$$\begin{aligned}
Ma_v|_{x=l} = & N_1 - N_2 + (1 - K(0)) \left( M \int_0^l \int_0^x G_{0tt}(x_1, t) dx_1 dx - \right. \\
& \left. \int_{-l}^l m(x) \int_0^x \int_0^{x_1} G_{0tt}(x_2, t) dx_2 dx_1 dx \right) - \\
& K_t(0) \left( M \int_0^l \int_0^x G_{0t} dx_1 dx - \int_{-l}^l m(x) \int_0^x \int_0^{x_1} G_{0t}(x_2, t) dx_2 dx_1 dx \right) - \\
& M \int_0^l \int_0^x \int_0^t K_{tt}(\gamma(t - t_1)) G_{0t_1}(x_1, t_1) dt_1 dx_1 dx + \\
& \int_{-l}^l m(x) \int_0^x \int_0^{x_1} \int_0^t K_{tt}(\gamma(t - t_1)) G_{0t_1}(x_2, t_1) dt_1 dx_2 dx_1 dx
\end{aligned} \tag{5.64}$$

and

$$\begin{aligned}
Ma_v|_{x=0} = & N_1 - N_2 - \int_{-l}^l m(x) \left[ \int_0^x \int_0^{x_1} ((1 - K(0)) G_{0tt}(x_2, t) - \right. \\
& \left. K_t(0) G_{0t}(x_2, t) - \int_0^t K_{tt}(\gamma(t - t_1)) G_{0t_1}(x_2, t_1) dt_1 \right) dx_2 dx_1 \Big] dx
\end{aligned} \tag{5.65}$$

where

$$G_0(x, t) = \frac{N_1 - N_2}{MEI} \int_x^l \int_0^{x_1} m(x_2) dx_2 dx_1 + \frac{G_1 + G_2}{2EI} \tag{5.66}$$

and for rotation

$$\begin{aligned}
J\Omega|_{x=-l} &= G_2 - G_1 - l(N_1 + N_2) - (1 - K(0)) \left[ \frac{l^2}{3} \times \right. \\
&\quad \left. \int_{-l}^0 \int_0^x G_{0tt}(x_1, t) dx_1 dx + \frac{1}{2} \int_{-l}^l x \int_0^x \int_0^{x_1} G_{0tt}(x_2, t) dx_2 dx_1 dx \right] + \\
&\quad K_t(0) \left[ \frac{l^2}{3} \int_{-l}^0 \int_0^x G_{0t}(x_1, t) dx_1 dx + \right. \\
&\quad \left. \frac{1}{2} \int_{-l}^l x \int_0^x \int_0^{x_1} G_{0t}(x_2, t) dx_2 dx_1 dx \right] + \\
&\quad \frac{l^2}{3} \int_{-l}^0 \int_0^x \int_0^t K_{tt}(\gamma(x_2)(t - t_1)) G_{0\tau_1}(x_2, t_1) dt_1 dx_1 dx + \\
&\quad \frac{1}{2} \int_{-l}^l x \int_0^x \int_0^{x_1} \int_0^t K_{tt}(\gamma(x_2)(t - t_1)) G_{0\tau_1}(x_2, t_1) dt_1 dx_2 dx_1 dx
\end{aligned} \tag{5.67}$$

$$\begin{aligned}
J\Omega|_{x=l} &= G_2 - G_1 - l(N_1 + N_2) + (1 - K(0)) \left[ \frac{l^2}{3} \times \right. \\
&\quad \left. \int_0^l \int_0^x G_{0tt}(x_1, t) dx_1 dx - \frac{1}{2} \int_{-l}^l x \int_0^x \int_0^{x_1} G_{0tt}(x_2, t) dx_2 dx_1 dx \right] + \\
&\quad K_t(0) \left[ \frac{l^2}{3} \int_0^l \int_0^x G_{0t}(x_1, t) dx_1 dx - \right. \\
&\quad \left. \frac{1}{2} \int_{-l}^l x \int_0^x \int_0^{x_1} G_{0t}(x_2, t) dx_2 dx_1 dx \right] - \\
&\quad \frac{l^2}{3} \int_0^l \int_0^x \int_0^t K_{tt}(\gamma(x_2)(t - t_1)) G_{0\tau_1}(x_2, t_1) dt_1 dx_1 dx + \\
&\quad \frac{1}{2} \int_{-l}^l x \int_0^x \int_0^{x_1} \int_0^t K_{tt}(\gamma(x_2)(t - t_1)) G_{0\tau_1}(x_2, t_1) dt_1 dx_2 dx_1 dx
\end{aligned} \tag{5.68}$$

and

$$J\Omega|_{x=0} = G_2 - G_1 - l(N_1 + N_2) - \frac{1}{2} \int_{-l}^l x \left[ \int_0^x \int_0^{x_1} \left( (1 - K(0))G_{0tt}(x_2, t) - K_t(0)G_{0t}(x_2, t) - \int_0^t K_{tt}(\gamma(x_2)(t - t_1))G_{0t_1}(x_2, t_1)dt_1 \right) dx_2 dx_1 \right] dx \quad (5.69)$$

where

$$G_0(x, t) = \frac{(G_2 - G_1 - l(N_1 + N_2)) \int_0^x \int_{x_1}^l x_2 m(x_2) dx_2 dx_1}{EI \int_{-l}^l x^2 m(x) dx} + \frac{x}{2EI} (N_1 + N_2) \quad (5.70)$$

### 5.4.3 A homogeneous viscoelastic beam

The derived equations (5.35)-(5.37) and (5.55)-(5.57) take a simpler form for perturbed rigid body motion of a homogeneous viscoelastic beam of uniform stiffness, density and viscosity. In this case  $m(x) = m$ ,  $E(x) = E$ ,  $I(x) = I$  and  $\gamma(x) = \gamma$  and the formulae (5.38) and (5.58) become

$$G_0 = (l^2 - x^2) \frac{N_1 - N_2}{4l} + \frac{G_1 + G_2}{2} \quad (5.71)$$

and

$$G_0 = x \left( \frac{x^2}{l^2} - 1 \right) \frac{N_1 + N_2}{4} + x(3l^2 - x^2) \frac{G_2 - G_1}{4l^3} \quad (5.72)$$

On inserting the latter into and we get respectively for vertical motion

$$Ma_v|_{x=-l} = N_1 - N_2 - \frac{l^3}{EI} \left( \dot{G}_{0tt}^{(l)}(1 - K(0)) - \dot{G}_{0t}^{(l)} K_t(0) - \int_0^t K_{tt}(\gamma(t - t_1)) \dot{G}_{0t_1}^{(l)} dt_1 \right) \quad (5.73)$$

$$Ma_v|_{x=l} = N_1 - N_2 - \frac{l^3}{EI} \left( \dot{G}_{0tt}^{(r)}(1 - K(0)) - \dot{G}_{0t}^{(r)}K_t(0) - \int_0^t K_{tt}(\gamma(t - t_1))\dot{G}_{0t_1}^{(r)} dt_1 \right) \quad (5.74)$$

and

$$Ma_v = N_1 - N_2 - \frac{l^3}{EI} \left( \dot{G}_{0tt}(1 - K(0)) - \dot{G}_{0t}K_t(0) - \int_0^t K_{tt}(\gamma(t - t_1))\dot{G}_{0t_1} dt_1 \right) \quad (5.75)$$

where  $M = 2ml$ ,  $\dot{G}_0^{(l)} = \frac{17}{60}(N_1 - N_2) + \frac{2}{3}(G_1 + G_2)$ ,  $\dot{G}_0^{(r)} = -\frac{2}{15}(N_1 - N_2) - \frac{1}{3}(G_1 + G_2)$  and  $\dot{G}_0 = \frac{3}{40}(N_1 - N_2) + \frac{1}{6}(G_1 + G_2)$  in (5.73), (5.74) and (5.75) respectively.

and for rotation

$$J\Omega|_{x=-l} = G_2 - G_1 - l(N_1 + N_2) - \frac{ml^4}{EI} \left( \dot{G}_{0tt}^{(l)}(-K(0)) - \dot{G}_{0t}^{(l)}K_t(0) - \int_0^t K_{tt}(\gamma(x)(t - t_1))\dot{G}_{0t_1}^{(l)} dt_1 \right) \quad (5.76)$$

$$J\Omega|_{x=l} = G_2 - G_1 - l(N_1 + N_2) - \frac{ml^4}{EI} \left( \dot{G}_{0tt}^{(r)}(1 - K(0)) - \dot{G}_{0t}^{(r)}K_t(0) - \int_0^t K_{tt}(\gamma(x)(t - t_1))\dot{G}_{0t_1}^{(r)} dt_1 \right) \quad (5.77)$$

and

$$J\Omega|_{x=0} = G_2 - G_1 - l(N_1 + N_2) - \frac{ml^4}{EI} \left( \dot{G}_{0tt}(1 - K(0)) - \dot{G}_{0t}K_t(0) - \int_0^t K_{tt}(\gamma(x)(t - t_1))\dot{G}_{0t_1} dt_1 \right) \quad (5.78)$$

where  $\dot{G}_0^{(l)} = -\frac{41}{1260}(N_1 + N_2) - \frac{17}{140}(G_2 - G_1)$ ,  $\dot{G}_0^{(r)} = \frac{2}{315}(N_1 + N_2) - \frac{1}{35}(G_2 - G_1)$  and  $\dot{G}_0 = \frac{11}{840}(N_1 + N_2) + \frac{13}{280}(G_2 - G_1)$  in (5.76) - (5.78) respectively.

For a Voigt beam the formulae (5.76) - (5.78) become

$$Ma_v|_{x=\mp} = N_1 - N_2 + \frac{ml^3}{\mu I} \left( \dot{G}_{0t}^{(l),(r)} - \frac{E}{\mu} \int_0^t e^{-\frac{E}{\mu}(t-t_1)} \dot{G}_{0t_1}^{(l),(r)} dt_1 \right) \quad (5.79)$$

and

$$J\Omega|_{x=\mp} = G_2 - G_1 - l(N_1 + N_2) - \frac{ml^4}{40\mu I} \left( \dot{G}_{0t}^{(l),(r)} - \frac{E}{\mu} \int_0^t e^{-\frac{E}{\mu}(t-t_1)} \dot{G}_{0t_1}^{(l),(r)} dt_1 \right) \quad (5.80)$$

## 5.5 Numerical results

Consider time-harmonic motion of a homogeneous viscoelastic beam. In this case the constitutive relations (5.1) become

$$\kappa = \frac{G}{IA} (1 + i\delta) \quad (5.81)$$

with

$$\delta = \int_0^\infty K \left( \frac{\gamma}{\omega} z \right) e^{iz} dz \quad (5.82)$$

where  $\omega$  is circular frequency. Here and below the factor  $e^{-i\omega t}$  is separated.

Let vertical motion of the beam caused by equal end forces, i.e.  $N(l) = -N(-l) = N_2$  and  $G(\pm l) = 0$  (see Figure 5.2). Thus, the equation (5.79) is in the form

$$Ma_v = -2N_2 \left[ 1 + \frac{3}{40} \lambda_v^2 (1 + i\delta) \right] \quad (5.83)$$

where

$$\lambda_v = \omega l^2 \sqrt{\frac{m}{EI}} \quad (5.84)$$

The latter formula also corresponds to a two-term asymptotic expansion of the exact solution, see Appendix A.2.

Numerical results are given in Figures 5.3 and 5.4 for the same values of the parameter  $\beta$  which is now expressed by

$$\beta = \frac{\mu}{l^2} \sqrt{\frac{m}{EI}} \quad (5.85)$$

In addition, we adapt here the notation  $a_v^* = -Ma/2N_2$  and define the parameter  $\delta$  in 5.87 as

$$\delta = \frac{\lambda_v \beta}{1 - i\lambda_v \beta} \quad (5.86)$$

As before, the two-term formula 5.87 extends the range of the applicability of Newton's second law to vertical motion of a bar. Similarly to the data displaced in Figures 4.3 and 4.2, we observe a better accuracy of the aforementioned formula at greater values of the parameter  $\beta$  responsible for the effect of viscosity.

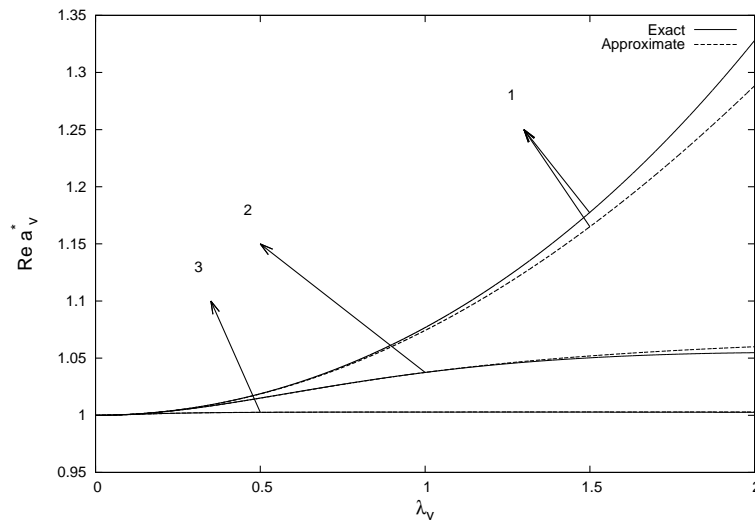


Figure 5.3: Vertical acceleration vs frequency (Real Part)

Rotation motion of the beam caused by equal end forces, i.e.  $N(l) = N(-l) = N_2$

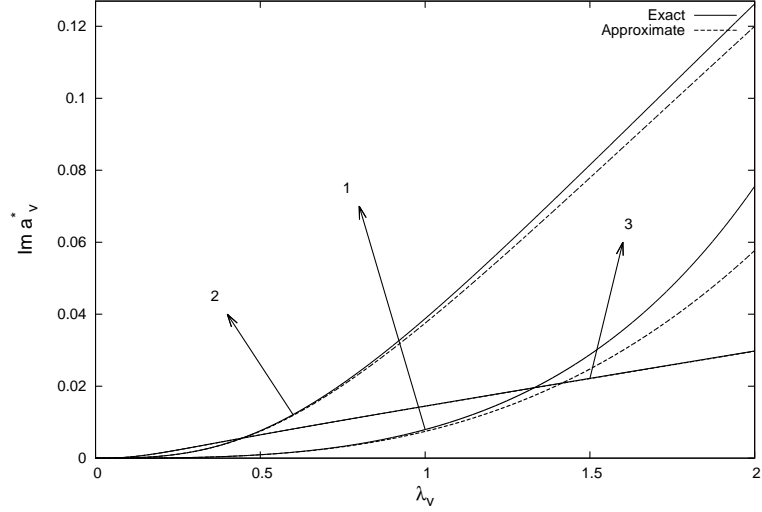


Figure 5.4: Vertical acceleration vs frequency (Imaginary Part)

and  $G(\pm l) = 0$  (see Figure 5.2). In this case the equation (??) is written as

$$J\varphi_{tt} = -\frac{2N_2}{3} \left[ 1 + \frac{3}{40} \lambda_v^2 (1 + i\delta) \right] \quad (5.87)$$

where

$$\lambda_v = \omega l^2 \sqrt{\frac{m}{EI}} \quad (5.88)$$

The latter formula also corresponds to a two-term asymptotic expansion of the exact solution, see Appendix A.3.

Numerical results are given in Figures 5.5 and 5.6 for the same values of the parameter  $\beta$  which is now expressed by

$$\beta = \frac{\mu}{l^2} \sqrt{\frac{m}{EI}} \quad (5.89)$$

In addition, we adapt here the notation  $a_v^* = -Ma/2N_2$  and define the parameter

$\delta$  in 5.87 as

$$\delta = \frac{\lambda_v \beta}{1 - i \lambda_v \beta} \quad (5.90)$$

The two-term formula 5.87 extends the range of the applicability of Newton's second law to rotation motion of a bar. Here we observe a better accuracy of the aforementioned formula at greater values of the parameter  $\beta$  responsible for the effect of viscosity.

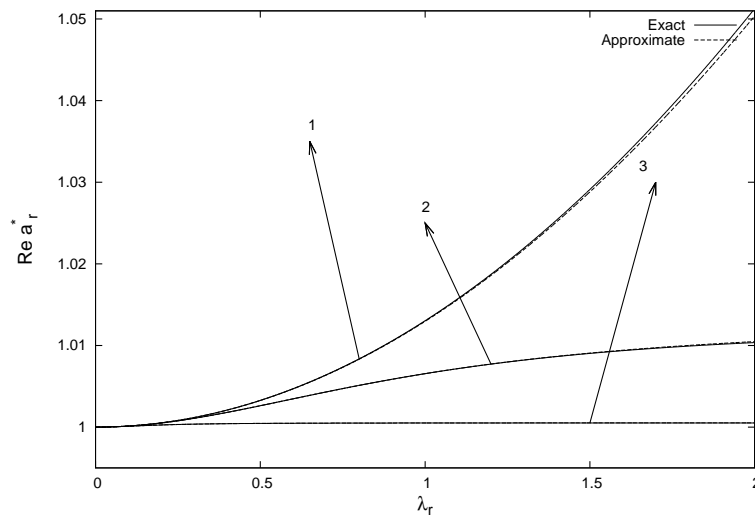


Figure 5.5: Rotation acceleration vs frequency (Real Part)

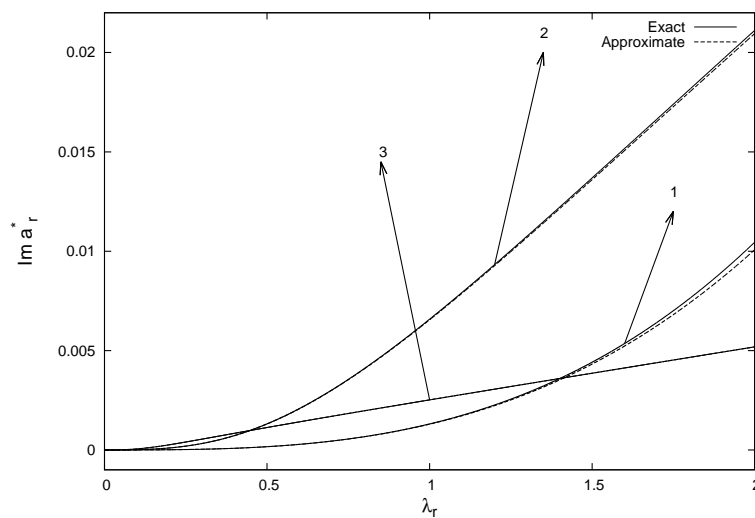


Figure 5.6: Rotation acceleration vs frequency (Imaginary Part)

# Chapter 6

## Application of the low-frequency model to a coupled impact

### 6.1 A homogeneous elastic rod

For simplicity consider time-harmonic motion of a homogeneous elastic rod of length  $2l$  ignoring the effect of viscosity ( $\mu = 0$ ). The equation of motion (4.1) becomes

$$F_x = mu_{tt} \tag{6.1}$$

and the relation between strain and force can be written as

$$e(x, t) = \frac{1}{EA} F(x, t), \tag{6.2}$$

where  $e = u_x$  is the longitudinal strain as above.

The boundary conditions corresponding to the end forces arising in a coupled impact

are given by

$$F(-l, t) = F_1(t), \quad F(l, t) = F_2(t) \quad (6.3)$$

Next by using dimensionless quantities

$$F_{*\xi} = u_{\tau\tau} \quad (6.4)$$

and

$$u_{*\xi} = \varepsilon F_* \quad (6.5)$$

we seek for the solution of the problem (6.4) - (6.5) in the form (4.15).

At leading order

$$f_{0\xi} = u_{0\tau\tau} \quad \text{and} \quad u_{0\xi} = 0 \quad (6.6)$$

subject to the boundary conditions

$$f_0(-1, \tau) = F_{1*}(\tau) \quad \text{and} \quad f_0(1, \tau) = F_{2*}(\tau) \quad (6.7)$$

Immediately, we get from the second equation (6.6)

$$u_0(\xi, \tau) = v_0(\tau) \quad (6.8)$$

Next, we have from the first equation (6.6) taking into account the imposed boundary conditions (6.7)

$$v_{0\tau\tau} = \frac{F_{2*} - F_{1*}}{2} \quad (6.9)$$

At the same time

$$f_0 = \frac{\xi(F_{2*} - F_{1*})}{2} + \frac{F_{2*} + F_{1*}}{2} \quad (6.10)$$

At next order

$$f_{1\xi} = u_{1\tau\tau} \quad \text{and} \quad u_{1\xi} = f_0 \quad (6.11)$$

with the homogeneous boundary conditions  $f_1(\pm 1, \tau) = 0$ . On integrating the second equation (6.11) we arrive at

$$u_1 = \frac{\xi^2(F_{2*} - F_{1*})}{4} + \frac{\xi(F_{2*} + F_{1*})}{2} + v_1 \quad (6.12)$$

The second derivative of (6.12) with respect to dimensionless time is given by

$$u_{1\tau\tau} = \frac{\xi^2(F_{2*\tau\tau} - F_{1*\tau\tau})}{4} + \frac{\xi(F_{2*\tau\tau} + F_{1*\tau\tau})}{2} + v_{1\tau\tau} \quad (6.13)$$

We also get from the first equation (6.11) and the homogeneous boundary conditions above

$$v_{1\tau\tau} = - \left( \frac{1}{3}F_{2*\tau\tau} + \frac{1}{6}F_{1*\tau\tau} \right) \quad (6.14)$$

Then, the acceleration of the right end of the rod is

$$u_{1\tau\tau}(1) = \frac{5}{12}F_{2*\tau\tau} + \frac{1}{12}F_{1*\tau\tau} \quad (6.15)$$

Similarly, the acceleration of the left end is

$$u_{1\tau\tau}(1) = \frac{5}{12}F_{2*\tau\tau} + \frac{1}{12}F_{1*\tau\tau} \quad (6.16)$$

or in the original variables

$$Ma_1 = F_2 - F_1 - \frac{l^2 m}{6EA} (7F_{2*tt} + 11F_{1*tt}) \quad (6.17)$$

and

$$Ma_2 = F_2 - F_1 + \frac{l^2 m}{6EA} (5F_{2*tt} + F_{1*tt}) \quad (6.18)$$

After subtracting (6.18) from the equation (6.17) we get

$$M(a_2 - a_1) = \frac{2l^2 m}{EA} (F_{2*tt} + F_{1*tt}) \quad (6.19)$$

On the other hand

$$F_{2tt} = F_{1tt} + Ma_{1tt} \quad (6.20)$$

Then

$$F_{1tt} = \frac{EA}{2l} (a_2 - a_1) - \frac{M}{2} a_{1tt} \quad (6.21)$$

and

$$F_{2tt} = \frac{EA}{2l} (a_2 - a_1) + \frac{M}{2} a_{1tt} \quad (6.22)$$

In terms of time harmonic motion the derived formulae (6.21) and (6.22) are given by

$$F_1 = \frac{EA}{2l\omega^2} (a_2 - a_1) - \frac{M}{2} a_1 \quad (6.23)$$

and

$$F_2 = \frac{EA}{2l\omega^2} (a_2 - a_1) + \frac{M}{2} a_1 \quad (6.24)$$

## 6.2 An inhomogeneous elastic rod of variable density

Consider time-harmonic motion of an inhomogeneous elastic rod of length  $2l$  ignoring the effect of viscosity ( $\mu = 0$ ). The equation of motion (4.1) becomes

$$F_x = m(x)u_{tt} \quad (6.25)$$

and the relation between strain and force is in the form (6.2)

$$e(x, t) = \frac{1}{EA}F(x, t)$$

The boundary conditions corresponding to the end forces arising in a coupled impact are given by (6.3). By using dimensionless quantities

$$F_{*\xi} = m_*(\xi)u_{\tau\tau} \quad (6.26)$$

and

$$u_{*\xi} = \varepsilon F_* \quad (6.27)$$

we are looking for the solution of the problem (6.26) - (6.27) in the form (4.15).

At the leading order

$$f_{0\xi} = m_*(\xi)u_{0\tau\tau} \quad \text{and} \quad u_{0\xi} = 0 \quad (6.28)$$

subject to the boundary conditions

$$f_0(-1, \tau) = F_{1*}(\tau) \quad \text{and} \quad f_0(1, \tau) = F_{2*}(\tau) \quad (6.29)$$

Immediately, we get from the second equation (6.28)

$$u_0(\xi, \tau) = v_0(\tau) \quad (6.30)$$

Next, we have from the first equation (6.28) taking into account the imposed boundary conditions (6.29)

$$v_{0\tau\tau} = \frac{F_{2*} - F_{1*}}{\int_{-1}^1 m_*(\xi) d\xi} \quad (6.31)$$

At the same time

$$f_0 = \frac{F_{2*} \int_{-1}^{\xi} m_*(\xi_1) d\xi_1 + F_{1*} \int_{\xi}^1 m_*(\xi_1) d\xi_1}{2} + \frac{F_{2*} + F_{1*}}{\int_{-1}^1 m_*(\xi) d\xi} \quad (6.32)$$

At next order

$$f_{1\xi} = m_*(\xi) u_{1\tau\tau} \quad \text{and} \quad u_{1\xi} = f_0 \quad (6.33)$$

with the homogeneous boundary conditions  $f_1(\pm 1, \tau) = 0$ . On integrating the second equation (6.33) we get

$$u_1 = \frac{1}{\int_{-1}^1 m_*(\xi) d\xi} \left( F_{2*} \int_0^{\xi} \int_{-1}^{\xi_1} m_*(\xi_2) d\xi_2 d\xi_1 + F_{1*} \int_0^{\xi} \int_{\xi_1}^1 m_*(\xi_2) d\xi_2 d\xi_1 \right) + v_1 \quad (6.34)$$

The second derivative of (6.34) with respect to dimensionless time is given by

$$u_{1\tau\tau} = \frac{1}{\int_{-1}^1 m_*(\xi) d\xi} \left( F_{2*\tau\tau} \int_0^\xi \int_{-1}^{\xi_1} m_*(\xi_2) d\xi_2 d\xi_1 + F_{1*\tau\tau} \int_0^\xi \int_{\xi_1}^1 m_*(\xi_2) d\xi_2 d\xi_1 \right) + v_{1\tau\tau} \quad (6.35)$$

From the first equation (6.33) and the homogeneous boundary conditions above we get

$$v_{1\tau\tau} = -\frac{1}{\left( \int_{-1}^1 m_*(\xi) d\xi \right)^2} \left( F_{2*\tau\tau} \int_{-1}^1 m_*(\xi) \int_0^\xi \int_{-1}^{\xi_1} m_*(\xi_2) d\xi_2 d\xi_1 d\xi + F_{1*\tau\tau} \int_{-1}^1 m_*(\xi) \int_0^\xi \int_{\xi_1}^1 m_*(\xi_2) d\xi_2 d\xi_1 d\xi \right) \quad (6.36)$$

Then, the acceleration of the right end of the rod is

$$u_{1\tau\tau}|_{\xi=1} = \frac{1}{\int_{-1}^1 m_*(\xi) d\xi} \left( F_{2*\tau\tau} \int_0^1 \int_{-1}^\xi m_*(\xi_1) d\xi_1 d\xi + F_{1*\tau\tau} \int_0^1 \int_\xi^1 m_*(\xi_1) d\xi_1 d\xi \right) - \frac{1}{\left( \int_{-1}^1 m_*(\xi) d\xi \right)^2} \left( F_{2*\tau\tau} \int_{-1}^1 m_*(\xi) \int_0^\xi \int_{-1}^{\xi_1} m_*(\xi_2) d\xi_2 d\xi_1 d\xi + F_{1*\tau\tau} \int_{-1}^1 m_*(\xi) \int_0^\xi \int_{\xi_1}^1 m_*(\xi_2) d\xi_2 d\xi_1 d\xi \right) \quad (6.37)$$

Similarly, the acceleration of the left end is

$$\begin{aligned}
u_{1\tau\tau}|_{\xi=-1} &= \frac{1}{\int_{-1}^1 m_*(\xi)d\xi} \left( F_{2*\tau\tau} \int_0^{-1} \int_{-1}^{\xi} m_*(\xi_1)d\xi_1d\xi + F_{1*\tau\tau} \int_0^{-1} \int_{\xi}^1 m_*(\xi_1)d\xi_1d\xi \right) - \\
&\frac{1}{\left( \int_{-1}^1 m_*(\xi)d\xi \right)^2} \left( F_{2*\tau\tau} \int_{-1}^1 m_*(\xi) \int_0^{\xi} \int_{-1}^{\xi_1} m_*(\xi_2)d\xi_2d\xi_1d\xi + \right. \\
&\left. F_{1*\tau\tau} \int_{-1}^1 m_*(\xi) \int_0^{\xi} \int_{\xi_1}^1 m_*(\xi_2)d\xi_2d\xi_1d\xi \right)
\end{aligned} \tag{6.38}$$

or in the original variables

$$\begin{aligned}
Ma_1 &= F_2 - F_1 + \frac{1}{EA} \left( F_{2*tt} \int_0^{-l} \int_{-l}^x m(x_1)dx_1dx + F_{1*tt} \int_0^{-l} \int_x^1 m(x_1)dx_1dx \right) - \\
&\frac{1}{EA \int_{-1}^1 m_*(\xi)d\xi} \left( F_{2tt} \int_{-l}^l m(x) \int_0^x \int_{-1}^{x_1} m(x_2)dx_2dx_1dx + \right. \\
&\left. F_{1tt} \int_{-l}^l m(x) \int_0^x \int_{x_1}^l m(x_2)dx_2dx_1dx \right)
\end{aligned} \tag{6.39}$$

and

$$\begin{aligned}
Ma_2 &= F_2 - F_1 + \frac{1}{EA} \left( F_{2*tt} \int_0^l \int_{-l}^x m(x_1)dx_1dx + F_{1*tt} \int_0^l \int_x^1 m(x_1)dx_1dx \right) - \\
&\frac{1}{EA \int_{-1}^1 m_*(\xi)d\xi} \left( F_{2tt} \int_{-l}^l m(x) \int_0^x \int_{-1}^{x_1} m(x_2)dx_2dx_1dx + \right. \\
&\left. F_{1tt} \int_{-l}^l m(x) \int_0^x \int_{x_1}^l m(x_2)dx_2dx_1dx \right)
\end{aligned} \tag{6.40}$$

After subtracting (6.40) from the equation (6.39) we get

$$M(a_2 - a_1) = \frac{1}{EA} \left( F_{2tt} \int_{-l}^l \int_{-l}^x m(x_1) dx_1 dx + F_{1tt} \int_{-l}^l \int_x^l m(x_1) dx_1 dx \right) \quad (6.41)$$

On the other hand

$$F_{2tt} = F_{1tt} + Ma_{1tt} \quad (6.42)$$

where  $M = \int_{-l}^l m(x) dx$ .

Then

$$F_{1tt} = \frac{MEA(a_2 - a_1) - M \int_{-l}^l \int_{-l}^x m(x_1) dx_1 dx a_{1tt}}{2Ml} \quad (6.43)$$

or

$$F_{1tt} = \frac{EA}{2l} (a_2 - a_1) - \frac{\int_{-l}^l \int_{-l}^x m(x_1) dx_1 dx}{2l} a_{1tt} \quad (6.44)$$

and

$$F_{2tt} = \frac{EA}{2l} (a_2 - a_1) - \left( \frac{\int_{-l}^l \int_{-l}^x m(x_1) dx_1 dx}{2l} - M \right) a_{1tt} \quad (6.45)$$

### 6.3 Evaluation of impact forces from experimental data

In the equation for the impact force (6.21) the coefficients may be estimated through least squares as

$$F_{1tt} = k_1(a_2 - a_1) + k_2 a_{1tt}. \quad (6.46)$$

Some of the results for the impact force and related spectra are demonstrated below for  $k_1 = -630100$  and  $k_2 = 65780$ . The results for Test 1 are illustrated in Figure 6.1,

containing the comparison of experimental and predicted derivatives of the force  $F_{1tt}$ , spectrum of acceleration at the left end of the rod, spectrum of difference between accelerations at both sides, spectrum of the force at the left end, and, finally, comparison of experimentally measured and theoretically predicted forces.

It is remarkable that as follows from the theoretical consideration in the previous section the spectrum of  $a_1 \sim a_2$  and the spectrum of the difference  $a_2 - a_1$  (or *Acceleration2 - Acceleration1* on Figures 6.1 and 6.2) has to begin at the origin. The violation of this requirement for available experimental data indicates that some further careful analysis of data representation is required. However, even so, the results for Test 1 show relatively good agreement between theoretical and experimental data.

We note that it is not always the case, see e.g. the results for Test 3, shown on Figure 6.2.

More data for other tests may be found below.

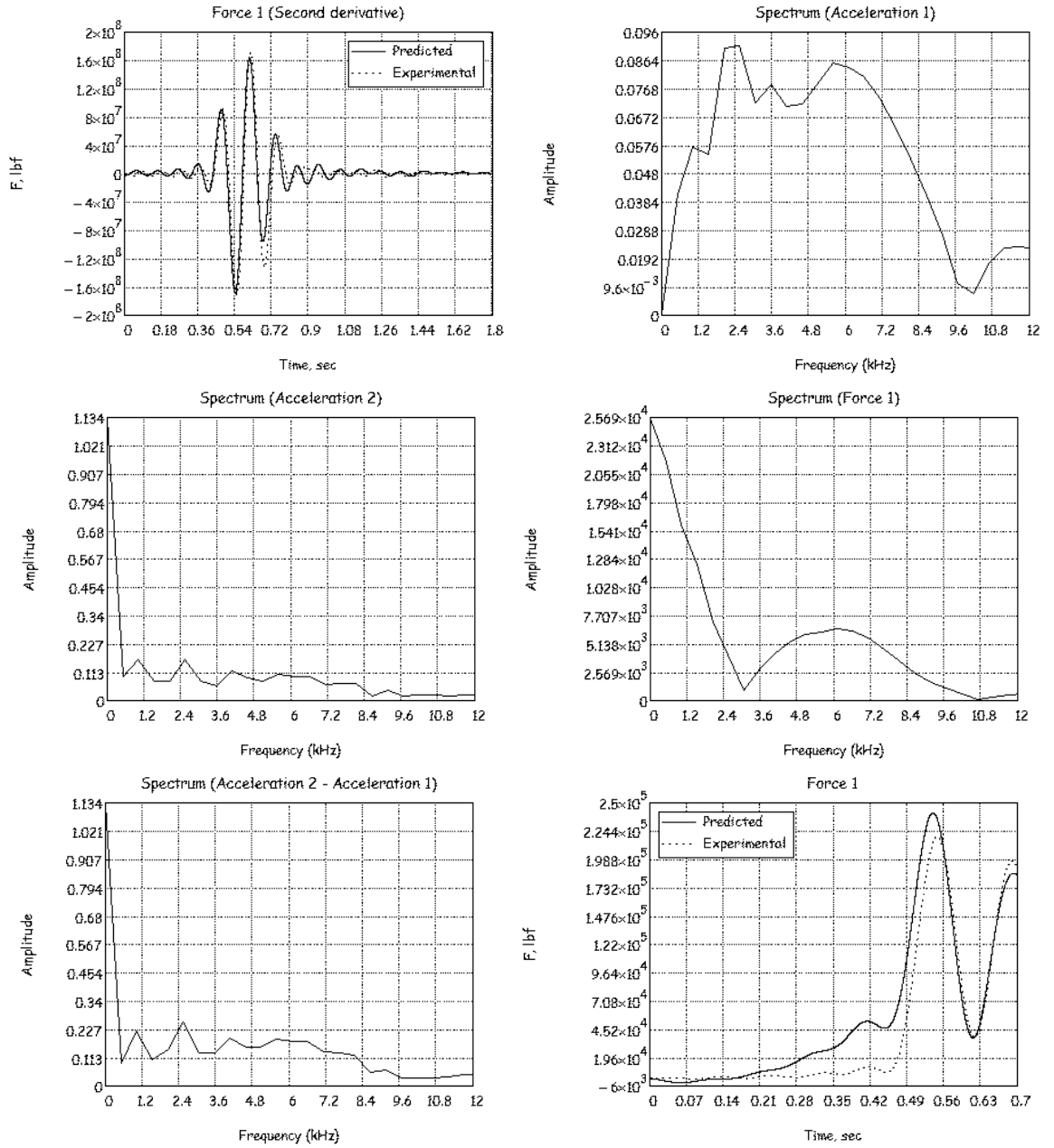


Figure 6.1: Numerical illustrations for test 1

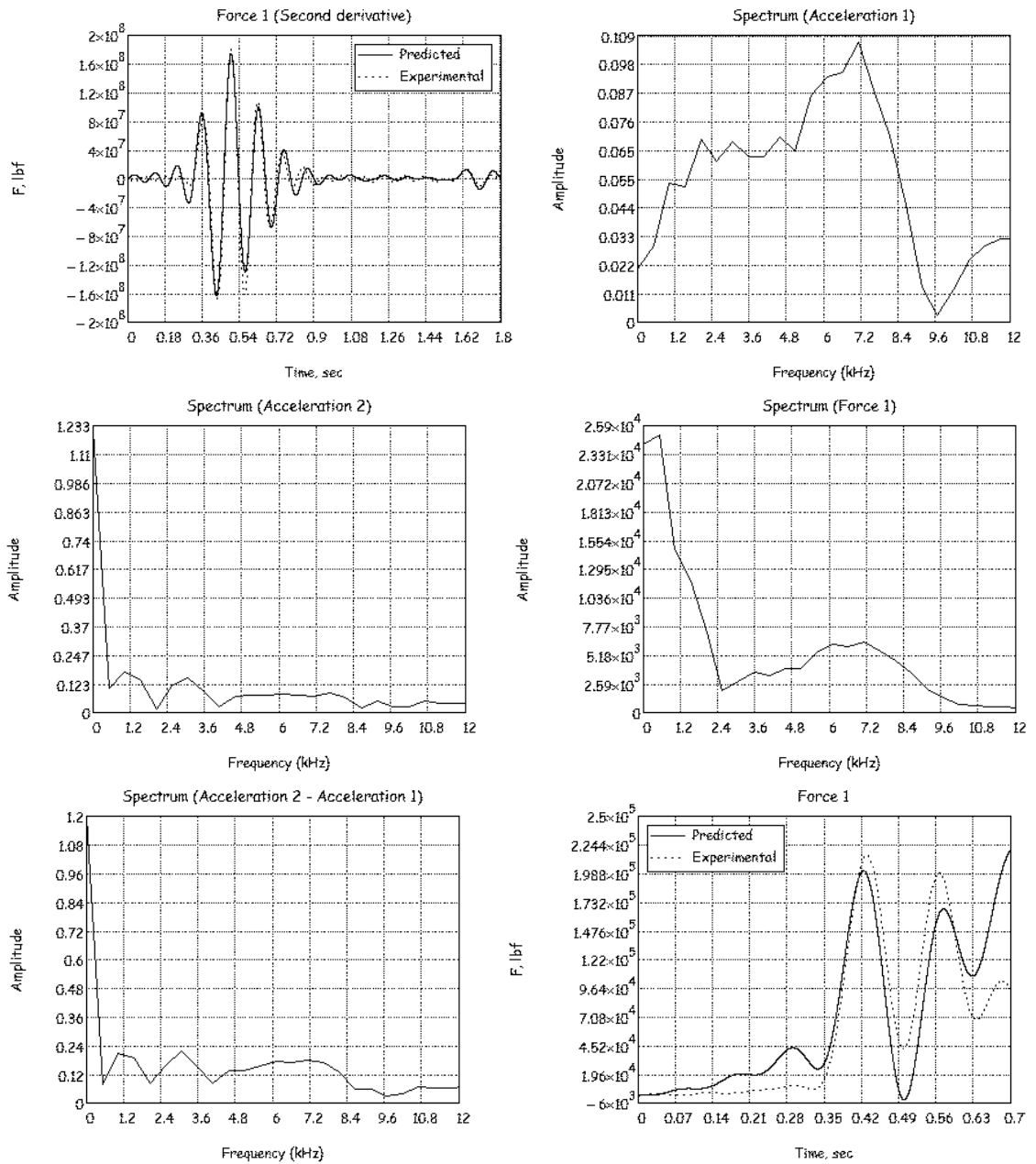


Figure 6.2: Numerical illustrations for test 3

Let us also present some evidence of necessity of some further investigation of the presented experimental data. As an example, we consider part of the recorded data for acceleration at the right end of the freight car, showing with red solid lines the positive values, and with the blue dotted lines the negative values, reflected into the upper half-plane, therefore, essentially, the graphs on Figure 6.3 show modulus of acceleration. It may be observed that the mean value of the data (and of course, the integral) are non-zero, with negative part overwhelming the positive one. This provides a clear evidence of further analysis of the recorded data.

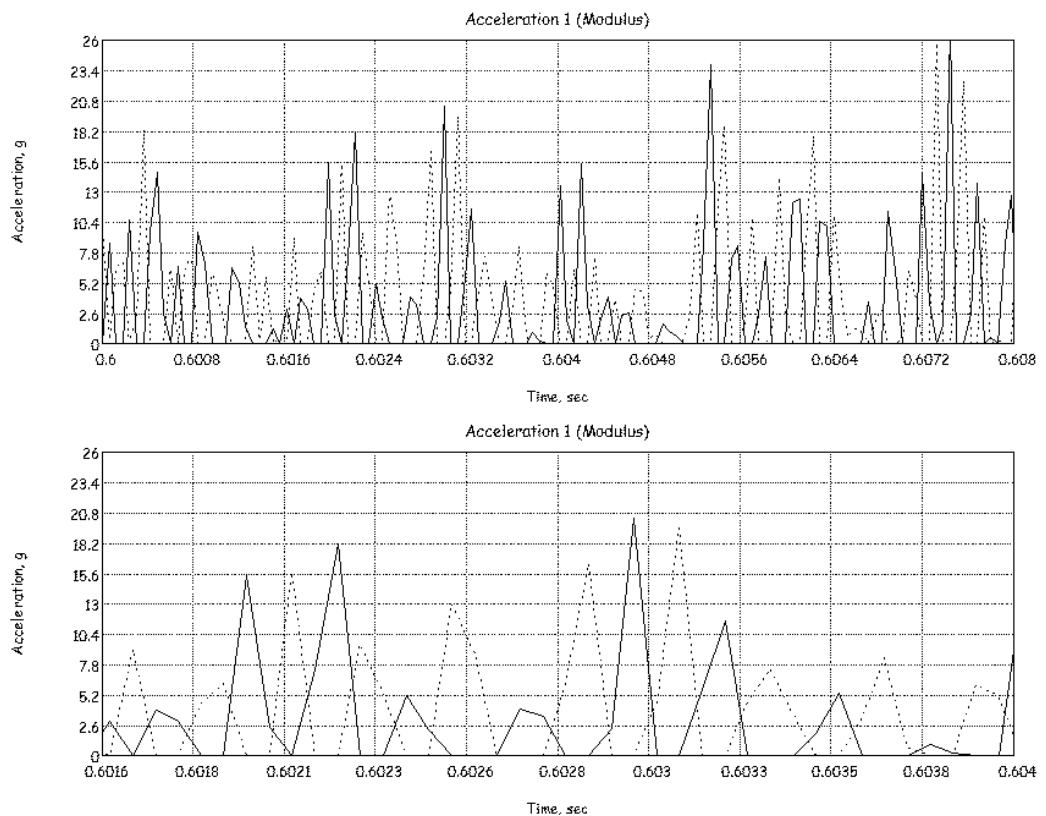


Figure 6.3: Evidence of further investigation for test 3

Below we present the results of comparison of the theoretical results for  $F_{1tt}$  versus provided experimental data. Calculations are presented for the rest 17 tests, with solid

line standing for theoretical calculations and dotted line depicting experimental results.

The values of the coefficients are taken as  $k_1 = -630100$  and  $k_2 = 65780$ .

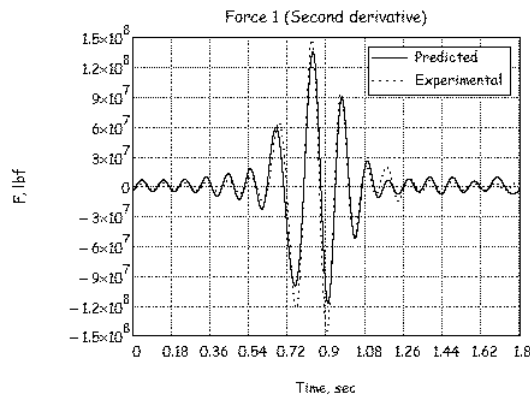


Figure 6.4: Numerical illustration (test 2)

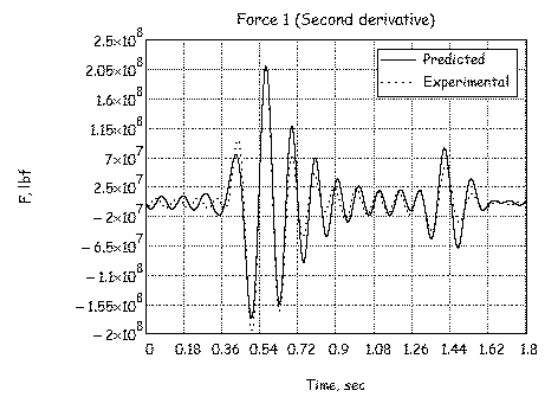


Figure 6.5: Numerical illustration (test 4)

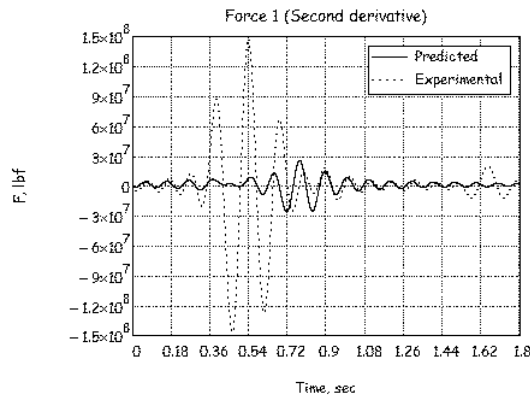


Figure 6.6: Numerical illustration (test 5)

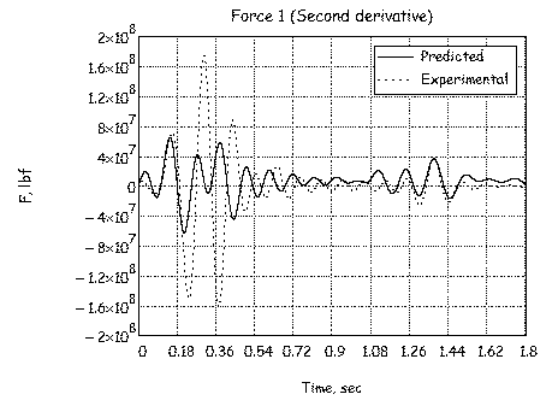


Figure 6.7: Numerical illustration (test 6)

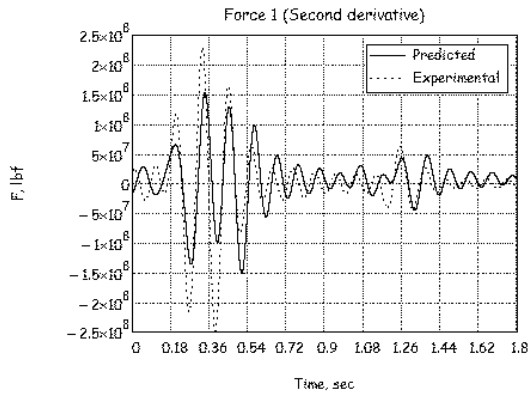


Figure 6.8: Numerical illustration (test 7)

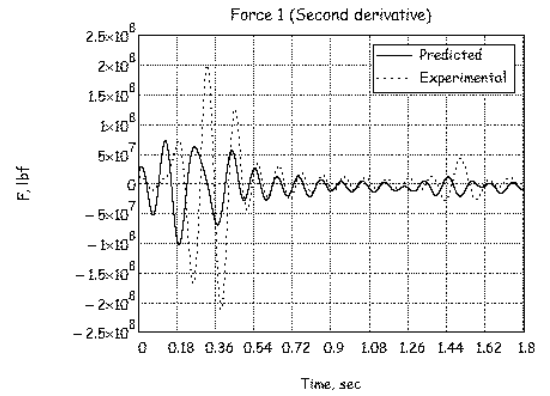


Figure 6.9: Numerical illustration (test 8)

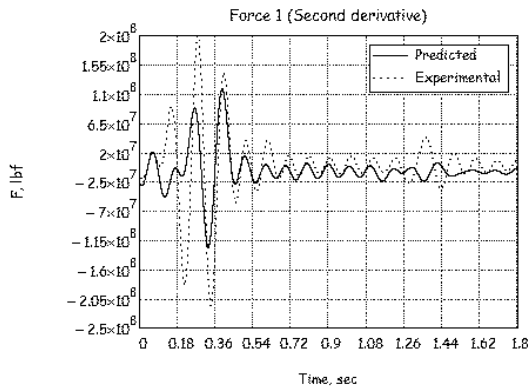


Figure 6.10: Numerical illustration (test 9)

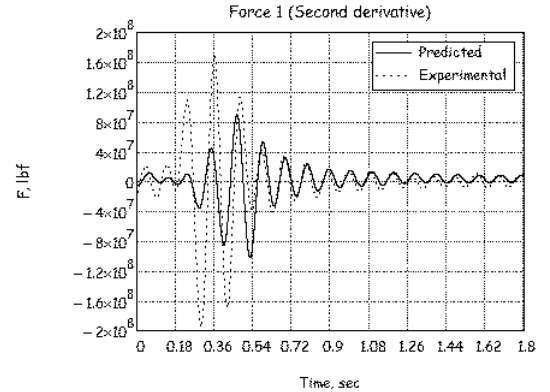


Figure 6.11: Numerical illustration (test 10)

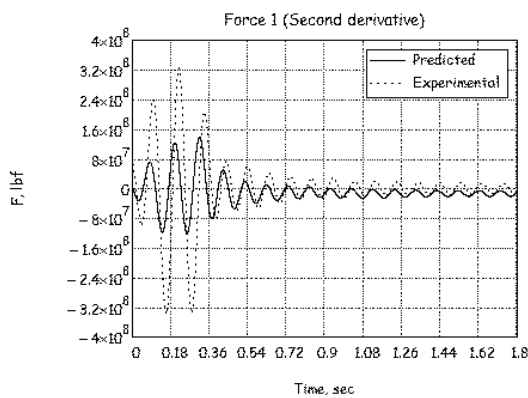


Figure 6.12: Numerical illustration (test 11)

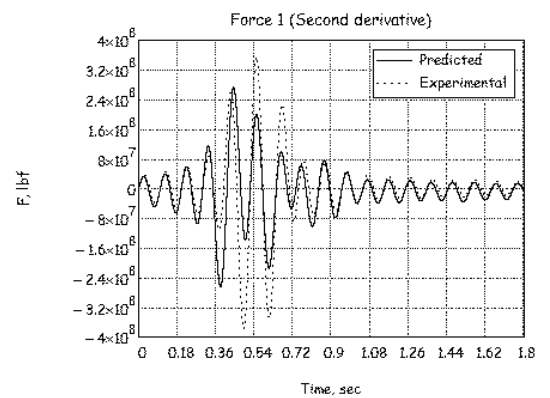


Figure 6.13: Numerical illustration (test 12)

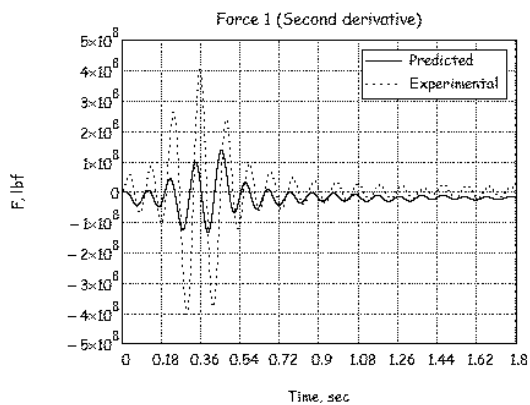


Figure 6.14: Numerical illustration (test 13)

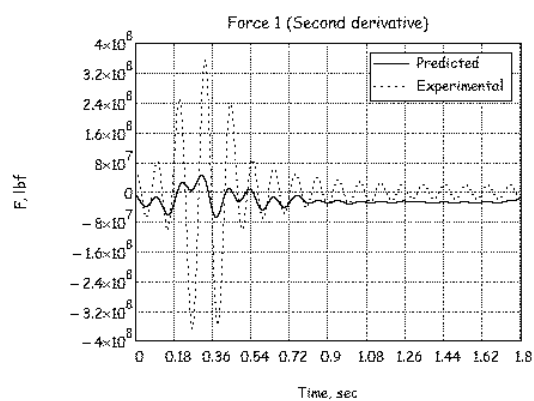


Figure 6.15: Numerical illustration (test 14)

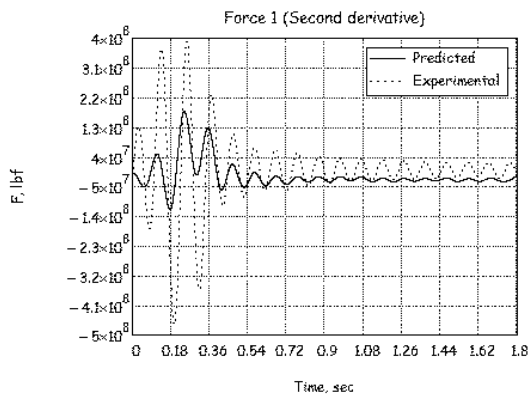


Figure 6.16: Numerical illustration (test 15)

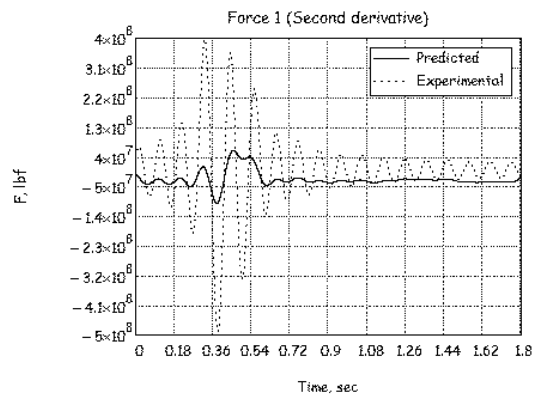


Figure 6.17: Numerical illustration (test 16)

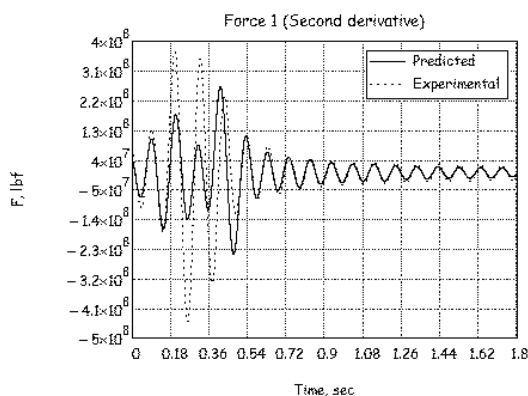


Figure 6.18: Numerical illustration (test 17)

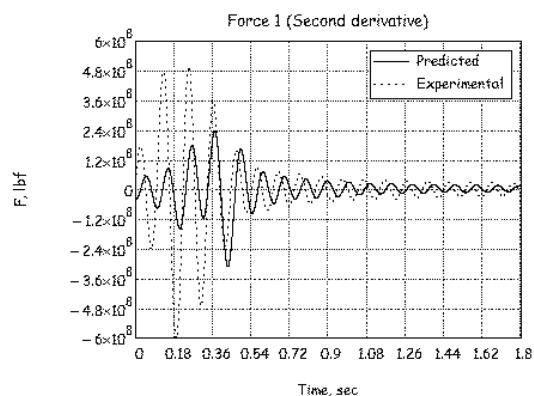


Figure 6.19: Numerical illustration (test 18)

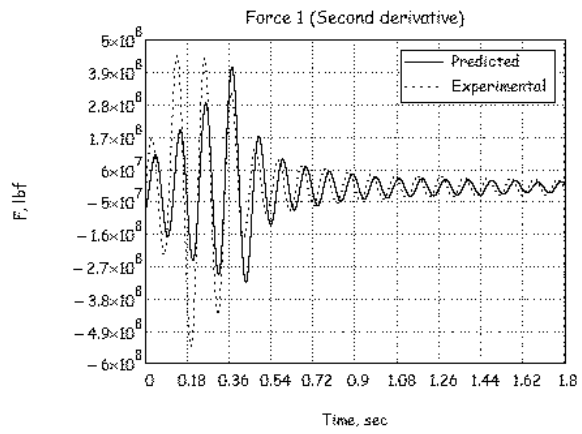


Figure 6.20: Numerical illustration (test 19)

# Conclusion

In this thesis, an approach for the prediction of contact forces arising at car-to-car impacts is developed. An ANN routine was designed for this case. Theoretical formulations within rigid body dynamics were adapted for training the ANN. Low-frequency corrections to rigid body dynamics were derived for extension and bending of an inhomogeneous viscoelastic bar. Implementation of the proposed methodology for analysis of experimental data leads to the following conclusions

- ANN seems to be a beneficial tool for predicting the contact forces in freight cars. At the same time, there is an issue related to achieving a required accuracy mainly due to a limited amount of tests.
- Rigid body dynamic models are useful for theoretical training of ANN. However, the validity of linear multibody models may be restricted because of nonlinearity of impact phenomena. On the other hand, the efficiency of general 3D continuum models is rather limited due to computational problems as well as lack of information on problem parameters, e.g. structure topology.
- The derived pseudo-rigid dynamic model incorporating the effect of internal structure demonstrates a wider range of validity than that started from the rigid body dynamic framework. The advantage of the aforementioned formulation has been

proved by comparisons with a real experimental setup in case of a coupled impact, see Chapter 6.

The developed perturbation procedure enables various extensions and is not restricted to the field of railway dynamics. In particular, a pretty similar analysis can be initiated for two-dimensional antiplane and plane problems for a viscoelastic rectangle subject to stresses prescribed along its sides. For an elongated rectangle there is an obvious possibility for applying higher-order asymptotic plate models, e.g. see [103, 104]. In this case not only one-dimensional equations of motion but also related boundary conditions should be refined using the dynamic version of the Saint-Venant's principle [105, 106]. Calculation of low-frequency corrections for more general geometries should rely on numerical calculations. However, the perturbation algorithm presented in the thesis should not be subject to major changes.

In addition, the proposed scheme is not restricted to the utilised linear viscoelastic model. More elaborate theories taking into account non-linearity and time inhomogeneity of viscous behaviour can be taken into consideration.

# Appendices

# Appendix A

## Exact solutions for homogeneous rods and beams

Substitute the formulae (4.85) and (5.81) into the equations of motion (4.1) and (5.1), (5.2) specified for a time-harmonic motion of a homogeneous bar and introduce dimensionless variables. Then, these equations take the form

$$u_{\xi\xi} + q_h^2 u = 0 \tag{A.1}$$

and

$$w_{\xi\xi\xi\xi} - q_{v,r}^4 w = 0 \tag{A.2}$$

where  $q_h^2 = \lambda_h^2(1+i\delta)$  and  $q_{v,r}^4 = \lambda_v^2(1+i\delta)$ . Subject them to the boundary conditions corresponding to the problems analyzed in the previous section, i.e.

$$u_\xi|_{\xi=-1} = 0, \quad u_\xi|_{\xi=1} = \frac{F_2 l(1+i\delta)}{EA} \tag{A.3}$$

$$w_{\xi\xi\xi}|_{\xi=\pm 1} = \mp \frac{N_2 l^3 (1 + i\delta)}{EI}, \quad w_{\xi\xi}|_{\xi=\pm 1} = 0 \quad (\text{A.4})$$

and

$$w_{\xi\xi\xi}|_{\xi=\pm 1} = \frac{N_2 l^3 (1 + i\delta)}{EI}, \quad w_{\xi\xi}|_{\xi=\pm 1} = 0 \quad (\text{A.5})$$

## A.1 Horizontal motion

We are looking the solution of the problem (A.1) subject to the boundary condition (A.3) in the form of

$$u(\xi) = C_1 e^{q_h \xi} + C_2 e^{-q_h \xi} \quad (\text{A.6})$$

First derivative of the (A.6) is given by

$$u_\xi(\xi) = C_1 q_h e^{q_h \xi} - C_2 q_h e^{-q_h \xi} \quad (\text{A.7})$$

After substituting (A.6) to he boundary condition (A.3) we get

$$\begin{aligned} C_1 &= \frac{F l e^{q_h} (1 + i\delta)}{2EA \sinh 2q_h} \\ C_2 &= \frac{F l e^{-q_h} (1 + i\delta)}{2EA \sinh 2q_h} \end{aligned} \quad (\text{A.8})$$

and finally

$$u(\xi) = -\frac{F_2 l (1 + i\delta) \cosh(q_h (1 + \xi))}{EA q_h \sinh 2q_h} \quad (\text{A.9})$$

In this case the horizontal acceleration of the center ( $\xi = 0$ ) is given by

$$a_h = \frac{F_2 q_h}{M \sinh q_h} \quad (\text{A.10})$$

Over the low-frequency band  $\lambda_h \ll 1$  we get  $q_h \ll 1$  assuming that  $\delta \sim 1$  ( $\gamma \sim \omega$ ) in (A.1). As a result, we arrive at the expansion

$$a_h = \frac{F_2}{M} \left( 1 + \frac{q_h^2}{6} + \dots \right) \quad (\text{A.11})$$

## A.2 Vertical motion

For the case of the vertical motion the solution of the problem (A.2) subject to the boundary condition (A.4) in the form of

$$w(\xi) = C_1 \cosh q_v \xi + C_2 \cos q_v \xi \quad (\text{A.12})$$

the third derivative is given by

$$w_{\xi\xi\xi}(\xi) = C_1 q_v^3 \sinh q_v \xi + C_2 q_v^3 \sin q_v \xi \quad (\text{A.13})$$

By substituting (A.13) to the boundary condition (A.4) we get

$$\begin{aligned} C_1 &= \frac{Fl^3(1+i\delta) \cos q_v}{EIq^3(\cos q_v \sinh q_v + \sin q_v \cosh q_v)} \\ C_2 &= \frac{Fl^3(1+i\delta) \cosh q_v}{EIq^3(\cos q_v \sinh q_v + \sin q_v \cosh q_v)} \end{aligned} \quad (\text{A.14})$$

and finally

$$w(\xi) = \frac{N_2 l^3 (1+i\delta)}{EI} \frac{\cos q_v \cosh \xi q_v + \cosh q_v \cos \xi q_v}{q_v^3 (\cos q_v \sinh q_v + \sin q_v \cosh q_v)} \quad (\text{A.15})$$

The associated acceleration of the center  $\xi = 0$

$$a_v = -\frac{2N_2}{M} \frac{q_v (\cos q_v + \cosh q_v)}{\cos q_v \sinh q_v + \sin q_v \cosh q_v} \quad (\text{A.16})$$

has the following low-frequency expansion

$$a_v = -\frac{2N_2}{M} \left( 1 + \frac{3}{40} q_v^4 + \dots \right) \quad (\text{A.17})$$

### A.3 Rotation

Similarly the rotation motion the solution of the problem (A.2) subject to the boundary condition (A.5) in the form of

$$w(\xi) = C_1 \sinh q_r \xi + C_2 \sin q_r \xi \quad (\text{A.18})$$

the third derivative is given by

$$w_{\xi\xi\xi}(\xi) = C_1 q_v^3 \cosh q_r \xi + C_2 q_r^3 \cos q_r \xi \quad (\text{A.19})$$

By substituting (A.19) to he boundary condition (A.4) we get

$$\begin{aligned} C_1 &= \frac{Fl^3(1+i\delta) \sin q_r}{EIq^3(\sin q_r \cosh q_r - \cos q_r \sinh q_r)} \\ C_2 &= \frac{Fl^3(1+i\delta) \sinh q_r}{EIq^3(\sin q_r \cosh q_r - \cos q_r \sinh q_r)} \end{aligned} \quad (\text{A.20})$$

and finally

$$\varphi(\xi) = \frac{N_2 l^3 (1+i\delta)}{EI} \frac{\sin q_r \cosh \xi q_r + \sinh q_r \sin \xi q_r}{q_r^2 (\sin q_r \cosh q_r - \cos q_r \sinh q_r)} \quad (\text{A.21})$$

The acceleration of the center  $\xi = 0$

$$a_r = -\frac{2N_2}{M} \frac{q_r^2 (\sin q_r + \sinh q_r)}{\sin q_r \cosh q_r - \cos q_r \sinh q_r} \quad (\text{A.22})$$

has the following low-frequency expansion

$$a_r = -\frac{2N_2}{3M} \left( 1 + \frac{11}{840} q_v^4 + \dots \right) \quad (\text{A.23})$$

# Appendix B

## Brief description of the developed software

The C# programmes with applications for analytical models (Kelvin-Voigt and Modified standard-linear ), finding force closure, processing and analysing experimental data, several artificial neural networks 'ANN' were developed. For implementation aforementioned applications the study materials and algorithms from [107]-[110] were used.

### B.1 Application 'Model'

Application 'Model' was created to facilitate the research and produce the results for analytical models, train artificial neural networks (ANN) and evaluate the results of models, ANN and the real life experiment data.

Application consists of the several modules:

- Implementation of analytical model with a linear spring 'Ideal Model' (see Figure B.1)

- Analytical model with a nonlinear spring and damper 'Damper Model' (see Figure B.2)
- Processing and analysis of experimental data 'Experiment Data' (see Figure B.3)
- Implementation of several artificial neural networks 'ANN' (see Figures B.4 and B.5)

Modules 'Ideal Model' and 'Damper Model' allow to generate any volume of data and set different analytical model characteristics such as stiffness, mass, initial velocity, viscosity and etc. It calculates accelerations, velocities and forces using analytical models with linear spring and nonlinear spring with viscous damper, generates and saves data sets to file for ANN training with different input and output parameters.

Module 'Experiment Data' allows to upload real experiment data, analyse it, generate and save the file for training of ANN.

Module 'ANN' has two types of neural networks: Multi Layer Perceptron (MLP) with Backpropagation "Backpropagation" and Radial Basis Function network "RBF". It takes the file with training data (which automatically randomly divided in to training and test data sets) and construct the MLP with different activation functions (e.g. linear, sigmoid, tanh, step, log) and numbers neurons and hidden layers. During the ANN training charts demonstrate progress showing the error and the average output error for the data provided. After training, you can save down the ANN and later upload it with a new data to continue training or to evaluate analytic model or real life experiment data.

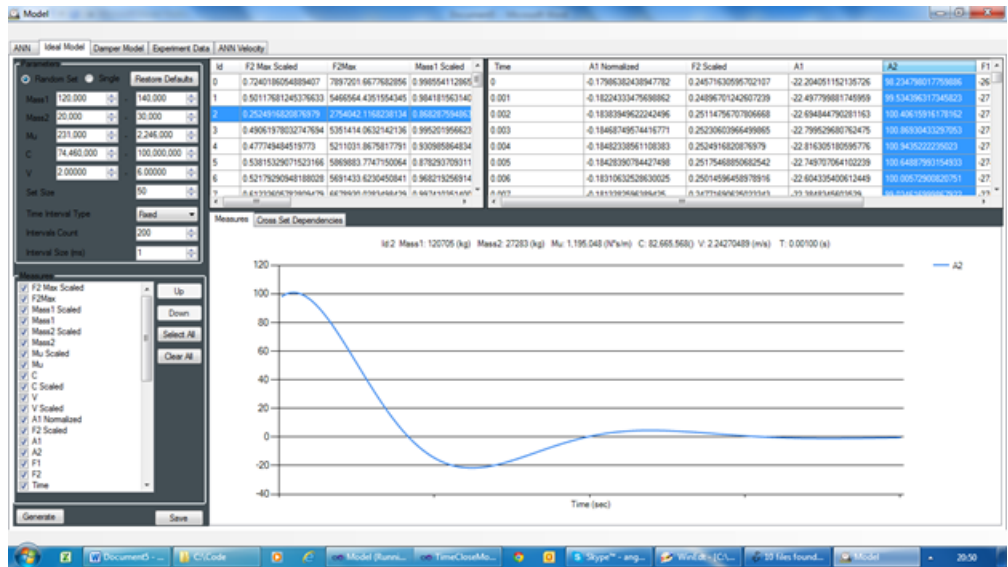


Figure B.1: Screenshot for module “Ideal Model”

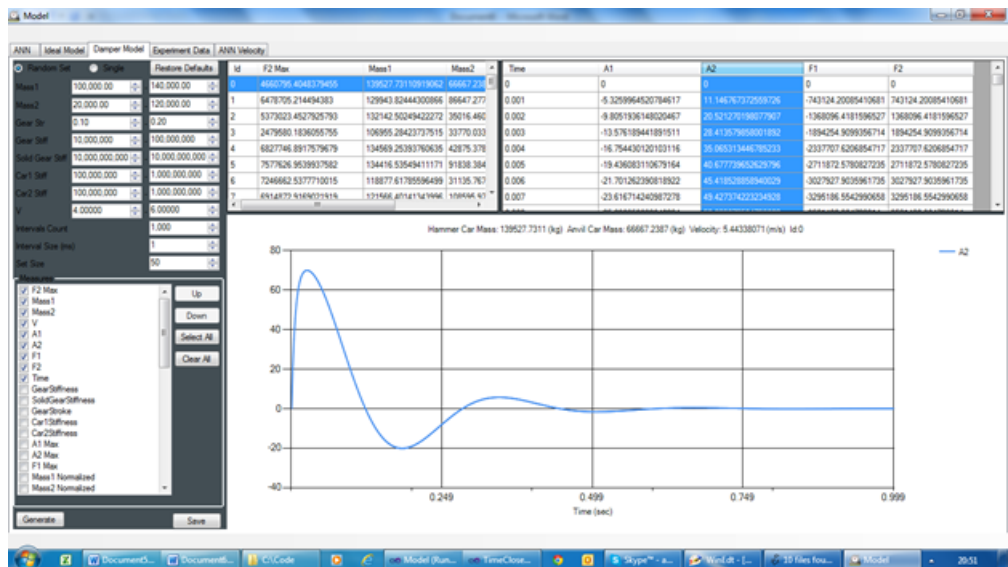


Figure B.2: Screenshot for module “Damper Model”

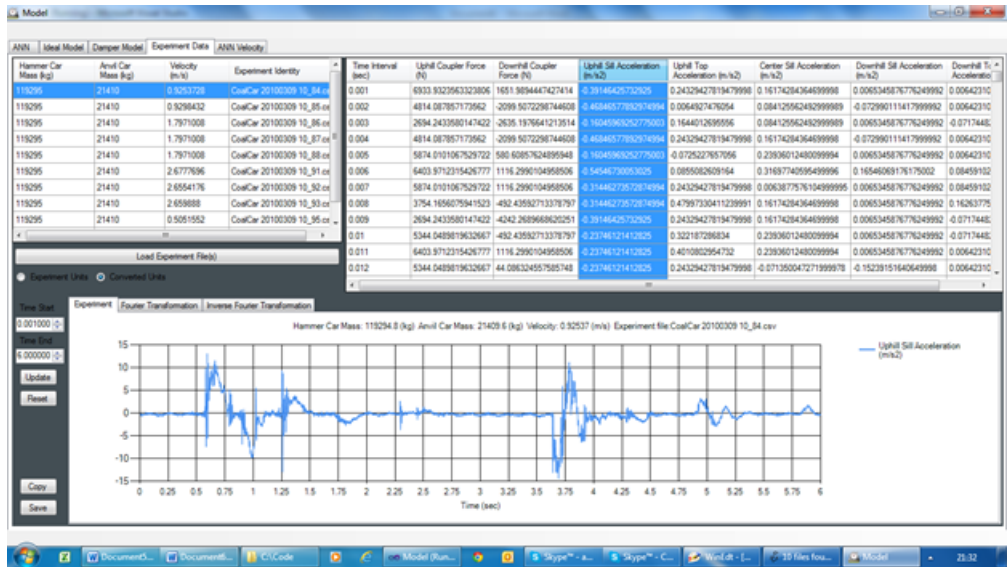


Figure B.3: Screenshot for module “Experimental Data”

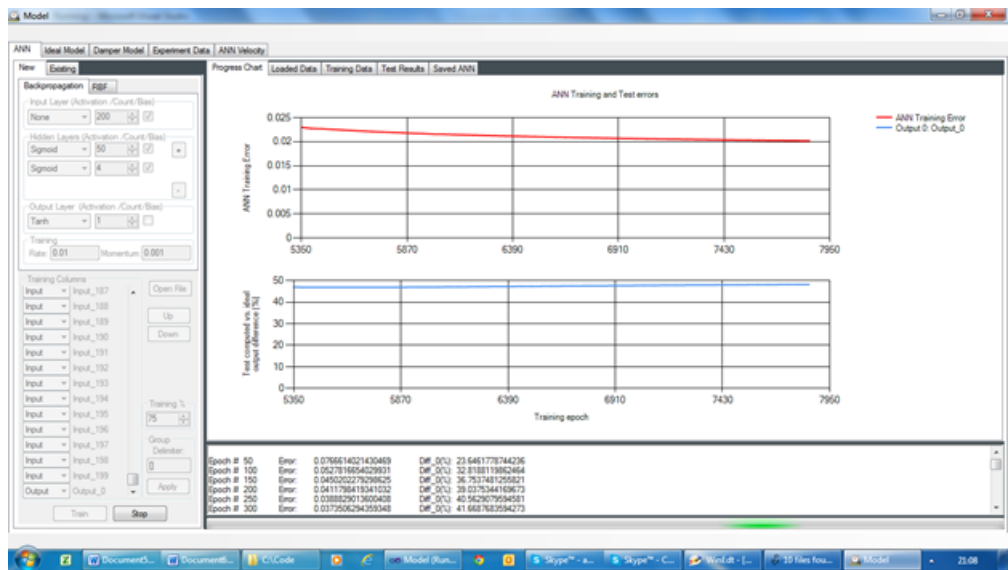


Figure B.4: Screenshot for ANN training

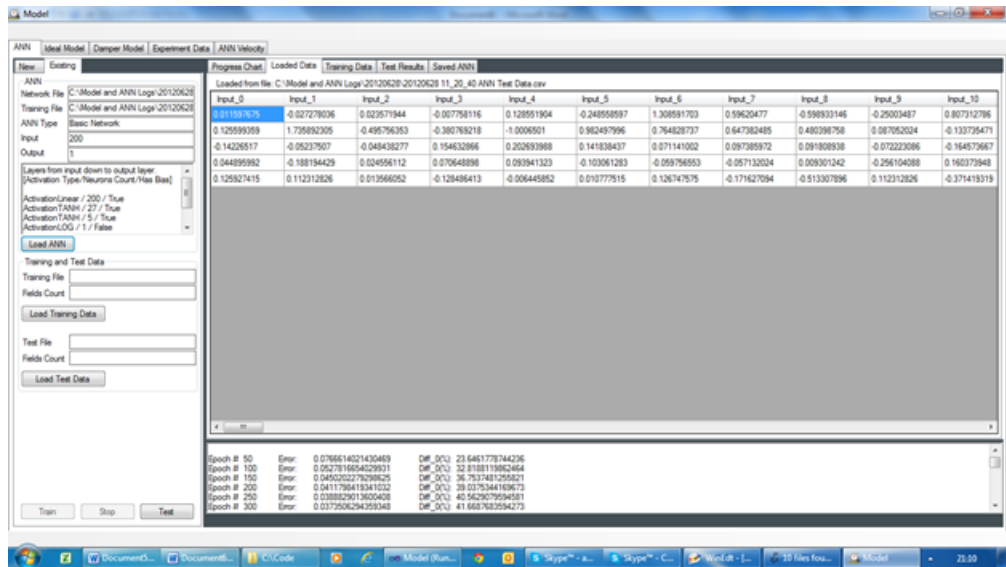


Figure B.5: Screenshot for loading ANN data

## B.2 Application 'Time Close Model'

Application 'Time Close Model' was developed to facilitate the research and produce for evaluation the reaction force using smoothing adaptive method and sin approximation.

Application consists of the several modules:

- Processing and analysis of experimental data
- Implementation of sin approximation method
- Implementation of smoothing adaptive method
- Generating ANN training data file

Application (see Figure B.6) allows to upload any volume of data, either real experiment data or data generated by the analytical models, analyse it, manually sets different

time intervals, increments and calculates closing forces and times and, finally, generate and save the file for training of ANN.

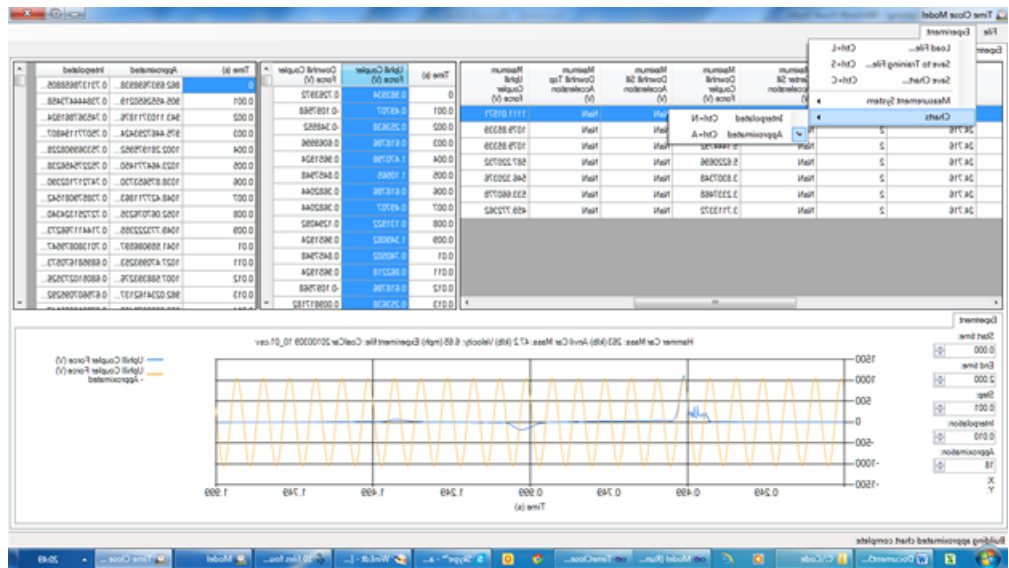


Figure B.6: Screenshot for Time Close Model

# Bibliography

- [1] C. Chen, M. Han, Y. Han. A numerical model for railroad freight car-to-car end impact. *Discr. Dyn. Nat. Soc.*, **927592**, 11, 2012.
- [2] W.McCulloch, W.H. Pitts. *A logical calculus of the ideas immanent in Neural Nets*. Bulletin of Mathematical Biophysics, V.5, 1943.
- [3] K. Hownik, M. Stinchombe and H. White. *Multilayer feedforward networks are universal approximators*. Neural Networks, **2(5)**, 359-366, 1989.
- [4] L. Fausett. *Fundamentals of Neural Networks*. Prentice Hall (UK), 248, 1994.
- [5] J. A. Anderson. *An Introduction to Neural Networks*. A Bradford Book, 672, 1995.
- [6] Yoh-Han Pao. *Adaptive Pattern Recognition and Neural Networks*. Addison Wesley, 309, 1989.
- [7] P. Song, P. Kraus, V. Kumar, P. Dupont. Analysis of rigid body dynamic models for simulation of system with frictional contacts. *ASME - J. of Applied Mechanics*, **68(1)**, 118-128, 2001.
- [8] C. W. Moussau, T.A. Laursen, M. Lidberg, R.L. Teylor. Vehile dynamics simulations with coupled multibody and finite element models. *Finite Elements in Analysis and Design*, **31(4)**, 295-315, 1999.

- [9] S. Hegard, H. Rahnejat, K. Hussain. Multi-body dynamics in full-vehicle handling analysis under transient manoeuvre. *Vehicle System Dynamics - Int. J. of Vehicle Mechanics*, **31(4)**, 1-24, 2000.
- [10] J. Kaplunov, A. Shestakova, I. Aleynikov and B. Hopkins. Theoretical Experimental Analysis of Transient Forces in Viscoelastic Chains *17th Workshop on Adv. in Exp. Mech. Portorozh, Slovenia*, 2013.
- [11] J. Kaplunov, A. Shestakova, I. Aleynikov and B. Hopkins. Perturbed rigid body motions of viscoelastic structures *Proc. 9th Int. Conf. Struct. Dyn. EUROODYN-2014, Porto, Portugal, 2014*, 3461-3464, 2014.
- [12] J. Kaplunov, A. Shestakova, I. Aleynikov, B. Hopkins, A. Talonov. Low - frequency perturbations of rigid body motions of a viscoelastic inhomogeneous bar. *Mech. of Time-Dep. Mat.*, 1573-2738, 2015.
- [13] A. Shestakova. An asymptotic approach to evaluate transient forces in freight cars. *EUROMECH-Colloquium 574, Eskisehir, Turkey*, 2015.
- [14] G.W. Milton, J.R. Willis. On modifications of Newton's second law and linear continuum elastodynamics. *Proc. R. Soc. Lond.*, **A 2079**, 855-880, 2007.
- [15] S. Goldman. *Vibration Spectrum Analysis*. Industrial Press Inc., 350, 2012.
- [16] L.H. Koopmans. *The Spectral Analysis of Time Series*. Academic Press, 366, 1995.
- [17] P. Stoica, R.L. Moses. *Spectral Analysis of Signals*. Prentice Hall, 480, 2005.
- [18] M.H. Holmes. *Introduction to Perturbation Methods*. Springer, 1995.
- [19] A.N. Tikhonov. Systems of differential equations containing a small parameter multiplying the derivative. *Mat. Sb.*, **31(73)**, 575-586, 1952.

- [20] F. Verhulst. *Methods and Applications of Singular Perturbations: Boundary Layers and Multiple Timescale Dynamics*. Springer, 2005.
- [21] B. M. Hopkins, D. Maraini, A. Seidel, and P. Shahidi. Empirical modeling of a rail tank car for struck coupler force estimation. *Proc. 2014 Joint Rail Conference, Colorado, USA, 2014*, Paper No. JRC2014-3713, pp. V001T06A002; 11 pages, doi:10.1115/JRC2014-3713.
- [22] S. Haykin. *Neural Networks: A Comprehensive Foundation*. CLC Press, 716, 1994.
- [23] J.A. Anderson. Data representation in neural networks. *AI Expert*, 30-37, 1990.
- [24] J. Laurence. Data preparation for a neural network. *AI Expert*, 34-41, 1991.
- [25] Y. Chauvin, D. E. Rumelhart. *Backpropagation: Theory, Architectures, and Applications*. Psychology Press, 576, 1995.
- [26] D. S. Broomhead, D. Lowe. *Radial basis functions, multi-variable functional interpolation and adaptive networks (Technical report)*. RSRE. 4148, 1988.
- [27] C. Cortes, V. Vapnic. Support vector networks. *Machine Learning*. **20**, 1-25, 1995.
- [28] A. J. Storkey, Romain Valabregue. The basins of attraction of a new Hopfield learning rule. *Neural Networks* **12.6**, 869-876, 1999.
- [29] T. Kohonen, O. Simula. Engineering Applications of the Self Organizing Map. *Proceeding of IEEE* 84, **10**, 1354-1384, 1996.
- [30] T. Kohonen, T. Honkela. *Kohonen Network*. Scholarpedia, 2007.

- [31] A. Fischer, C. Igel. Training Restricted Boltzmann Machines: An Introduction. *Pattern Recognition* **47**, 25-39, 2014.
- [32] D.E. Rumelhart, C.E. Hinton, R.J. Williams, *Learning internal representations by error propagation*. Parallel Distributing Processing, The MIT Press, 1986.
- [33] C. Bishop. *Neural Network for Pattern Recognition*. Clarendon Press, 504, 1995.
- [34] M. A. W. Saduf. Comparative Study of Back Propagation Learning Algorithms for Neural Networks. *Int. J. of Advanced Research in Computer Sci. and Software Eng*, **3**, 12, 2013.
- [35] Y.H. Zweiri, L.D. Seneviratne, K. Althoefer. Stability analysis of three term back propagation algorithm. *Neural Networks Journal*, **18**, 1341-1347, 2005.
- [36] R. J. Schalkoff. *Artificial Neural Networks*. McGraw-Hill, 422, 1997.
- [37] J. Park, I. W. Sandberg. Universal Approximation Using Radial-Basis-Function Networks. *Neural Computation*, **3**, 2, 246-257, 1991.
- [38] Yu Hen Hu, Jenq-Neng Hwang. *Handbook of Neural Network Signal Processing*. CRC Press, 408, 2001.
- [39] S. Iwnicki. *Handbook of railway vehicle dynamics*. CRC Press, 552, 2006.
- [40] M. Ansari, E. Esmailzadeh, P. Younesian. Longitudinal dynamics of freight trains. *Int. J. of Heavy vehicle system*, **16**, 1/2, 102-131, 2009.
- [41] A. Sommerfeld. *Mechanics: Lectures on Theoretical Physics*. **1**, 53, 1956.
- [42] C. Lanczos. *The Variational Principles of Mechanics*. Dover Publications Inc, 92, 1970.

- [43] R.E. Roberson, R. Schwertassek. *Dynamics of Multibody system*. Springer, 460, 1988.
- [44] J. Wittenburg. *Dynamics of Systems of Rigid Bodies*. Teubner, 224, 1977.
- [45] A. A. Shabana. *Dynamics of Multibody system*. Cambridge University Press, 393, 2013.
- [46] R. Schwertassek, R.E. Roberson. A state-space dynamical representation for multi-body mechanical system part 1: system with tree configuration. *Acta Mechanica*, **50(3-4)**, 141-161, 1984.
- [47] H. J. Fletcher, L. Rongved, E.Y.Yu. Dynamics analysis of a two-body gravitationally oriented satellite. *Bell System Techn. J.*, **42(5)**, 2239-2266, 1963.
- [48] R.E. Roberson, W. Wittenburg. A dynamical formalism for an arbitrary number of interconnected rigid bodies with reference to the problem of satellite attitude control. *Proceeding of 3rd Int. Federation of Automatic Control Congress London*, UK, 1966.
- [49] K. Hutter, K. Johnk. *Continuum Methods of Physical Modeling*. Springer, 660, 2004.
- [50] Y. A. Khulief, A. A. Shabana. A continuous force model for the impact analysis of flexible multibody systems. *Mechanism and Machine Theory*, **22**, 213224, 1987.
- [51] H.M. Lankarani, P. E. Nikravesh. A contact force model with hysteresis damping for impact analysis of multi-body system. *J. Mech. Des.*, **112**, 369-376, 1990.
- [52] R. M. Brach. *Mechanical impact dynamics, rigid body collisions*. J. Wiley, 1991.

- [53] W. Goldsmith. *Impact, the Theory and Physical Behavior of Colliding Solids*. E. Arnold Ltd, 379, 1960.
- [54] Y. A. Khulief, A. A. Shabana. A continuous force model for the impact analysis of flexible multibody systems. *Mechanism and Machine Theory*, **22**, 213224, 1987.
- [55] W.J. Stronge. *Impact Mechanics*. Cambridge University Press, 304, 2004.
- [56] K.H. Hunt, R.F. Crosseley. Coefficient of restitution interpreted as damping in vibroimpact. *J. Appl. Mech.*, **7**, 440-445, 1975.
- [57] H. M. Lankarani, P. E. Nikravesh. Continuous contact force models for impact analysis in multibody systems. *Nonlinear Dynamics*, **5**, 2, 193-207, 1994.
- [58] M. Machadoa, P. Moreiraa, P. Floresa, H.M. Lankaranib. *Compliant contact force models in multibody dynamics: Evolution of the Hertz contact theory*. *Mech. and Mach. Theory*, **53**, 99121, 2012.
- [59] R.V. Dukkipati. *Vehicle Dynamics*. Narosa Publishing House, 600, 2000.
- [60] J.D. Hoffman. *Numerical Methods for Engineers and Scientists*. CRC Press, Second Edition, 2001.
- [61] K.A. Atkinson. *An Introduction to Numerical Analysis (2nd ed.)* Wiley, 712, 1989.
- [62] N.M. Newmark. A method of computation for structural dynamics. *J. of Eng. Mech.*, ASCE, **85(3)**, 67-94, 1959.
- [63] J. Mei, Z. Liu, W. Wen, P. Sheng. Effective mass density of fluid-solid composites. *Phys. Rev. Lett.* **96**, 024301, 2006.

- [64] J.R. Willis. Variational and related methods for the overall properties of composites. *Adv. Appl. Mech.*, **21**, 178, 1981.
- [65] P. Sheng, X.X. Zhang, Z.Liu, C.T. Chan. Locally resonant sonic materials. *Phys. B. Condens. Matter.*, **338**, 201205, 2003.
- [66] M. Milgrom. Modification of the Newtonian dynamics as a possible alternative to the hidden mass hypothesis. *Astrophys. J.*, **270**, 1983a 365370, 1983.
- [67] G. Papanicolau, A. Bensoussan, J.-L. Lions. *Asymptotic Analysis for Periodic Structures*. Elsevier, 699, 1978.
- [68] J.G. Berryman. Long-wavelength propagation in composite elastic media. I. Spherical inclusions. *J. Acoust. Soc. Am.*, **680**, 18091819, 1980.
- [69] M. Bellieud, G. Bouchitte. Homogenization of a soft elastic material reinforced by fibers. *Asymptot. Anal.*, **32-2**, 153183, 2002.
- [70] M. Camar-Eddine, G. W. Milton. Non-local interactions in the homogenization closure of thermoelectric functionals. *Asymptot. Anal.*, **32** , 2762, 2002.
- [71] K. D. Cherednichenko. Two-scale asymptotics for non-local effects in composites with highly anisotropic fibres. *Asymptot. Anal.*, **49**, 3959, 2006.
- [72] Z. Addressamad, J. Kostin, G. Panasenko, V.P. Smyshlyaev. Memory effect in homogenisation of a viscoelastic Kelvin-Voigt model with time-dependent coefficients. *Math. Models Methods Appl. Sci.*, **9**, 1603-1630, 2009.
- [73] R. Luciano, J.R. Willis. Bounds on non-local effective relations for random composites loaded by configuration-dependent body force. *J. Mech. Phys. Solids*, **48**, 18271849, 2000.

- [74] N.S. Bakhvalov, G.P. Panasenko. *Homogenization: averaging processes in periodic media*. Springer Netherlands, 36, 1989.
- [75] R.V. Craster, L.M. Joseph, J. Kaplunov. Long-wave asymptotic theories: The connection between functionally graded waveguides and periodic media. *Wave Motion*, **51**, 581-588, 2013.
- [76] E. Nolde, R.V. Craster, J. Kaplunov. High frequency homogenization for structural mechanics. *J. of the Mech. and Ph. of Solids*, **59-3**, 651671, 2011.
- [77] R.V. Craster, J. Kaplunov, J. Postnova. High-frequency asymptotics, homogenisation and localisation for lattices. *J Mech. Appl. Math.*, **63(4)**, 497-519, (2010).
- [78] L.V. Fausett. *Fundamentals of Neural Networks: Architectures, Algorithms And Applications*. Pearson, 461, 1993.
- [79] N. K. Bose, P. Liang. *Neural Network Fundamentals with Graph Algorithms and Applications*. McGraw-Hill, 478, 1996.
- [80] R. Stein. Selecting data for neural networks. *AI Expert*, 42-47, 1993.
- [81] R. Stein. Preprocessing data for neural networks. *AI Expert*, 32-37, 1993.
- [82] J.S. Simonoff. *Smoothing Methods in Statistics, 2nd edition*. Springer, 338, 1998.
- [83] R. Callan. *The essence of Neural Networks*. Prentice Hall (UK), 248, 1998.
- [84] K. Gurney. *An introduction to Neural Network*. UCL Press, 234, 1997.
- [85] G.E. Nasr, E.A. Badr, C. Joun. Cross Entropy Function in Neural Networks: Forecasting Gasoline Demand. FLAIRS Conference, 381-384, 2002.

- [86] J. Heaton. *Introduction to Neural Networks for C*. 2nd Edition, Heaton Research, Inc., 2008.
- [87] F. Rosenblatt. The perceptron: a probabilistic model for information storage and organization in the brain, *Psychological Review*, **65**, 386-408, 1958.
- [88] V. Kurkova. Kolmogorov's theorem and multilayer neural networks. *Neural Networks*, **5(3)**, 501-506, 1992.
- [89] M.R. Hestenes, E. Stiefel. Methods of Conjugate Gradients for Solving Linear Systems. *The J. of Research of the Nat. I. of Stand. and Tech.*, **49(6)**, 409-436, 1952.
- [90] H. Shao, H. Zheng. A new bp algorithm with adaptive momentum for FNNs training. *GCIS*, 16-20, 2009.
- [91] D.J. Swanston, J.M. Bishop, R.J. Mitchell. Simple adaptive momentum: new algorithm for training multilayer perceptrons. *J Electronic Letters*, **30**, 1498-1500, 1994.
- [92] C.C. Yu, B.D. Liu. A backpropagation algorithm with adaptive learning rate and momentum coefficient. *IEEE*, 2002.
- [93] Y.H. Pao. *Adaptive pattern recognition and neural networks*. Addison-Wesley, 326, 1989.
- [94] R. Fletcher, C.M. Reeves. *Function minimization by conjugate gradients*. Computer Journal, **7**, 149-154, 1964.
- [95] M. Hazewinkel. *Runge-Kutta method*. Springer, 2001.

- [96] G. Da-Hu, S.A. Meguid. Stability of Runge-Kutta methods for delay differential system with multiple delays. *IMA Journal of Num. An.*, **19**, 3, 349-356, 1999.
- [97] S.W. Smith, *The Scientist and Engineer's Guide to Digital Signal Processing*. California Technical Pub, 1st edition, 626, 1997.
- [98] G.P. Tolstov, *Fourier Series (Dover Books on Mathematics)* Dover Publications, 1976, 352.
- [99] T. Hastie, R. Tibshirani, J. Friedman. *The Elements of Statistical Learning: Data Mining, Inference, and Prediction*. Springer, 745, 2009.
- [100] H. Park, K. Kim. An adaptive method for smooth surface approximation to scattered 3D points. *Computer-Aided Design*, **27(12)**, 929-939, 1995.
- [101] R.M. Cristensen. *Viscoelasticity: An Introduction. 2nd addition*. Academic Press, N.Y., 359, 1982.
- [102] Yu.N. Rabotnov. *Elements of hereditary solid mechanics*. Mir Publishers, Moscow, 387, 1980.
- [103] R. Craster, J. Kaplunov *Dynamic Localization Phenomena in Elasticity, Acoustics and Electromagnetism (CISM International Centre for Mechanical Sciences)*. Springer, 256, 2013.
- [104] A.L. Goldenveizer, J.D. Kaplunov, E.V. Nolde. On Timoshenko-Reissner type theories of plates and shells. *Int. J. of Solids and Structures*, **30(5)**, 675-694, 1993.
- [105] E. Babenkova and J. Kaplunov. The two-term interior asymptotic expansion in the case of low-frequency longitudinal vibrations of an elongated elastic rectangle.

- Proc. of the IUTAM Symposium on Asymptotics, Singularities and Homogenisation in Problems of Mechanics, Solid Mechanics and its Applications*, **113**, Kluwer, 123-131, 2003.
- [106] E. Babenkova and J. Kaplunov. Low-frequency decay conditions for a semi-infinite elastic strip. *Proc. R. Soc. Lond.*, **A 460**, 2153-2169, 2003.
- [107] J. Sharp *Microsoft Visual C# 2013. Step by Step*. Microsoft Press, 824, 2013.
- [108] S.T. Welstead. *Neural Network and fuzzy logic applications in C/C++*. Wiley, 494, 1994.
- [109] T. Masters. *Practical Neural Network Recipes in C++*. Academic Press, 493, 1993.
- [110] J. Rodgers. *Object-oriented Neural Networks in C++* Academic Press, 310, 1997.
- [111] G.S. Gorelic. *Oscillations and waves*. Moscow publisher of physical and mathematical lit., 572, 1959.
- [112] B. Maxfield. *Essential Mathcad for Engineering, Science, and Math, Second Edition*. Academic Press, 501, 2009.